TÉCNICO LISBOA

Zeolite-supported catalysts for CO_2 methanation: The influence of transition metals incorporation in the performances

DIOGO MIGUEL FRANCO CANASTREIRO

Thesis to obtain the Master of Science Degree in

CHEMICAL ENGINEERING

Supervisors:
Dr. Prof. Patrick da Costa
Dr. Maria del Carmen Bacariza Rey

EXAMINATION COMMITTEE

Chairperson: Dr. Prof. Maria Teresa Duarte
Supervisor: Dr. Maria del Carmen Bacariza Rey
Members of Committee: Dr. Prof. Ana Cristina Gomes Ferreira da Silva Parreira

October 2021

Acknowledgements

The ability to reflect allows us to do better in the future. Thus, with the current journey coming close to its end, one must reflect upon those that without their assistance all this wouldn't have been possible. Therefore, I would like to take this opportunity to express my deepest thanks to the following.

A special thank you to Doctor Carmen Bacariza, the supervisor I didn't knew I'd get, for all her unfathomable support, availability and guidance. It would have been a lot harder without her and her immeasurable spirit.

To Professor Doctor Patrick da Costa, my supervisor, for his availability and motivation, as well as his incentive for wider goals.

To both, it was a privilege to work alongside you.

To Professor Doctor Carlos Henriques, for his availability and support throughout these past few months.

To Professor Doctor José Madeira Lopes, for his guidance and assistance.

And an academic acknowledgement to both Daniela Spataru and Leonardo Pedrosa, for their respective assistance and companionship on the long hours spent in the laboratory.

A particular appreciation for my friend Ricardo Pereira, for his sound and constant advises made this a more tolerable labor.

To family and friends for all their unconditional support and patience through the whole process.

Resumo

A metanação de CO_2 foi apontada como uma alternativa promissora para o armazenamento de energia renovável através do conceito de *power-to-gas*, permitindo simultaneamente uma redução das emissões dióxido de carbono.

Destarte, com o objetivo de melhorar a atividade de catalisadores à base de zeólitos para a reação de metanação do CO_2, foi estudada a incorporação de diversos metais de transição (Fe, Ni, Co e Cu) nesses mesmos suportes. Deste modo, foi avaliado o efeito do tipo de metal assim como a dopagem do catalisador mais ativo com pequenos teores dos metais menos interessantes.

No primeiro conjunto de testes catalíticos, o Ni provou ser o metal mais ativo para a reação, pelo que, foi então o escolhido para a síntese de catalisadores bimetálicos com 1 wt% de Fe, Co e Cu e 15 wt% Ni. Nesta série, o Fe foi responsável por uma melhoria na dispersão metálica do Ni$^\circ$, levando aos melhores resultados catalíticos. Por último, avaliou-se ainda o efeito do teor de Fe (1, 2 ou 3 wt%), tendo sido o catalisador com um 1 wt% o mais interessante, possivelmente devido ao enfraquecimento das interações metal-suporte com o aumento do teor de Fe, obtendo então valores de conversão de CO_2 de 71.5 % e de seletividade de CH_4 de 98.25% para os 350°C.

Palavras-chave

Metanação de CO_2; Metais de Transição; Power-to-Gas; Zeólitos; Catálise Térmica.

Abstract

CO_2 methanation has been appointed as a promising alternative for the storage of renewable energy through the *power-to-gas* concept, whilst also allowing for the reduction of this gas injurious emissions.

Thus, aiming to improve the activity of zeolite-based catalysts for the carbon dioxide methanation reaction, a study was performed on the incorporation of several transition metals (Fe, Ni, Co and Cu) on those same supports. Hence, the effect of the type of metal was evaluated, as well as the doping of the most active catalyst with the other metals.

In the first set of catalytic tests, Ni proved to be the most active added metal, hence, it was chosen for the synthesis of bimetallic catalysts containing 1 %wt of Fe, Co and Cu and 15 %wt of Ni. In this series, iron was responsible for an improvement on the metallic dispersion of Ni $^{\circ}$, leading up to the best catalytic results. Therefore, the effect of the iron loading (1, 2 or 3 %wt) was also evaluated, being the catalyst with 1 %wt the most interesting, possibly due to the weakening of the metal-support interactions as the iron loading increased, thus obtaining CO_2 conversion values of 71.5 % and CH_4 selectivity values of 98.25% for 350°C.

Keywords CO_2 Methanation; Transition Metals; Power-to-Gas; Zeolites; Thermal Catalysis.

Contents

1 Introduction **15**

2 State of the Art **17**

2.1 Methanation as a Natural Gas production method . . . 18

2.1.1 Hydrogen . . . 19

2.1.2 Power-to-Gas . . . 19

2.1.3 Pre-treatment . . . 21

2.1.4 Separation of CO_2 and CH_4 . . . 21

2.2 Reactional Mechanism . . . 22

2.2.1 Pure CO_2 Splitting . . . 23

2.2.2 CO_2 Hydrogenation . . . 24

2.2.3 Methanation of CO_2 . . . 24

2.2.4 CO_2 Hydrogenation to Methanol . . . 25

2.2.5 DME Synthesis from Methanol . . . 26

2.2.6 Methanol Conversion to C_2+ hydrocarbons . . . 26

2.2.7 WGSR/PROX . . . 26

2.2.8 Thermodynamics of the Sabatier Reaction . . . 27

2.3 Thermal Catalysis . . . 28

2.3.1 Active Metals . . . 29

2.3.2 Monometallic vs Bimetallic catalysts . . . 29

2.3.3 Promotion of Ni-based catalysts with Fe, Co and Cu . . . 29

2.3.4 Deactivation of Catalysts . . . 31

2.4 Bimetallic Catalysts Study . . . 31

2.5 Zeolite-supported catalysts for CO_2 Methanation . . . 33

2.5.1 Improving the properties of the support . . . 33

2.5.2 Incorporation of Promoters . . . 33

2.6 Thesis Objective . . . 33

3 Methods and Catalyst Preparation **35**

3.1 Synthesis of the Catalysts . . . 35

3.1.1 Preparation of the CsUSY support . . . 35

3.1.2 Incorporation of Metals . . . 35

3.2 Physico-chemical characterizations . . . 36

3.2.1 X-Ray Diffraction (XRD) . . . 36

3.2.2 Temperature-Programmed Reduction with H_2 (H_2 TPR) . . . 36

3.2.3 Thermogravimetric Analysis (TGA) . . . 37

3.2.4 N_2 Adsorption . . . 38

3.2.5 Transmission Electron Microscopy (TEM) . . . 38

3.3 Catalytic tests . . . 38

3.3.1 Experimental Unit . . . 38

3.3.2 Calculation of CO_2 conversion, CH_4 selectivity and yield . . . 40

4 Results and Discussion **42**

4.1 Effect of the Metal Nature . . . 42

4.1.1 XRD . . . 42

4.1.2 H_2-TPR . . . 43

4.1.3 TGA . . . 44
4.1.4 N_2 Adsorption . . . 44
4.1.5 TEM . . . 45
4.1.6 Catalytic Results . . . 46
4.1.7 XRD of spent catalysts . . . 47
4.2 Effect of 15Ni doping with other transition metals . . . 49
4.2.1 XRD . . . 49
4.2.2 H_2-TPR . . . 49
4.2.3 TGA . . . 50
4.2.4 TEM . . . 50
4.2.5 Catalytic Results . . . 51
4.2.6 XRD of spent catalysts . . . 52
4.3 Effect of Fe Loading . . . 54
4.3.1 XRD . . . 54
4.3.2 H_2-TPR . . . 54
4.3.3 TGA . . . 55
4.3.4 TEM . . . 55
4.3.5 Catalytic Results . . . 57
4.3.6 XRD of spent catalysts . . . 58

5 Conclusions and Future Perspectives 61

6 References 63

7 Annexes 74
7.1 Annex 1: Peak angles in the XRD diffractogram ($^\circ$) . . . 74
7.2 Annex 2: Tecnico-Economical study into the system . . . 75
7.3 Annex 3: Mass Loss (%) vs Temperature . . . 76
7.4 Annex 4: Other Technologies for the conversion of CO_2 . . . 79
7.4.1 Electrochemical Conversion . . . 79
7.4.2 Solar Thermochemical Conversion . . . 80
7.4.3 Photochemical Conversion . . . 81
7.4.4 Biochemical Conversion . . . 81
7.5 Annex 5: CO_2 Procurement . . . 83
7.5.1 Cleaning the Cement . . . 83
7.6 Annex 6: Aspen simulation of thermodynamic conditions for methanation and methanolation . . . 85
7.6.1 Temperature . . . 85
7.6.2 Pressure . . . 86
7.6.3 N_2 Dilution . . . 87
7.6.4 H_2/CO_2 ratio . . . 88
7.7 Annex 7: Uses for Methanation . . . 89
7.8 Annex 8: Catalysts used for Methanol Conversion . . . 90
7.9 Annex 9: Plasma . . . 92
7.9.1 Plasma Catalysis . . . 92
7.9.2 Catalysts for Plasma-Assisted Methanation . . . 93
7.9.3 Physicochemical Interactions of Plasma and Catalyst . . . 93

List of Figures

1 Carbon dioxide emissions (on the left), and the global average temperature (on the right) along the years These emissions solely represent CO_2 and not the remaining GHG (Global Carbon Budget 2019) [9]. . . . 17
2 Carbon-cycle on a closed loop system. . . . 18
3 Amount of different polluting materials (in thousand of tons per TWh) needed for a construction of each type of energetic plant, per unit of eletricity generated. [6] . . . 19
4 Power-to-Gas strategy connects the electrical and the natural gas grids, allowing for the renewable storage of energy in the form of synthetic natural gas, as well as many possible uses even beyond the energy sector. [29] . . . 20
5 Illustrated comparison charge/discharge period and storage capacity of different electricity storage systems. CAES: compressed air energy storage; PHS: pumped hydro storage. [30] . . . 20
6 Schematic of all possible reactional pathways for the carbon dioxide methanation, in pink. All intermediates are represented by the gray dots. The gray lines represent plausible links between the primary pathways. [41] . . . 22
7 Representative mechanism for thermal methanation of CO_2 over a Ni-based ceria-zirconia catalyst. [43] . . . 22
8 Representative mechanism for plasma-assisted carbon dioxide hydrogenation over a Ni/USY zeolite. . . . 23
9 Calculated theoretical thermal conversion (left axis) and corresponding energy efficiency (right axis) as a function of temperature for the pure splitting of CO_2 into CO and O_2. . . . 24
10 Possible reaction pathways for CO_2 conversion to methanol. . . . 25
11 Water gas shift reaction mechanism [72] . . . 27
12 Results obtained by McBride *et al.* [113] for an increase of pressure and temperature, for a) CO_2 conversion, and b) CH_4 selectivity. . . . 28
13 Graphical representation of the yield of CH_4 obtained for each different catalyst, comparing its different preparation methods. [76] . . . 32
14 Scheme of the catalytic tests unit, for 1 bar, adapted with permission from [116]. . . . 39
15 X-Ray Diffractograms for the calcined (on the left) and reduced (on the right) samples, referring to the first study. . . . 42
16 H_2-TPR profiles obtained for the 15X catalysts. . . . 43
17 N_2 Adsorption Isotherms obtained for the support and catalysts of the first study. . . . 45
18 Images of each catalyst corresponding to the first study, obtained through Transmission Electron Microscopy, after their reduction. . . . 46
19 Methanation tests results for each one of the monometallic samples, after a reduction at 470 °C. In which each graph corresponds to a) CO_2 conversion; and b) CH_4 selectivity. . . . 46
20 Methane yield obtained for 15X catalysts after reduction at 470 °C. . . . 47
21 X-Ray Diffractograms for the spent samples belonging to the first study. . . . 48
22 X-Ray Diffractograms for the calcined (on the left) and reduced (on the right) samples, for the second study. . . . 49
23 H_2-TPR profiles obtained for 15Ni1X catalysts. . . . 50
24 Images of each catalyst corresponding to the second study, obtained through Transmission Electron Microscopy, after their respective reduction. . . . 51
25 Methanation test results for each one of the bimetallic samples of the second study. In which each graph corresponds to a) CO_2 conversion; and b) CH_4 selectivity. . . . 51
26 Methane yield obtained for each one of the bimetallic catalysts. . . . 52
27 XRD patterns for spent 15Ni1X samples. . . . 53
28 X-Ray Diffractograms for the calcined (on the left) and reduced (on the right) samples, for the third study. . . . 54
29 H_2-TPR profiles obtained for 15NixFe catalysts. . . . 55

30 TEM micrographs obtained for 15NixFe catalysts after reduction at 470 °C. 56
31 Methanation test results for the iron-based bimetallic samples of the third study. In which each graph corresponds to a) CO_2 conversion; and b) CH_4 selectivity. 57
32 Methane yield obtained for each one of the iron-based bimetallic catalysts. 58
33 X-Ray Diffractograms for the spent samples belonging to the third study. 59
34 Mass Loss (%) as a function of temperature for 15X catalysts. 76
35 Mass Loss (%) as a function of temperature for the bimetallic catalysts pertaining the second study. 77
36 Mass Loss (%) as a function of temperature for the iron-based bimetallic catalysts. 78
37 Diagram representing the principles of a solid proton conducting electrolysis cell (a) solid oxide electrolysis cell (b) an alkine electrolysis cell (c) for the conversion of CO_2 and/or H_2 79
38 Schematic of the two-step solar thermochemical conversion cycle for CO_2 and H_2 splitting based on metal oxide redox reactions. 80
39 Schematic of the photochemical reduction of CO_2 by water on a metal oxide catalyst. 81
40 Schematic of the photo-bioreactor application for CO_2 conversion. [12] 82
41 Separation techniques available for the removal of CO_2 on the post-combustion stage. [182] . 83
42 Graph representing the quantity of each respective product obtained for the ASPEN simulation, as a function of temperature, for a H_2/CO_2 ratio of 3, pressure of 1 bar, no catalyst. 85
43 Graph representing the conversion of CO_2 as a function of temperature, for a H_2/CO_2 ratio of 3, pressure of 1 bar, without a catalyst. 86
44 Graph representing the selectivities of CH_3OH and CH_4 as a function of pressure, for a H_2/CO_2 ratio of 3, constant temperature of 25 °C, without a catalyst. 86
45 Graph representing the conversion of CO_2 as a function of pressure, for a H_2/CO_2 ratio of 3, constant temperature of 25 °C, without a catalyst. 87
46 Graph representing the thermodynamic conversion of 200 kmol/h of N_2 into NO, NO_2 and N_2O as a function of temperature. 87
47 Graph representing the products obtained for the conversion of CO_2 with H_2 for a ratio of four between the two, as a function of temperature. 88
48 Fraction of electron energy transferred to different channels of excitation, as well as to the ionization and dissociation of CO_2. [12] 94

List of Tables

1 Molar composition of natural gas [16]. . . . 18
2 A selection of the best results found in the literature, obtained for three promoters (Fe, Co and Cu) for Ni-based catalysts. . . . 30
3 Depiction of all the prepared catalysts throughout the study, divided by their respective studied effect. . . . 35
4 Operational conditions used for the pretreatment and methanation tests. . . . 40
5 Grain size obtained for each catalyst, at each one of the phases it underwent, for the first study. 43
6 Hydrophobicity indexes calculated for the 15X catalysts. . . . 44
7 Textural Properties in Calcined Catalysts. . . . 45
8 NiO and Ni$^{\circ}$crystallite sizes obtained for the 15Ni1X catalysts after calcination and reduction. . 49
9 Hydrophobic indexes obtained for 15Ni1X catalysts. . . . 50
10 NiO and Ni$^{\circ}$crystallite sizes obtained for the 15NixFe catalysts after calcination and reduction. 54
11 Hydrophobic indexes obtained for 15NixFe catalysts. . . . 55
12 Peak angles corresponding to each compound on the X-ray diffractograms. . . . 74
13 Prices for each one of the components involved in the process. Water was despised as its value is far lower than the others. . . . 75
14 Mass balance performed for both the Sabatier reaction and the reverse water gas shift reaction, according to their respective selectivity. . . . 75
15 Profit and Gross Margin obtained both for green and fossil fuel hydrogen. . . . 75
16 Descriptive table of previously used catalysts for the conversion of CO_2 into methanol and their respective results. . . . 90
17 Comparison with some of the catalysts reported in the literature for CO_2 methanation under DBD plasma assisted conditions. . . . 93
18 Bond Dissociation Energies (E_diss), Vibrational Energies (E_vib), First Electronically Excited State (E_elect), Ionization Energies (E_ion), and Electron Impact Dissociation Energy Thresholds ($E_diss, impact$) for the CH_4 and CO_2 molecules, all the variables in eV. . . . 94

Glossary

- BECCS: Bioenergy with Carbon dioxide Capture and Storage
- CTM: CO_2-to-Methanol
- DAC: Direct Air Capture
- DBD: Dielectric Barrier Discharge
- DFT: Density Functional Theory
- DME: Dimethyl Ether
- eV: electron Volt
- H_2-TPR: Temperature Programmed Reduction with H_2
- HTS: High Temperature Shift
- IPC: In-Plasma Catalysis
- IPCC: Intergovernmental Panel on Climate Change
- LNG: Liquified Natural Gas
- LTS: Low Temperature Shift
- MeOH: Methanol
- NASA: National Aeronautics Space Administration
- NTP: Non-Thermal Plasma
- PM: Particulate Matter
- PPC: Post-Plasma Catalysis
- PROX: Preferential Oxidation
- PtG: Power-to-Gas
- PtH: Power-to-Hydrogen
- PtM: Power-to-Methane
- PtDME: Power-to-DME
- RWGS: Reverse Water-Gas Shift
- SEI: Specific Energy Input
- SNG: Synthetic Natural Gas
- TEM: Transmission Electron Microscopy
- TGA: Thermogravimetric Analysis
- USY: Ultra-Stable Y Zeolite
- UV: Ultraviolet radiation
- VOC: Volatile Organic Compounds
- W: Watts
- WGSR: Water-Gas Shift Reaction
- XAFS: X-ray Absorption Fine Structure
- XRD: X-Ray Diffraction

1 Introduction

Climate change is, without a shadow of doubt, the most important challenge that humans will have to overcome, as a group, attaining for the best within themselves. For without any effort, it is estimated that an increase to the earth's average temperature of around 4.8°C is bound to occur up until the year 2100. [1]

As a way of reaching the desired environmental goals, the conventional methodologies to energy production should be substituted with their greener options, aiming for renewable, more efficient, and cleaner options which may attain and fulfil the economical, societal and ecological concerns of this issue.

This investigation presents itself therefore as a contribution towards the research of alternative methods for attaining economical and green energy supply, whilst also intending to get rid of the sector's main problem: carbon dioxide.

CO_2 methanation thus reveals itself as a promising renewable energy process, with a neutral carbon-footprint. This system thus takes carbon dioxide and, procuring to maximize its valorization, associates it with green hydrogen, and at a relatively low temperature and pressure, procures to convert it into methane, hence inserting it into the Power-to-Gas strategy.

This process has been thoroughly studied for supported metallic catalysts. From within all the referred supports used throughout the vast literature, two may be highlighted, which are alumina based catalysts and the zeolites, being that the latter usually present a higher stability.

It is within this scope that the current dissertation inserts itself: it intends to synthesize, characterize and test several series of catalysts, in order to obtain the best synergies and results for the studied reaction. The first part of this investigation pretended to research which interactions would be obtained between a series of transition metals (Ni, Fe, Co and Cu) and the CsUSY zeolite. The best within these catalysts was then taken and, on a second study, was added a small percentage (1% (wt/wt)) of a second metal, procuring for which metals would generate the best catalytic synergies. The third part of the study arose from the results of the second, and was meant to assess which would be the optimal content of the second metal added.

All of the developed samples were characterized through Thermogravimetric Analysis (TGA), X-Ray Diffraction (XRD), N_2 Adsorption Analysis, Temperature-Programmed Reduction with H_2 (TPR-H_2) and Transmission Electron Microscopy (TEM). In addition, catalytic tests were carried out for atmospheric pressure, and within a range of temperature from 200 to 450 °C, in order to ascertain the best conditions for each catalyst.

The current dissertation was organised according with the following fashion: *State of the Art*, where a context for the present work can be found; *Methods and Catalyst Preparation*, where the conditions for the catalyst's preparation and evaluation were presented; *Results and Discussion*, where the analysis of the results is carried out in a systematic way, separated for each study; *Conclusion*, where the main results to be taken out of the current study are presented, as well as some insightful suggestions towards further studies are made; and *Annexes*, where further and smaller investigations onto the theme were carried out, and are thus presented.

2 State of the Art

Carbon dioxide is the main component of greenhouse gases [2], and this man-made disruption of the carbon cycle can have catastrophic consequences towards the survival of both humanity and a large number of many other species, which may lead to a catastrophic reiteration of what was previously seen in the Permian–Triassic mass extinction [3].

According to the Intergovernmental Panel on Climate Change (IPCC) [4], the best mitigation scenarios involve a concentration of 450 ppm CO_2 eq. in 2100, but for that, the models rely on the availability and widespread deployment of bioenergy with carbon dioxide capture and storage (BECCS). As of July 5th of 2021, it is believed that carbon dioxide has a global average concentration of 418.45 ppm. [5] [1] And since humans keep producing about 51 billion tons of CO_2 eq. into the atmosphere per year [6], there isn't much hope of attaining this goal in the near future without any direct air capture (DAC) technology and further utilisation and/or deposition of said collected carbon.

It is hard to define the exact number for the cost of removing one ton of carbon from the air, however it has been established as at least 170 € [6]. Multiplying this value with the total amount of carbon emissions would result in a loss of 8.7 trillion € on a yearly basis. In other words, using the DAC system to solve the carbon problem would consume approximately 12.1% of the world's economy, with each passing year. Hence, at the current rate and processual cost, it would be quite impossible to perform.

According with the Global Carbon Budget for 2020 [7], in order to reach the 1.5 °C increase on global temperature, there's still a budget of CO_2 eq. emissions of 440 billion tonnes, which considering the amount currently produced (51 billion tonnes yearly [6]) would give humanity about 9 years until its attainment. This 1.5 °C increase is the same value stipulated as the limit by the Paris Agreement to 2050. [8] This limiting and dangerous value is therefore being attained approximately 20 years sooner than previously anticipated.

Since 1850 until 2018, the worldwide emissions of carbon dioxide have been steadily increasing until the current 37 bilion tonnes, [9] [6] as can be ascertained by figure 1. On the left, it is demonstrated how the carbon dioxide emissions have gone up since 1850. On the right it is shown how the global average temperature is rising along with emissions.

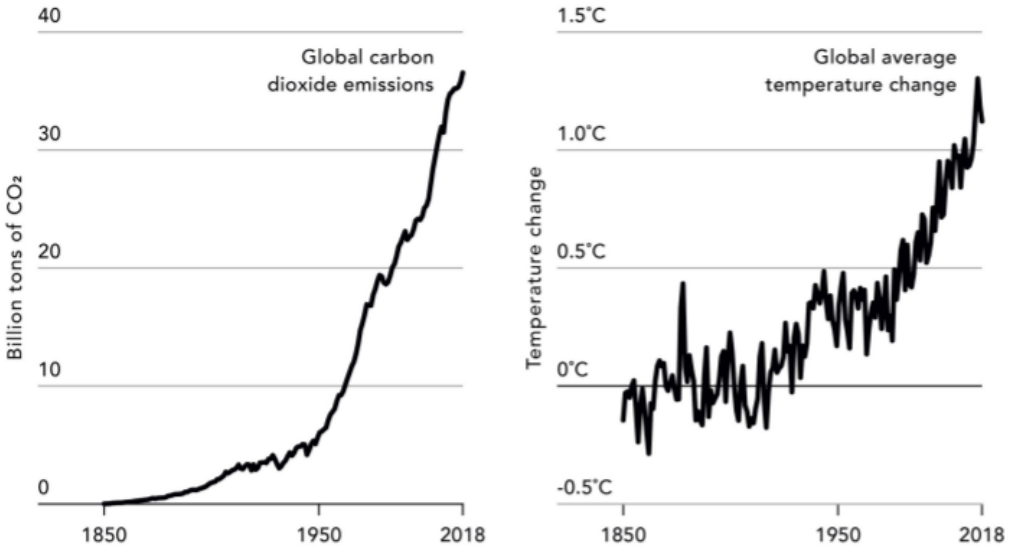

Figure 1: Carbon dioxide emissions (on the left), and the global average temperature (on the right) along the years These emissions solely represent CO_2 and not the remaining GHG (Global Carbon Budget 2019) [9].

[1] This value for current carbon dioxide present in the atmosphere represents an increase of 0.74% comparing with the value from the prior year. At the present rate of increase, it is expected to reach the 450 ppm stipulated by IPCC in less than 11 years.

2.1 Methanation as a Natural Gas production method

Although worrysome when released in the atmosphere, carbon dioxide could also be our saviour [2], by being a desired feedstock for a multitude of processes, from which many useful value-added chemicals can be made. [11] For that, these interesting reactions involve the conversion of CO_2 with a co-reactant acting as a hydrogen source (CH_4, H_2 or H_2O). There are essentially two pathways to achieve this: the indirect and the direct oxidative. In the former, the main product obtained is syngas, which can afterwards be converted to almost any commercial chemical or fuel, through methanol and/or Fischer-Tropsch synthesis, but usually associated to a high energetic cost. However, for the latter, the energy-intensive intermediate is eliminated, by converting the reactants directly into hydrocarbons (e.g. methane), short-chained olefins (e.g. ethylene, propylene) and oxygenated products (e.g. methanol, formaldehyde, dimethyl ether, formic acid). [12] Some examples of possible methods for the CO_2 transformation are methanation, methanolation, and the production of increasingly complex (and thus value-added) carbon-containing molecules. [13]

However, solely the production of methane doesn't allow for it's direct application as a fuel. In order for this to happen, certain criteria have to be met, such as molar composition, as shown in table 1. For that, an upgrading of the reactor's outlet current has to be performed, as shall be seen further on section 2.1.4. Nevertheless, it is feasible and profitable. Previous reports, such as Muller *et al.* [14], can attain for a 95% conversion of CO_2 towards methane in pilot-scale plants. And the first industrial-scale power-to-methane plant was developed by *ETOGAS* for *Audi AG* in Germany. [15]

Table 1: Molar composition of natural gas [16].

Natural gas	CH_4	Heavier hydrocarbons	CO_2	N_2	H_2S
% (mol)	85-92	9	0.2-1-5	0.3	1.1-5.9

Methanation, the conversion of carbon oxides into methane, is one of the most promising processes for the fixation of the carbon dioxide [17]. Methane is a potential-filled product, since it can be used either as a synthetic substitute for natural gas (SNG) [18], as a feedstock for steam reforming, or even as a source of energy in power plants, allowing for a global cycle between the CH_4 combustion and the CO_2 hydrogenation [19], as can be described by figure 2. For the present reasons, CO_2 emissions could thus not only be employed as cheap, but also as having a neutral cost carbon feedstock, this way counterbalancing the mismatch in renewable energy supply and demand. [11]

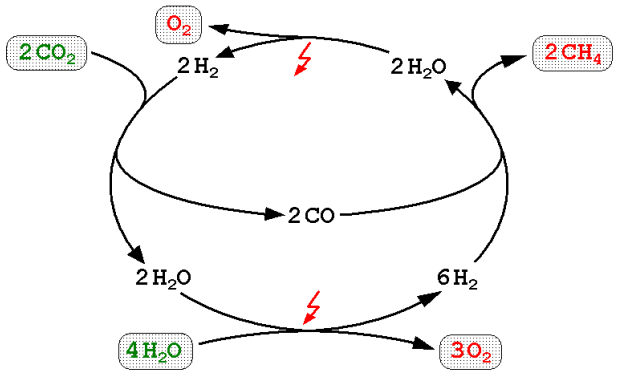

Figure 2: Carbon-cycle on a closed loop system.

In addition to this, natural gas production plants are the number one when it comes to efficiently using materials with a large carbon footprint, such as cement, steel and glass, as is shown in figure 3. That means that for each TWh of electricity produced, natural gas was the one which consumed the lesser resources that go into building and running the power plant. [6] Thus, and considering the similarity between a natural gas and SNG (through methanation) productions, if this were to be implemented on a large-scale, it could potentially solve all energetic problems at the smallest ecological cost.

[2] Upon performing a relatively simple calculation, in which one assumes that all released carbon can be captured and used towards the methanation process, it can be ascertained that this method could potentially supply 12.2 Billion people with their annual per capita energy consumption (considering values referring to 2019) [10], which corresponds to supplying 159% of the energy the world currently needs. These values do not take into account the amount of energy necessary for the process in case.

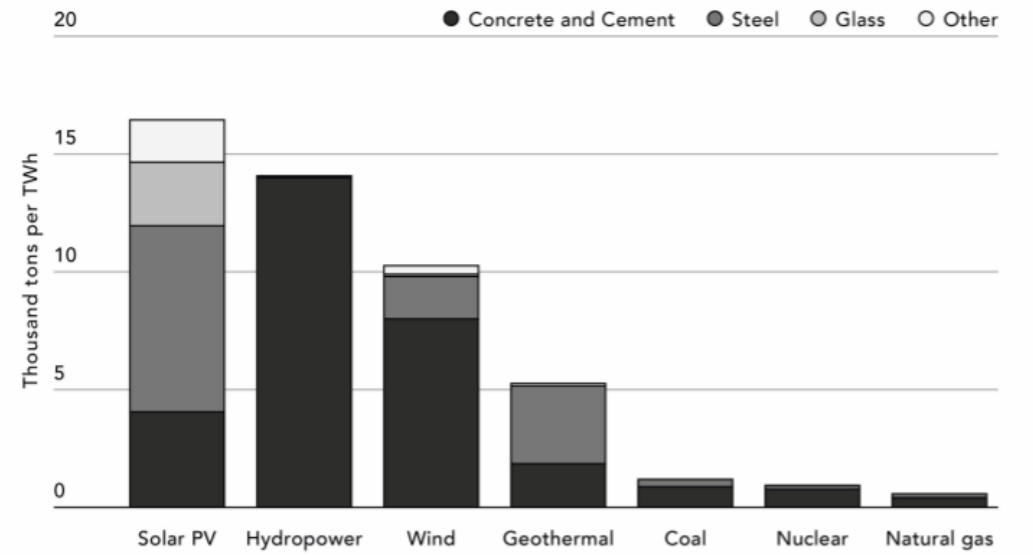

Figure 3: Amount of different polluting materials (in thousand of tons per TWh) needed for a construction of each type of energetic plant, per unit of eletricity generated. [6]

A further study on the alternative uses for CO_2 methanation reaction can be found in Annex 7, section 7.7 of the present report.

2.1.1 Hydrogen

In recent times, progress has been made in hydrogen production technologies, through water electrolysis, which has raised the likeness of the utilization of the methanation process [20], since the lack of a renewable, reliable and inexpensive hydrogen source has widely been accused of being the main impediment.

Hydrogen has mainly four sources: natural gas, oil, coal and electrolysis, which account for 48%, 30%, 18% and 4% of the world's hydrogen production, respectively [21] [22]. The main hydrogen production processes correspond to water electrolysis, steam/catalytic reforming, natural gas/coal gasification and oxidation of methane. [23] [22] Besides electrolysis, there are also some other possible renewable methods for hydrogen production including biomass fermentation, renewable liquid reforming (e.g. ethanol), and photoelectrochemical water splitting, although these methods aren't ready for a big scale deployment yet. [24]

The main renewable method (water electrolysis) is a more energy intensive process, yet it can be performed with profit when using renewable energy. [25] Recently, Denmark has announced that it was going to build an 'energy island' which intends to use wind energy to perform the water electrolysis reaction, therefore producing hydrogen, which is expected to power all of Denmark's electrical needs and even supply energy for neighboring countries. [26]

Although hydrogen is a powerful fuel on itself, technical issues arise when it comes to its high-scale production, storage and utilisation. These include a lack of efficient engine technology that can run safely on hydrogen, safety concerns due to its high reactivity with oxygen, and also the difficulty of developing long-term storage, pipeline and engine equipment. [25] For this reason, its conversion to ammonia, methanol and methane is preferred. [11]

2.1.2 Power-to-Gas

Due to the expansion of the hydrogen production, it results thereafter the recent uprise of Power-to-Gas (PtG) technologies, which intends to transform the hydrogen power obtained from renewable sources into a high-energy density gaseous fuel. [27] [28] The process starts with the production of H_2 through water electrolysis, which then leads to the reaction of that produced hydrogen with carbon dioxide, producing methane, through the Sabatier equation, which can be observed in section 2.2.3.

Due to its renewable origin and its carbon neutral process, PtG has been widely appointed as an option for the transport sector to comply with the targets of the energy transition, since it offers a substantial greenhouse

gas reduction. [27] In addition to PtG, this green hydrogen can be used in a range of pathways that promise to alleviate energy generation from electricity demand, whilst assisting in reducing energetic surpluses by supplying a better method of energetic storage. [29] An illustration of all these processes described can be observed in figure 4.

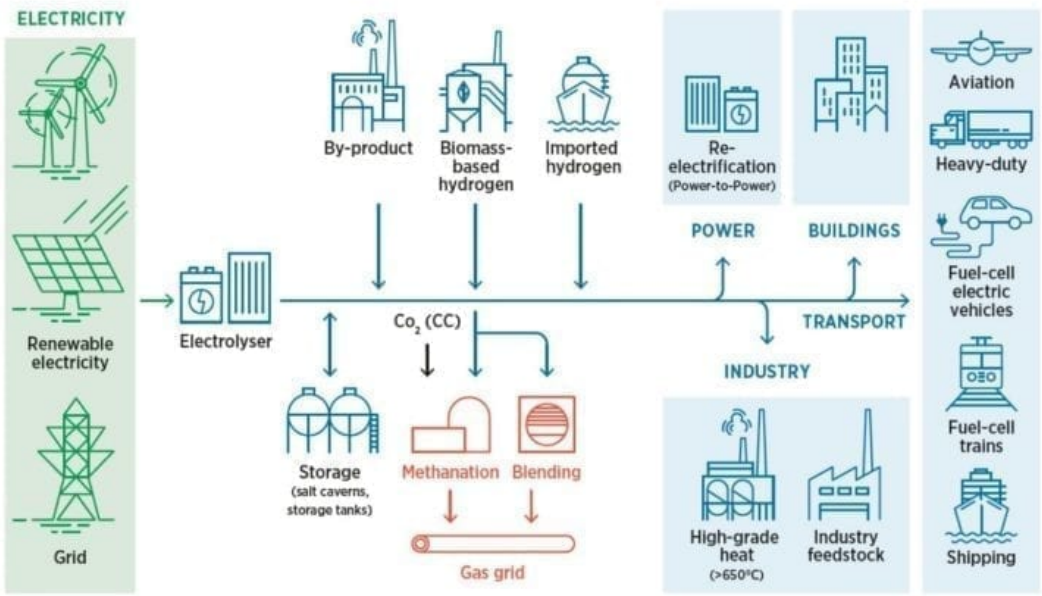

Figure 4: Power-to-Gas strategy connects the electrical and the natural gas grids, allowing for the renewable storage of energy in the form of synthetic natural gas, as well as many possible uses even beyond the energy sector. [29]

As previously referred, the application of this PtG approach into the SNG production has potential for playing a major role in resolving the issues involving energy storage, especially by increasing its capacity and its durability. As an illustration of it, figure 5 [30] represents a diagram comparing different storage technologies, for the discharge time as a function of its storage capacity. As depicted, SNG is the most capable fuel presented for both characteristics compared, making it a long-lasting and high-capacity energy storage method. [30]

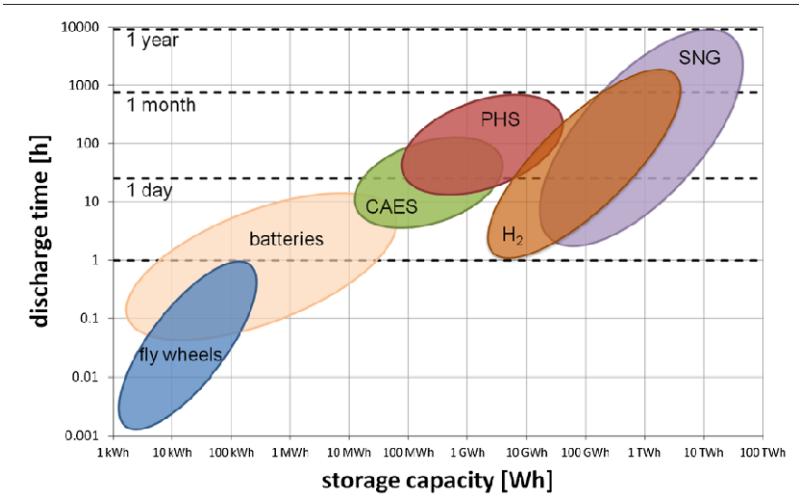

Figure 5: Illustrated comparison charge/discharge period and storage capacity of different electricity storage systems. CAES: compressed air energy storage; PHS: pumped hydro storage. [30]

In 2019, there was a record of already existing 143 Power-to-Gas projects, aiming to produce hydrogen and/or methane, in a total of 22 countries. [29] Being one of the most renowned, the "STOREGO" is a project funded by the European Union's "Horizon 2020 research and Innovation programme", which comprises a

partnership between 27 organizations and companies from all over Europe, all invested in the research, development and widespread of PtG technologies. [31] A further study on where it could be an interesting location for a novel CO_2 methanation industry and why can be found in Annex 5, section 7.5 of the present report.

2.1.3 Pre-treatment

The cleaning of the gases is an important part inherent to this process. Depending on which process this carbon dioxide originates from, their respective detrimental compounds can be quite different. For biogas, the main impurities in the feed current that require pre-treatment are H_2S, HCl, NOx and NH_3, which would poison any Ni-based catalyst. [32] Whilst for the cement industries, the main problem concerns the separation of CO_2 from oxygen.

In petrochemical industries, **hydrogen sulphide** is most commonly removed through the Claus Process, which consists on the conversion to elementary sulphur [33], however it is also possible to perform it with eletrochemical membranes [34], or through adsorption with a polar adsorbent surface (and the absorbents are usually natural or synthetic zeolites, activated carbons, and metal oxides) [35].

Ammonia can be removed through catalytic destruction, or through ammonia scrubbing, either in addition to water or sulfuric acid, resulting in ammonium sulfate, which can be further collected and sold, as it has commercial value as a fertilizer. [32]

Hydrogen chloride should be easily removed through filtration or by water wash cleaning units. [36]

In addiction to the cleaning needed previously to the reactor, it needs an upgrading afterwards too.

2.1.4 Separation of CO_2 and CH_4

An issue inherent to this process has to do with the separation of the unconverted CO_2 from CH_4, in order to upgrade methane into SNG. Luckily, there are already some technologies in use developed by the natural gas industry intended for the removal of CO_2. The main ones being the organic scrubbing, the water scrubbing, the chemical absorption, the pressure swing adsorption, the cryogenic separation and the membrane separation [37] [38].

From all these referred technologies available, **water scrubbing** is the simplest and cheapest process, yet well developed towards the removal of CO_2 and H_2S from natural gas. However, **chemical absorption** is the most extensively used for CO_2 removal, wherein an amine aqueous solution reacts and absorbs acid gases (mainly CO_2 and H_2S) [38]. Although it is the most used process, it still arises some issues, since it has a high energy consumption, leads to corrosion and exposure to foaming.

Membranes have, quite recently, been appointed as a promising technology meant to overcome these drawbacks. [39] Separation through membranes operates based on the concentration gradient of the absorbent through the membrane. Smaller molecules such as H_2, CO_2 and H_2S have a higher permeation rate, which allows for a better separation from CH_4. The efficiency of the process in question will however depend on which membrane is chosen, and often the losses of methane can be relatively high. In addition, membranes have yet a relatively high price, and a short life cycle. [40]

2.2 Reactional Mechanism

There are essentially three pathways for the activation of CO_2 and consequential conversion into methane, when working at thermal catalysis conditions. These reactional pathways can be observed in the Figure 6. [41] [42] All of these pathways were observed in experimental testing while using a Ni catalyst [42] [43], however the carboxylate pathway appears to be mainly obtained through catalysts such as Cu and Fe. [44] [41]

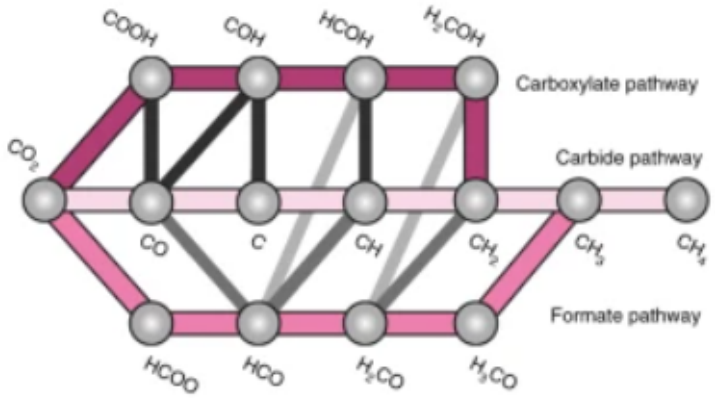

Figure 6: Schematic of all possible reactional pathways for the carbon dioxide methanation, in pink. All intermediates are represented by the gray dots. The gray lines represent plausible links between the primary pathways. [41]

This schematic representation (figure 6) does not consider the stability of each intermediate, so it could be misleading. Hence a further reading on the activation energies for each respective reaction step is necessary.

Ussa Aldana *et al.* [43] performed a study on CO_2 methanation using Ni-based ceria-zirconia catalysts, obtaining a better catalytic activity when compared with Ni-silica, which can be explained by the importance of weak basic sites for the adsorption of CO_2. In addition, through operando FTIR spectroscopy, it was first discovered that the main mechanism for thermal CO_2 methanation didn't involve nor require the formation of a CO intermediate. This research resulted in the mechanism described in figure 7, which resulted in the discovery of the carboxylate pathway.

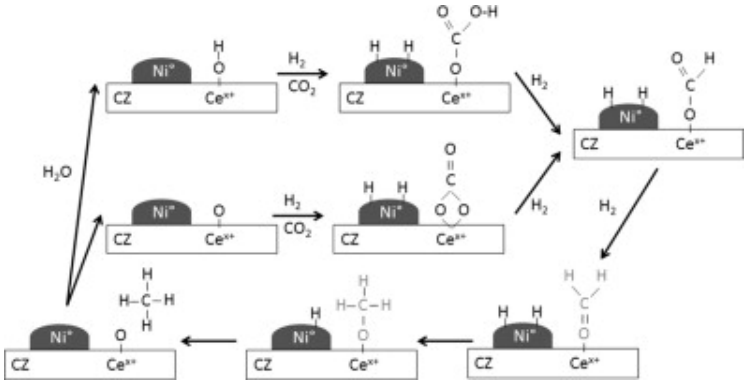

Figure 7: Representative mechanism for thermal methanation of CO_2 over a Ni-based ceria-zirconia catalyst. [43]

For most catalysts, the rate-determining step for the process corresponds to the CO_2 activation [45] [46], as described in equation 1, which consists of the chemisorption of CO_2 and in the electron transfer from the catalyst to the CO_2 [47] [48]. Through Density Functional Theory (DFT), it can be perceived that the CO_2 activation occurs through the electron transfer between different orbitals. [49]

Afterwards, hydrogen acts as an electron donor/reducing agent that is oxidized into water, whilst carbon dioxide, on the other hand, is reduced into methane. [28]

In addition, oxygen vacancies on metal oxide surfaces and Lewis acid sites have been shown to enhance CO_2 activation [50] [51], stabilize intermediates [52] and reduce sintering [53].

Albeit it being plentiful, that previous knowledge was all obtained for thermal catalysis. Hence, there was no certainty whether such pathways would be followed in non-conventional catalysis, such as plasma-assisted catalysis. For that, Azzolina-Jury and Thibault-Starzyk [54] performed a study on CO_2 methanation under glow discharge plasma conditions at low pressure over a Ni/USY zeolite catalyst. The authors then proposed a mechanism in which CO_2 molecules were excited by the plasma, dissociated into CO in the gas phase and adsorbed on the metal Ni species of the catalyst as monodentate formates, which were later transformed into linear carbonyls under plasma assistance. Afterwards, carbonyls were reported to be hydrogenated, forming CH species on the nickel substrate, and later converting into CH_4. Such mechanism can be observed in figure 8. And upon comparing with figure 6, it is possible to affirm that this mechanism proposed by the authors follows the carbide pathway.

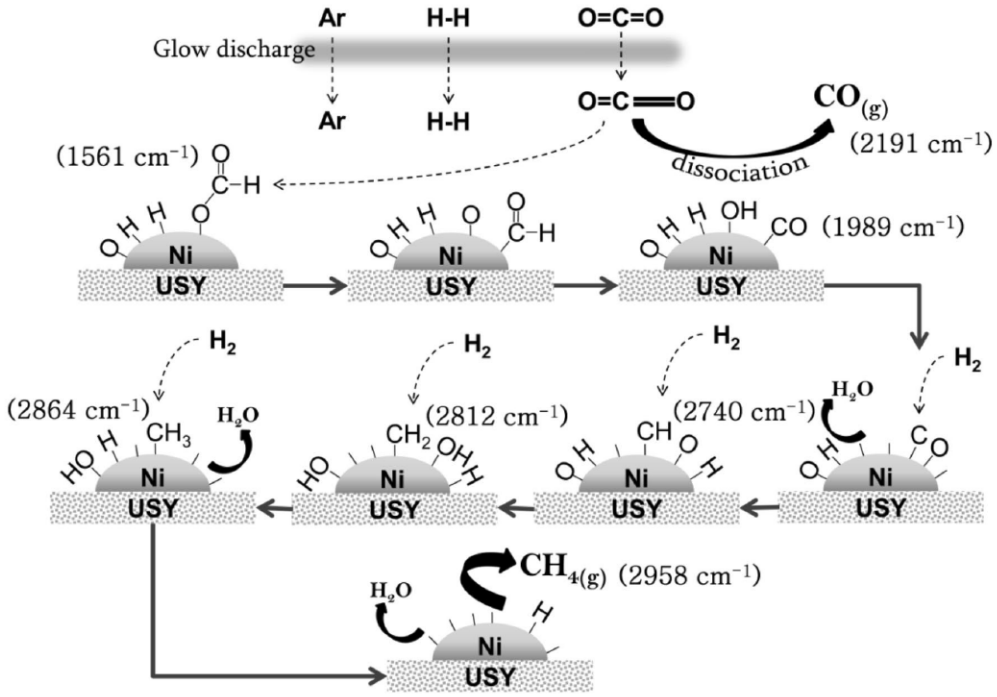

Figure 8: Representative mechanism for plasma-assisted carbon dioxide hydrogenation over a Ni/USY zeolite.

But yet, a series of questions remain unanswered. Is this the single mechanism occurring in the vast amount of reactive species within plasma? What percentage of importance has each mechanism? What is the relation between the catalyst and each specific mechanism? What influences the way each mechanism prevails? Not only are the answers to these questions unknown for plasma catalysis, but also for thermal catalysis. A thorough investigation into the mechanisms of this reaction could prove fruitful, since its study could provide a deep understanding on the reaction, allowing for a better prediction on which catalysts and physicochemical conditions should be used, instead of the trial and error method that has prevailed in the current field.

In addition to that, the intended process has a set of secondary reactions competing with it. Some of those are CO methanation, Boudouard reaction, reverse water-gas shift reaction, methane cracking, inverse methane CO_2 reforming, and both CO_2 and CO reduction [55] [56], which can therefore modify the products selectivity.

2.2.1 Pure CO_2 Splitting

As described previously, for one of the pathways (carbide), this reaction is needed to obtain the product. Thermal CO_2 splitting isn't very effective, which should already be expected, since CO_2 is a very stable molecule, with a strong carbon-oxygen bond (of 783 kJ/mol) and a Gibbs free energy of formation (ΔG^o =

-394 kJ/mol), requiring a substantial energy supply for any conversion to take place. [12]

$$CO_2 \rightarrow CO + \frac{1}{2}O_2 \tag{1}$$

However, the elevated value of enthalpy for this dissociation (ΔH^o=+283 kJ/mol) doesn't necessarily mean its conversion is not feasible. This is the most difficult step of the intended process, yet with the assistance of plasma and/or catalysts, it can become easier.

There's also an interesting relationship between this reaction's conversion (since it's the limiting step), and the energy efficiency obtained as a function of the temperature, as can be ascertained by the figure 9. [12]

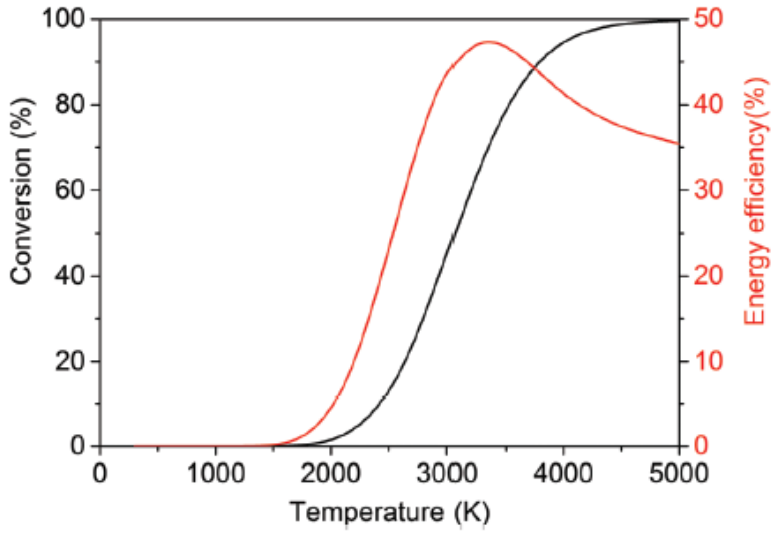

Figure 9: Calculated theoretical thermal conversion (left axis) and corresponding energy efficiency (right axis) as a function of temperature for the pure splitting of CO_2 into CO and O_2.

For thermal conversion, without the removal of one of the products of this dissociation (i.e. CO or O_2), the equilibrium of this single reaction will always tend towards the left. Only at relatively high temperatures would this reaction be feasible, thus becoming energetically inefficient. [12]

2.2.2 CO_2 Hydrogenation

There are multiple possible hydrogenation reactions for CO_2. These depend essentially on the ratio of molecules of H_2 reacting with the CO_2, as can be seen by the equation 2 (for one molecule of H_2), equation 4 (for three hydrogen molecules) and equation 3 (for four).

$$CO_2 + H_2 \rightarrow CO + H_2O \tag{2}$$

This reaction (shown in equation 2) is equal to the reverse water-gas shift reaction, and has a positive enthalpy (ΔH^o=+40.9 kJ/mol). [57]

While CO_2 hydrogenation appears a challenging reaction, due to the high stability of CO_2, considerable progress has been made towards converting carbon dioxide to single carbon products (e.g., carbon monoxide, methane, methanol, and even formic acid [58]) through direct hydrogen reduction or hydrothermal-chemical reduction in water. [59] [60] [61] [62]

2.2.3 Methanation of CO_2

The most important equation to the current thesis corresponds to the methanation of CO_2 (also known as the Sabatier reaction), in which carbon dioxide reacts with hydrogen, forming methane, as can be observed accordingly with equation 3. [17] [63] CO_2 methanation remains the most advantageous reaction with respect

to thermodynamics (ΔH^o=-165.3 kJ/mol), and since the reaction is considerably faster than other reactions which form hydrocarbons or alcohols. [64]

$$CO_2 + 4H_2 \rightarrow CH_4 + 2H_2O \tag{3}$$

However, due to the high oxidation of the carbon, its reduction consists of an eight-electron process, which significantly limits the reaction kinetics and requires a catalyst with high rates and selectivities. [12] [17]

The process has been widely studied, and CO_2 conversions higher than 95%, and CH_4 selectivities frequently reaching the 100% at temperatures around 420 °C have already been achieved and spread through industrial production. However, at industrial scale, this process can only become viable when the H_2 is produced from renewable energy and the CO_2 comes from cheap accessible waste streams. [17] [65]

Two different routes for CO_2 methanation have been discovered. The first one considers CO as intermediate formed by dissociation of CO_2 into CO. CO is then dissociated into C and O atoms on the active sites and further hydrogenated into methane by dissociated H_2 on the metal particles. The second route does not consider CO as intermediate and CO_2 is directly hydrogenated into methane via carbonates/formates [55]. But these routes tend to vary accordingly with the different catalysts used, so a prediction of which pathway is going to undergo is difficult.

2.2.4 CO_2 Hydrogenation to Methanol

Methanol's production reaction through CO_2 hydrogenation needs to involve the coupling of CO_2 into a bifunctional catalyst. In this reaction, the CO_2 and H_2 are converted to CH_3OH over a partially reduced oxide surface (e.g., Cu, In, and Zn) or noble metals via a CO or formate pathway, as can be observed in the figure 10. [66]

$$CO_2 + 3H_2 \rightarrow CH_3OH + H_2O \tag{4}$$

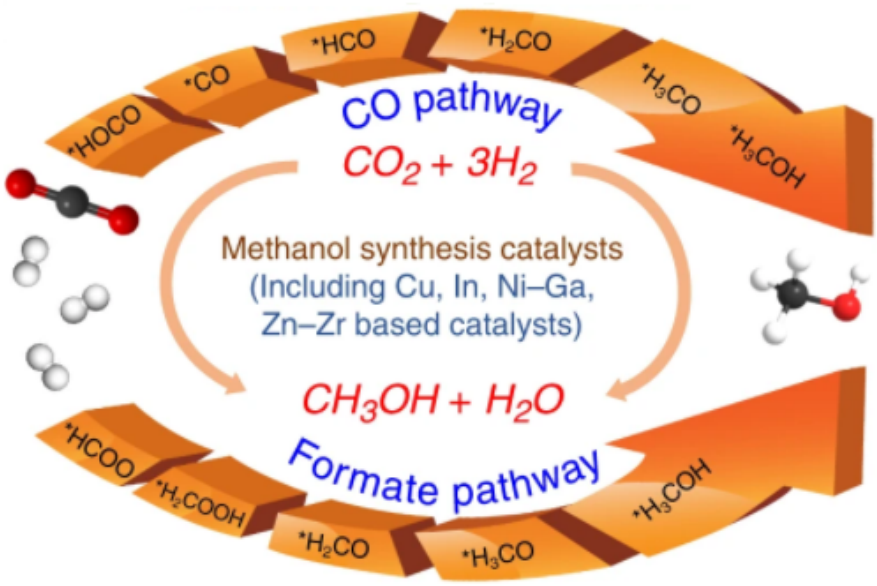

Figure 10: Possible reaction pathways for CO_2 conversion to methanol.

CH_3OH synthesis from CO_2 hydrogenation is overall exothermic (ΔH^o=-49.9 kJ/mol), however, the rate-determining step, which is the activation of CO_2 (as described in equation 2), has a positive enthalpy, for which CO_2 and H_2 will only react under high temperatures and multicomponent heterogeneous catalysts. [12] [67]

It has been show that the addition of promoters such as K, La, Pd, Ga and Ba can improve the adsorption strength of CO_2, stabilize surface intermediates and enhance CH_3OH selectivity. [68] [69]

The selective hydrogenation of CO_2 into methanol is a process that is currently operated on industrial scale. Although, this industrial production usually relies on syngas on a 3 to 1 ratio, while CO_2 is added to deal with the excess H_2 in the feed, and the produced water is recycled via the WGSR. [12]

A further study on which catalysts would be beneficial for this reaction can be found in Annex 8, section 7.8 of the present report.

2.2.5 DME Synthesis from Methanol

Dimethyl ether can be obtained through the reaction of methanol dehydrogenation, as can be seen by equation 5. In this reaction, methanol is dehydrated or coupled over zeolites or alumina. [70]

$$2CH_3OH \rightarrow CH_3OCH_3 + H_2O \tag{5}$$

DME synthesis reaction is developed industrially around 250 °C, and has to be controlled before it reaches 400 °C, since the catalyst begins to deactivate at around this temperature. DME can be used as an additive to natural gas, up to 20% (v/v), as an aerosol propeller, and as an additive or substituent for diesel. [70]

2.2.6 Methanol Conversion to C_2+ hydrocarbons

Other equations can be observed, from methanol into hydrocarbons with multiple possible number of carbons, as can be seen by equations 6 and 7.

$$nCH_3OH + H_2 \rightarrow CH_3(CH_2)_{n-2}CH_3 + nH_2O \tag{6}$$

$$nCH_3OH \rightarrow CH_2CH(CH_2)_{n-3}CH_3 + nH_2O \tag{7}$$

Accordingly, bifunctional or hybrid catalysts are composed of a CH_3OH synthesis catalyst and a CH_3OH dehydration/coupling catalyst, which can convert CO_2 into high-value C^{2+} compounds, including DME, hydrocarbons like gasoline, and light olefins. An efficient catalyst for these high-value C^{2+} products should be active for both CH_3OH synthesis and dehydration/coupling under the same conditions.

2.2.7 WGSR/PROX

The Water-Gas Shift Reaction (WGSR) can also be known as the Preferential Oxidation (PROX), and refers to the oxidation of carbon monoxide in a gas mixture, performed under a catalyst. This reaction can be observed in equation 8.

This is an important reaction for this process, since, in its reverse form, it could be an additional conversion mechanism for CO_2, facilitating the most difficult step, by performing the first step of the carbide pathway, shown in figure 6. Although, there is a predicament, since it unnecessarily consumes H_2, which is the most valuable of the reactants used.

$$CO + H_2O \rightleftharpoons H_2 + CO_2 \tag{8}$$

The ideal catalyst for this reaction involves a metal (such as platinum, platinum/iron, platinum/ruthenium, gold nanoparticles) placed upon a ceramic support. [71]

It is currently mainly used in fuel cells, in carbon monoxide removal steps in other processes, and in the production of ammonia, hydrocarbons, methanol and hydrogen.

The mechanism for this reaction can be observed in the figure 11.

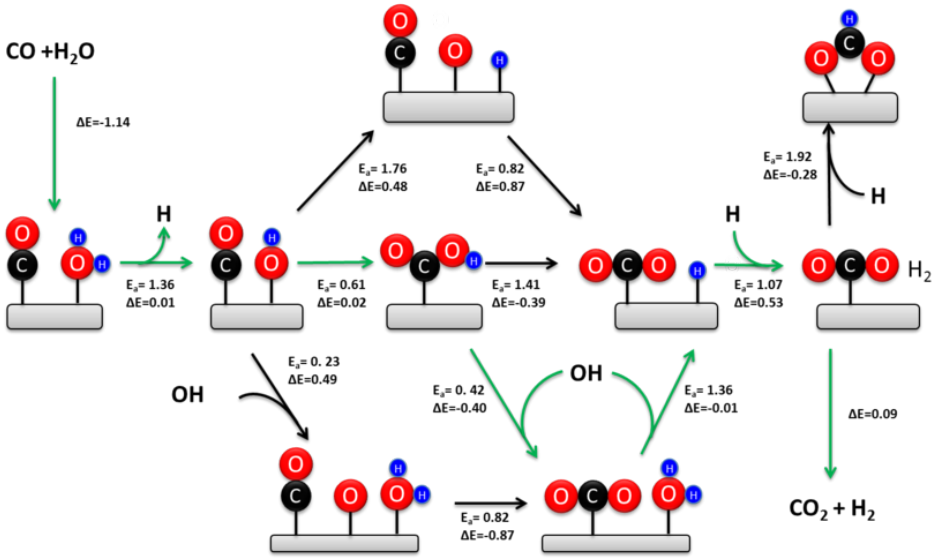

Figure 11: Water gas shift reaction mechanism [72]

Normally, under the conditions used (atmospheric pressure and low temperature), the reverse water-gas shift reaction has been found to be dominant, whilst in the plasma CO_2 hydrogenation process. [73]

2.2.8 Thermodynamics of the Sabatier Reaction

As for the most important reaction for the process considered, it is important to also evaluate its thermodynamics, in order to better understand the conditions needed to upgrade its process. And for that, a series of variables was analysed, and the best conditions procured.

- **Pressure**: According with McBride *et al.* [74], when there is an increase in pressure, the range of highly reactional temperature also increases, hence higher conversions can be obtained for higher temperatures, as can be seen by figure 12. A similar phenomenon occurred for CH_4 selectivity. [75]

- **Temperature**: Considering this is an exothermic reaction, it is favored at relatively low temperatures (between 250 and 450 °C). The viable temperature range enlarges with the pressure increase. However, with the further increase of temperature, the reverse water gas shift reaction is favourable, thus dropping CH_4 selectivity. [75]

- H_2/CO_2 **ratio**: CO_2 conversion and CH_4 selectivity are highly affected by this ratio. For lower than stoichiometric ratios (H_2/CO_2 « 4), a significant formation of carbon deposits is expected [74]. Whilst higher ratios (H_2/CO_2 » 4), are usually beneficial for the conversion of CO_2, due to the Le Chatelier Principle and also for the suppression of carbon depositions. [75] However, H_2 is the most costly burden of the process, hence it wouldn't be feasible to increase it significantly unless a cheap and green supply of hydrogen could be arranged.

- **Steam**: Steam and any other form of water added in the feeding stream reduces the conversion of CO_2, since it will act as an inhibitor, due to being one of the reactions products. However, Gao *et al.* [75] proved that adding steam into the reactants feed could help avoid carbon formation to a large extent on the surface of the catalysts.

- **Oxygen**: Trace amounts of oxygen in the feedstock would be practically impossible to avoid. Gao *et al.* [75] proved that its presence is detrimental to the CO_2 conversion, mainly due to the existence of side reactions of oxygen with hydrogen, specially for higher temperatures. Thus, the removal of any trace amounts of oxygen prior to the reaction could be beneficial to its yield.

- **Methane**: Similarly to what happens when water is added to the feedstream, the addition of methane can lead to a reduction of the CO_2 conversion, due to the Le Chatelier Principle. In addition, a higher amount of carbon deposition was found with the addition of methane to the feed. [75]

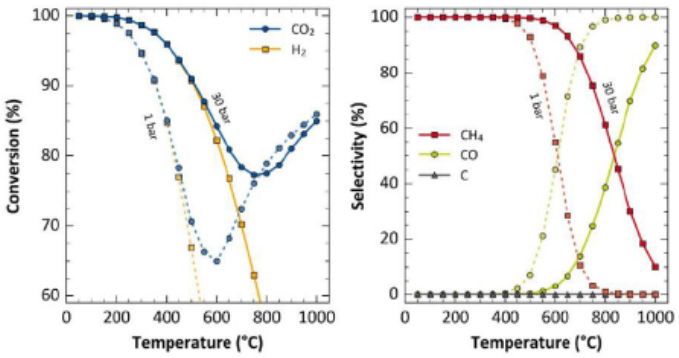

Figure 12: Results obtained by McBride *et al.* [113] for an increase of pressure and temperature, for a) CO_2 conversion, and b) CH_4 selectivity.

Succinctly, solely based on the thermodynamics point of view, the CO_2 methanation reaction should be carried out under relatively low temperature (<450 °C), to a relatively low pressure, however higher than atmospheric, and with a feed ratio where H_2/CO_2 is a little over 4. In addition, on the feed stream, any content of methane, oxygen and steam should be removed or eliminated previously to the reaction, since they can be responsible for losses in activity.

Envisioning the efficient implementation of an operating reactional process, a good cooling system should be implemented, which is needed due to the highly exothermic reaction considered, as a method of keeping temperature at stable and relatively low levels.

A further study onto the thermodynamics of the current process was developed through the simulation program ASPEN Plus V11, which can be found in Annex 6, section 7.6 of the present report.

2.3 Thermal Catalysis

Thermal methanation is possible because CH_4 is thermodynamically favoured over other CO_2 hydrogenation products, such as CO, for low temperatures (below 550 °C), and such as CH_3OH, for a ratio of H_2/CO_2 of 4 [77]. Hence, as CH_4 yields reach its peak at relatively low temperatures (300 to 400 °C) [78], this is a relatively straightforward process, as was previously seen in section 2.2.

Thermal CO_2 hydrogenation has been studied by many researchers, over a wide range of supports, which are important for the active phase dispersion, activity and stability [54]. The main supports studied are Al_2O_3 [17] [73] [79] [80] [81], SiO_2 [82], TiO_2 [82], ZrO_2 [80] $Ce-Zr$ mixed oxides [43], and more recently zeolites have been getting a lot of attention [19] [83], since Ni-doped ultra-stable faujasites (USY) have been reported to present higher stability, while maintaining the thermal catalytic activity.

In addition, the activity and performance of a catalyst can be further improved via modification of the support. Whether through addition on the lattice of the metal oxide support, or through the formation of a segregated metal oxide phase which is supported on the surface of the support, it can lead to an increase in the basicity of the support, which would lead to an acceleration of the CO_2 adsorption step. [77] [84] With this interest in mind, a study onto an addition of cesium (as a compensating cation) into the USY support was previously performed, and came to the conclusion that its addition is beneficial, as shall be further explained in section 2.5.1.

And when it comes to the active metals used, a lot of them have been adopted as catalysts for thermal CO_2 hydrogenation, obtaining specially interesting results for both noble and transition metals. [77] The choice of which of these metals catalysts to use can significantly affect the product distribution of the intended reaction. According with research previously developed, Ni [81] [19] and Ru [85] catalysts result in higher productions of CH_4, while Pd, Pt [82], Mn [73], Rh, Mo and Au catalysts favor CH_4, CO and CH_3OH productions, whilst Cu [73] can even focus on the formation of CH_4, C_2H_6 and C_3H_8. Nickel has been the most studied catalyst for this reaction, and has been reported as the most interesting one, due to its high activity and low cost.

Currently, thermal CO_2 methanation is already an industrial process achieving high conversions of CO_2 and CH_4 yields. However, there is yet still a need to optimize this process (decrease agressive reaction conditions, increase catalyst's activity, selectivity and stability), in order to maximize the rentability and widespread availability of the process. This method could be optimized mainly through investigation towards a better synergy between catalyst and conditions used for thermal catalysis, but also through the development

and research of plasma technology. [86]

Although thermal CO_2 methanation is the main focus of study for this process, there are also other possible methods. Such is the case for Plasma Catalysis, which can is explored further in Annex 9, in section 7.9. And other possible and more experimental processes can also be found in Annex 4, section 7.4 of the present report.

2.3.1 Active Metals

The catalysts most commonly used for the carbon dioxide methanation process are supported metals. [87] On this type of catalysts, the active metals can be found dispersed on the support corresponding to a variable dimension crystallite-form. This form and dispersion depend on the nature and the size of the metal, as well as the preparation method of the catalyst. [88]

Le *et al.* [89] developed a study on the activity of multiple metals for the CO_2 methanation reaction, arriving to the conclusion that the metals activity is organized according with the following order: Ru > Fe > Ni > Co > Rh > Pd > Pt. These are all transition and noble metals, which have proven highly active, and widely used for oxide supports.

The most used and widely-studied metal is nickel. This is due to its high activity, selectivity towards methane and its low cost. [81] [19] Despite being one of the most used metals, there are still many issues related with nickel usage on catalysts, such as sintering, reoxidation and carbon deposition. [87]

However, ruthenium (Ru) has proven a strong competition, being highly stable and active. In addition, it also presents a high selectivity towards methane and a great resistance to oxidizing atmospheres, thus preventing the catalysts' deactivation. Considering all this, nickel is still usually preferred, since it is quite cheaper than ruthenium. [90] [87]

For iron (Fe), although its monometallic catalysts have proven a low activity and a low selectivity towards methane, their bimetallic catalysts have revealed quite remarkable results, as shall be seen further in section 2.3.3. Cobalt, in opposition, can have a relatively high activity on its own, as well as a great selectivity towards methane. However, when associated with nickel-based catalysts, it doesn't create clear synergies with it, and possesses an inferior activity than nickel itself, as shall be seen in section 4.3.5.

As was previously stated, palladium (Pd) and platinum (Pt) are also frequently used for the CO_2 methanation process, however have been widely appointed as having a higher selectivity for carbon monoxide. [82] [91]

2.3.2 Monometallic vs Bimetallic catalysts

Monometallic catalysts are defined by the presence of solely one metal element associated with its support. In oposition, bimetallic possess two metals. Nickel is acknowledged as the best metallic promoter used for this process, not just in terms of activity, but also due to its low cost and high natural abundance. [77] However, some issues arise when using Ni-based catalysts, such as insufficient low-temperature activity, low dispersion and reducibility, as well as nanoparticle sintering. Luckily, some of these issues can be fixed by the addition of a second metal element into the Ni-based catalyst. The connection of those different metals can result in a number of synergetic effects, usually increasing performance, stability and diminishing costs.

Regarding which metals could result in the best synergy with Ni have been profusely investigated. These metals may include transition metal additives, such as V, Cr, Mn, Fe, Co, Y and Zr, in which Zr and Y are mostly used as dopants to modify the lattice of the metal oxide support.

2.3.3 Promotion of Ni-based catalysts with Fe, Co and Cu

Fe and Co, when combined with Ni-based catalysts, allow for the formation of alloys, which will directly disrupt nickel's electronic properties [92], and that can either lead to an increase in activity/stability, or result in a catalyst deactivation, depending on the ratio of metal intermixing used. [93]

Fe is, by far, the most studied metal when associated with Ni. This is due to its low price, high availability and its high solubility in the Ni lattice, facilitating the NiFe alloy formation. [94] According with Kang *et al.* [95] the optimal ratio for these metals should be 70% Ni and 30% Fe, whilst Sehested *et al.* [96] obtained an optimal percentage of 77% for Ni.

Co is also a commonly used promoter for Ni-based catalysts, since Co can easily dissolve into the lattice of Ni, and possesses easy transitions between oxidation states, which induce modifications in the electronic properties of the catalyst. [97] And according with Guo *et al.* [98], the optimal ratio of Co/Ni corresponds to 0.4.

The addition of Cu can be a tad difficult to defend as beneficial. When this metal is singularly used as a catalyst for this reaction, a relatively high selectivity towards methanol is observed [99]. When it's in addition to Ni-based catalysts, sometimes the CO_2 methanation reaction is inhibited, giving preference to the RWGS reaction [100]. And sometimes, Cu can increase the selectivity of other carbon based compounds, such as C_2H_6 and C_3H_8 [73], which could be highly beneficial for the fuel gases production. Although, for methane selectivity, it usually obtains a lower one than that of just Ni-based catalysts. [73] However, in some cases, as proven by Summa *et al.* [101], Cu as a promoter is beneficial. Using a hydrotalcite-derived catalyst promoted with 15 wt% Ni and 1.3 wt% Cu, a high selectivity (above 98%) and conversion (up to 86%) was obtained at 350 °C. In addition, it could also be stated that the promotion with Cu can strongly increase the number of basic sites, especially those with medium strength. The total number of basic sites is the highest in the sample containing 1% of Cu.

Ren *et al.* [73] performed a relatively similar study to the current, where a series of transition metals were added to a 30%Ni/USY catalyst and some interesting conclusions could be drawn. First, only Ni-Fe obtained a better selectivity towards methane than the 30% Ni monometallic catalyst, whilst both Ni-Fe and Ni-Co obtained a better conversion than solely Ni. Ni-Cu was the catalyst leading to lower performances, although obtaining relatively high selectivities for higher hydrocarbons at low temperatures. A study where which Fe loading would be optimal was the focus (3, 5 or 7 %), and thus concluded that 3% was the best ratio both for CO_2 conversion, and CH_4 selectivity.

A summary for some of the best results obtained for these three promoters can be observed in table 2.

Table 2: A selection of the best results found in the literature, obtained for three promoters (Fe, Co and Cu) for Ni-based catalysts.

Promoter (in addition to Ni)	Catalyst Composition	Preparation Method	Conditions Used	Best Performance Obtained	Ref.
Fe	17% Ni_3Fe $/Al_2O_3$	Urea deposition-precipitation	WHSV=60 000 $ml\_\{CO_2\}\ g^{-1}$ H_2/CO_2=4	χ_{CO_2}=78% S_{CH_4}=99.5% (350 °C)	[102]
Fe	15 wt% Ni and 1 wt% Fe $/ZrO_2 - 5 - V$	Incipient wetness coimpregnation	H_2/CO_2=4	χ_{CO_2}= +/- 82% S_{CH_4}=96% (500 °C)	[103]
Fe	30% Ni and 3% Fe $/ZrO_2$	Wet impregnation	GHSV=10 000 h^{-1} H_2/CO_2=4 P=0.5Mpa	χ_{CO_2}=82 S_{CH_4}=90 (230 °C)	[73]
Fe	15% Ni and 5% Fe /surface modified activated carbon	Incipient wetness impregnation	WHSV=60 000 mL/gh H_2/CO_2=4	χ_{CO_2}=77% S_{CH_4}=98% (400 °C)	[104]
Co	10% Ni and 3% Co /ordered mesoporous alumina	Evaporation-induced self assembly (EISA)	WHSV=10 000 mL/gh H_2/CO_2=4	χ_{CO_2}=78% S_{CH_4}=99% (400 °C)	[92]
Co	15%Ni and 3% Co $/CeO_2 - ZrO_2$	Wet impregnation	WHSV=12 500 mL/gh H_2/CO_2=4	χ_{CO_2}=83% S_{CH_4}=94% (300 °C)	[105]
Co	2%Co (+/- 35% Ni) /NiO-MgO	Sonochemical Synthesis and Wet impregnation	GHSV=47 760 h^{-1} H_2/CO_2=4	χ_{CO_2}=90% S_{CH_4}=99% (400 °C)	[106]
Co	12.5%Co-15%Ni $/Al_2O_3$	Wet impregnation	GHSV=9000 $mL/gcath$ H_2/CO_2=4	χ_{CO_2}=76.2% S_{CH_4}=96.39% (400 °C)	[107]
Cu	15% Ni and 1.3% Cu /hydrotalcite	Co-precipitation	GHSV=12 000 ml/gh H_2/CO_2=4	χ_{CO_2}=86% S_{CH_4}=98% (350 °C)	[101]

2.3.4 Deactivation of Catalysts

Catalysts often lose activity over time, which can be usually compensated with a temperature increase to boost its activity. Albeit all this, the catalyst's activity is always finite, and either its regeneration or its substitution become a necessary process. The main processes through which catalysts can deactivate are:

- **Poisining** is when a species irreversibly adsorbs on the active sites of the catalyst, thus rendering them useless for the process. Poisoning decreases the number of active sites, thus the average distance that reactant molecule have to diffuse through the pore structure increases, which end up decreasing the speed of the reaction that the catalyst was supposed to be increasing. [108]
- **Coking** corresponds to the deposition of hydrocarbons on the catalysts surface. The mechanism can be known as coking or even as fouling, although to the latter is usually given a broader meaning for all kinds of depositions. Coking is a process that depends on the feed, on the density of active sites, and on the nature of the catalyst employed. Coke can lead to catalyst deactivation due to active sites coverage and through pore blockage. [109]
- **Sintering** is a physical and thermal phenomenon that leads to agglomeration, which is a reduction in the surface to volume ratio of the catalyst. It usually results in the loss of active sites, due to the alteration of the catalyst's structure. Both the catalyst support and the active metal sites can be sintered upon exposure to whether high temperatures or high pressures. Hence, catalyst sintering can be avoided by controlling the temperature and pressure at which the reaction is carried out. [110]

In addition to these, which can be classified as the main concerns for nickel-based catalysts, some other more general concerns can be raised for the following deactivation processes: (i) thermal degradation, (ii) vapor compound formation accompanied by transport, (iii) vapor-solid and/or solid-solid reactions, and (iv) attrition/crushing.

Catalyst regeneration would be the optimal goal, since this could make the process highly more economical, as well as saving up raw materials. This process is however only possible when the deactivation has been due to surface contamination, as opposition to poisoning, which deems the catalyst as practically impossible to regenerate. [111]

According with Ewald *et al.* [112], carbon deposition can be considered to have a negligible influence on deactivation for nickel-based catalysts on the CO_2 methanation reaction. However, it has discovered that a more severe deactivation was attributed to the water formed during reaction, thus resulting in hydrothermal aging conditions, which therefore accelerate the nickel particle sintering process, leading to deactivation. In addition to that, a decrease of BET surface area was also experienced, as a general increase of the larger pores occurred, while smaller ones were blocked due to the nickel particle sintering and consequential growth.

2.4 Bimetallic Catalysts Study

This section of the present report intends to report whether the addition of a second metal promoter can be beneficial towards the catalysts activity.

Mutz *et al.* [102] performed a study using a 17 wt% Ni_3Fe bimetallic catalyst, supported on $\gamma - Al_2O_3$. This catalyst was prepared using a homogeneous deposition-precipitation process. This catalyst has shown better low-temperature performance, especially for higher pressures, that when compared with a monometallic Ni catalyst. For it's optimal conditions, which were reached at 358 °C and 6 bar, it obtained a conversion of CO_2 of 71% and a selectivity towards methane higher than 98%, whilst also maintaining a high stability.

Branco *et al.* [113] performed a research onto bimetallic catalysts of Ni connected with multiple different lanthanides, such as Ce, Pr, La, Sm, Dy and Yb, with a ratio of Ni/lanthanide of 5, and supported on silica. The supported catalysts were prepared by incipient wetness impregnation technique, whilst the silica was obtained through electrospinning. In an overall review, the lanthanides have proven to increase the catalyst's activity, due to their 4f block element doping effect, which results in a positive influence to the basicity, decreases the catalysts particle size, and increases its stability. The best results were obtained for the Sm and Pr metals, presenting both a selectivity towards CH_4 of 98%. However, the best activity was obtained for the praseodymium catalyst, which presented an activity per active site better than that of the references used. The order of activity that was found for the studied metals follows the order Pr>Sm>Ce>La>Dy>Yb>Ni, which appears to be exactly the reverse order of the apparent activation energy found for the kinetic regime: 30, 34, 37, 39, 43, and 58 kJ/mol, respectively.

In another study performed by Branco *et al.* [76], the performance of a selection of cerium-based bimetallic oxides was evaluated, such as $3NiO.CeCO_2$, $Co_3O_4.CeO_2$ and $1.5Fe_2O_3.CeO_2$, which were prepared through two sol-gel methods (epoxide addition and Pechini), and by electrospinning, which was used in order to obtain compounds with different morphologies. This study verified that the catalytic performance shows a dependence with i) the type of d block elements used on the catalyst, ii) its production method, and iii) the catalysts morphology. The best results were those obtained over the nickel-based catalysts, which were prepared by the electrospinning technique, as can be observed in figure 13.

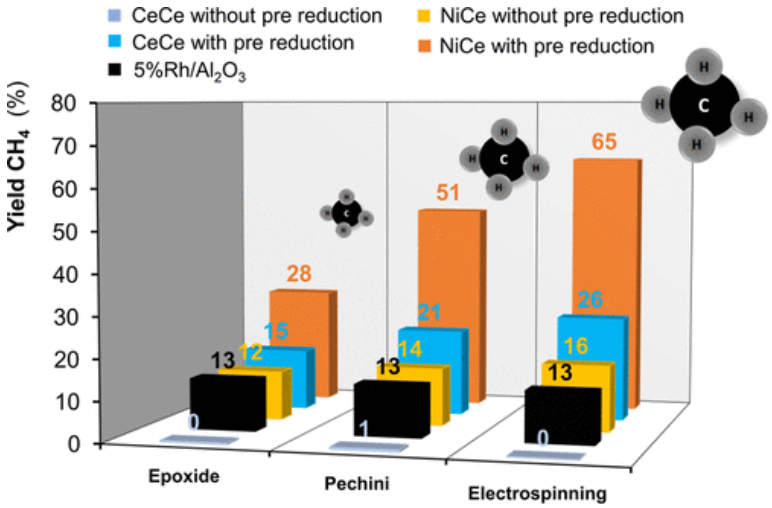

Figure 13: Graphical representation of the yield of CH_4 obtained for each different catalyst, comparing its different preparation methods. [76]

Dong *et al.* [114] performed a study evaluating the performance of a Ni-Re bimetallic catalyst for the CO_2 methanation process. The supported metals were prepared through facile co-impregnation method, and the support was reused from an industrial waste. This catalyst obtained a conversion of CO_2 of 99.55%, and a selectivity for CH_4 of 70.27%, for the following conditions: 400 °C, 1 atm, 2000 h^{-1}, and H_2 : CO_2 : N_2=4:1:0.5. Also, the addition of the Re metal to the catalyst was also stated to enhance the catalyst's anti-sintering and anti-coking abilities.

Zhang *et al.* [115] performed a study upon the foam silica supported $LaNi_{1-x}Co_xO_3$ perovskite nanocrystrals catalyst. It was prepared through citric acid assisted impregnation method. The specific $LaNi_{0.95}Co_{0.05}O_3$ was the proportion studied that obtained the better results. CO_2 conversion of 72% at 400 °C, 60000 gh^{-1}, 0.1 MPa, and obtained over 90% of selectivity towards CH_4.

Through the comparison of multiple commercial catalysts (only containing one metal compound, such as Ni or Ru) with their bimetallic counterparts, it is quite obvious that the addition of small proportions of other metals to the catalyst can be beneficial. This is quite more obvious when the main metal considered is nickel, since the addition of another metal has been repeatedly reported to decrease this nickel's sintering, - which is one of its main issues, - thus ending up increasing stability.

2.5 Zeolite-supported catalysts for CO_2 Methanation

In an enlightening study performed by Bacariza *et al.* [116], a series of effects were evaluated for the preparation and testing of nickel-promoted USY catalysts, such as:

- the preparation method;
- the calcination temperature;
- the Ni content;
- the pre-reduction temperature.

The study on the preparation method intended to compare the effect of the incorporation of nickel through ion exchange and through incipient wetness impregnation. And it proved that the impregnation method was far better, due to the enhanced reducibility of the Ni species, mainly present as NiO in the impregnated sample.

On the calcination temperature effect study, a comparison between temperatures (400, 450, 500 and 600 °C) was performed, which proved that it is quite indifferent which temperature its used, however 500 °C is considered by the author the optimal temperature, since it's higher yet the closest to the pre-reduction temperature used (470 °C), which is expected to confer a higher stability, since no deep modifications should be expected.

The study on the Ni content proved that the increase of said content confers an increase in activity as well, asserting 25%Ni/USY as the most active catalyst. However, this enhancement in activity is not a significant beneficial effect, as opposed to the previous increases. This behaviour is due to sintering, occurring for higher concentrations of Ni, thus favouring the occurrence of agglomeration processes, conferring 15%Ni/USY the optimal Ni content status. Furthermore, a study was performed for its stability, which proved that Ni/USY zeolites are stable catalysts for CO_2 methanation reaction, for at least 10h.

The last study was performed for the pre-reduction temperature, and it also proved that, within the studied temperatures (470, 550, 600 and 700 °C), it is relatively indifferent at which one the reduction is performed, hence 470 °C is considered the optimal temperature, since it is the most economic option.

2.5.1 Improving the properties of the support

In addition, the promoter which was selected to link with the support framework was Cs^+. This was due to the zeolites basicity, which arises from the charge of the oxygens present in the framework of the zeolites lattice. This effect can be countered through the tuning of the compensating cation nature, due to their nature, whilst also giving additional sites for CO_2 activation. According with Vos *et al.* [117], for FAU structures, basicity increased with the size of the exchangeable cation. Whilst Pirngruber *et al.* [118], also has proven that Cs (in addition to a Y-zeolite) obtains the highest order of CO_2 adsorption capacity. For the zeolites framework, the interactions between Cs^+ and the oxygens were also considered the most stable.

In another study performed by Temiloluwa [119], it was proven that exchanging a commercial HUSY zeolite with Cs^+ was beneficial not only to the CO_2 adsorption and consequently to its conversion, but also to the selectivity towards CH_4 whilst also proving more active through the stability tests.

2.5.2 Incorporation of Promoters

Nickel is the most active metal promoter for the methanation reaction. However, Ni-based catalysts suffer from problems such as sintering and deactivation at low temperatures, which is mainly due to their interaction with CO molecules and the formation of nickel sub-carbonyls. For that reason, Nickel often benefits from the addition of promoters and stabilizers, which serve the purpose of inhibiting the deactivation processes. [116]

In addition, when the correct compounds are added, these promoters can also enhance the samples basicity, by providing additional active sites for CO_2, such is the case of MgO.

2.6 Thesis Objective

As previously observed, CO_2 methanation performance is highly dependent on the active metal chosen. For the case of zeolite-supported catalysts, which were found as promising for the CO_2 methanation in literature, no systematic studies have dealt with the influence of transition metals nature on the properties and

performances. Based on literature, in the present work three studies were carried out using a previously optimized USY zeolite as support:

- Effect of the transition metals nature for catalysts with 15 wt% of metal;
- Effect of 15 wt% Ni catalysts doping with 1 wt% of Fe, Cu or Co;
- Effect of doping metal loading.

3 Methods and Catalyst Preparation

In the present chapter, the preparation method of the studied catalysts shall be explained, as well as the techniques used for their characterization. A description of the installation and which operational conditions used will also be presented.

3.1 Synthesis of the Catalysts

Three distinct studies were performed: one where it is intended to study the individual promoting transition metals (Fe, Co, Ni and Cu) associated with the CsUSY zeolite support. For the second part, the most active metal (Ni) for the CO_2 methanation reaction was selected and then used as the main promoter, whilst the other metals were added in a much lower concentration (1% w/w). For the third part, for the best selection of promoters, the second metal (Fe) was then varied their content, to assert the best possible catalyst was found. A summary of the studies performed can be found in the table 3.

Table 3: Depiction of all the prepared catalysts throughout the study, divided by their respective studied effect.

Study	Code	Ni (wt%)	M (wt%)	Preparation method	Tcalc (°C)	Tred (°C)
Support	CsUSY	–	–	Ion exchange	500	470
Metal nature effect	15Ni	15	–	impregnation		
	15Cu	15	-	Co-impregnation		
	15Co	15	-	Co-impregnation		
	15Fe	15	-	Co-impregnation		
Transition metal doping effect	15Ni1Cu	15	1	impregnation		
	15Ni1Co			impregnation		
	15Ni1Fe			impregnation		
Fe loading effect	15Ni2Fe	15	2	Co-impregnation		
	15Ni3Fe	15	3	n.d.		

3.1.1 Preparation of the CsUSY support

All of the previously referred catalysts have as starting material the CBV 780 zeolite from *Zeolyst International*, comprising a HUSY zeolite (acid form of the USY zeolite, <0.02% (w/w) of Na), containing an Si/Al ratio of 38. This compound was mixed with a solution of $CsNO_3$ (1M), and stirred for 4h at room temperature. Three ion exchanges were performed, intermixed with filtration and washing with distilled water until a pH of 7 was obtained, followed by a drying at 100 °C overnight.

Each support thus contains around 1.5 %wt of cesium, corresponding to an exchange degree of 34%, thus one third of the negative charges are being compensated by the Cs^+, and the remaining two thirds by H^+.

Afterwards it followed a calcination of the dried sample, intending to remove any trace of nitrates from the support. This calcination was performed in two steps, first at 200 °C for 1h, then at 500 °C for 6h, respectively, for an air flow of 60 ml min^{-1} $g^{-1}_{zeolite}$ and a heating rate of 2 °C/min. Hence, a CsUSY support was obtained. This same support preparation method was followed throughout all the catalyst's preparations.

3.1.2 Incorporation of Metals

Different types of samples were prepared throughout all of the three studies performed. For the first study, a series of four monometallic samples were prepared by impregnating 15 wt% of Ni, Cu, Co or Fe over the previously described zeolite. As shown in Table 3, catalysts were named as 15Ni, 15Cu, 15Co and 15Fe. The incipient wetness impregnation consisted in the deposition of a solution containing the precursor salts over the support.

For nickel, the precursor salt used was $Ni(NO_3)_2 \bullet 6H_2O]$ (nickel nitrate hexahydrate) from *Sigma-Aldrich*. For iron, it was used the precursor salt $Fe(NO_3)_3 \bullet 9H_2O$ (iron(III) nitrate nonahydrate) from *Sigma-Aldrich*. For cobalt, it was used the precursor salt $Co(NO_3)_2 \bullet 6H_2O$ (cobalt(II) nitrate hexahydrate) from *Sigma-Aldrich*. Whereas for copper, the precursor salt was $Cu(NO_3)_2 \bullet 3H_2O$ (cupric nitrate trihydrate) from *Fluka*.

After impregnation and drying overnight at 80 °C, catalysts were calcined following the same procedure described above for the synthesis of the zeolite support. In the second study, three catalysts containing 15 wt% of Ni and 1 wt% of Cu, Co or Fe were prepared by co-impregnation method followed by drying (80 °C, overnight) and calcination. These catalysts were named as 15Ni1Cu, 15Ni1Co and 15Ni1Fe. Finally, after identifying the most outstanding catalyst, the effect of the second metal loading was analysed. In this way, two additional catalysts were prepared by co-impregnation following the procedure already described, and being the chosen loadings 2 and 3 wt% for the doping metal (Fe) and 15 wt% for Ni. Catalysts were named as 15Ni2Fe and 15Ni3Fe, respectively.

3.2 Physico-chemical characterizations

The synthesized catalysts were characterized using X-Ray Diffraction, Temperature-Programmed Reduction with H_2, N_2 Adsorption, Thermogravimetric Analysis, and also Transmission Electron Microscopy.

3.2.1 X-Ray Diffraction (XRD)

X-Ray Diffraction is a technique that provides detailed information about the crystallographic structure, the chemical composition and the physical properties. The intensity of the diffracted x-rays depends on the atomic content (nature, number and relative position of atoms) on the elementary mesh, and also on the dimension of the crystallites. [126]

XRD peaks are made through constructive interference of a monochromatic beam of x-rays, which were scattered at specific angles in each set of lattice places of the sample. Each peak intensity is determined by the atomic position within the lattice planes. [127] The position of the peak on the diffractogram along with the distribution of their relative intensities can be compared with the databases for each one of the materials, thus allowing for a factual identification of the various molecules present on the framework of the catalyst.

Crystals refer to regular arrays of atoms, where X-rays, which are essentially waves of electromagnetic radiation, are scattered by those atoms' electrons. And through the incidence of monocromatic radiation on the sample with a wavelenght λ, a small portion of its intensity is reradiated as a spherical wave, thus scattering with a separation d. These spherical waves will be in sync, and their path-length difference will then be $2dsin\theta$, as can be seen through the Bragg's Law, in equation 9. [128]

$$n\lambda = 2dsin\theta \tag{9}$$

Where n represents any integer and θ is known as the Bragg's angle.

Afterwards, by applying Scherrer's equation (equation 10), it is possible to determine the particle size of the metals.

$$d_p = \frac{0.9\lambda}{Bcos\theta} \tag{10}$$

On which d_p represents the average particle diameter for the metallic crystallites, and B is the line broadening at half the maximum intensity (best known as FWHM). [129]

For the present study, the XRD system was used with the solid-powder samples, mainly aiming to determine the average particle size, and to identify any damage that may have been done to the zeolite's structure after the metal's impregnation. The equipment that was used is mainly composed of a diffractometer *Bruker AXS Advance D8*, one monochromator, one goniometer (for the variation of the incidence angle) and a detector 1D (SSD 160) with a nickel filter, utilizing radiation at a wavelength of λ= 1.5418 Å, and at 40 kV and 40 mA. The scan interval was defined from 5 °until 80 °, increasing with a time of 0.5 seconds between angles.

3.2.2 Temperature-Programmed Reduction with H_2 (H_2 TPR)

Temperature Programmed Reduction with H_2 is a technique used for the characterization of solid materials, specially heterogeneous catalysts, in order to find the most efficient reduction conditions. It consists of submitting an oxidized catalyst percursor to a programmed temperature rise, while a reducing gas mix flows over it. [125]

Prior to the procedure, a treatment of the surface of the catalyst is required. Afterwards, a U-tubed container is filled with the catalyst, and positioned in a furnace with a temperature control equipment. Temperature

measurement is performed with a thermocouple. The air is flushed out with inert gas (argon), and when ready the flow controllers are used to inject some hydrogen. The final composition of the outlet gaseous mixture is measured throughout the study, by passing through a coil, which is deep within ice, and where the condensation of steam and other gases occur, and then passing through a thermal conductivity detector (TCD), which will thus monitor the consumption of H_2. The temperature at which hydrogen is consumed is then registered by the detectors as the temperature at which reduction has taken place.

This is a highly relevant characterization method, because it allows for a better understanding of the conditions the reduction should have, prior to the catalytic tests. The graphed profile obtained for H_2-TPR usually supplies information not only on the ability of each one of the metallic species to be reduced, but also on the type and position of each different species present on the support.

For this technique, an *Autochem II* equipment from *Micromeritics* was used. All the samples were tested according with the same following conditions: the pre-treatment was performed at 250 °C using argon as inert gas. After cooling until 20 °C, the TPR developed with the presence of a flow of 95% argon and 5% H_2, between the temperatures of 20 and 900 °C with a heating rate of 10 °C/min.

3.2.3 Thermogravimetric Analysis (TGA)

TGA is a thermal method used to determine a material's thermal stability, its chemical composition and the functional groups of compounds, by monitoring the weight change that occurs as a sample is heated at a constant rate. [122]

This is an important procedure to perform for the current study, since it can account for the reactional losses (e.g. drying, reduction) or gains of weight (e.g. oxidation, adsorption) that happen specially on gas-solid systems, allowing for a high control over the study of the catalyst's stability. [123]

For the present thesis, all of the samples were analysed using the TGA-DSC (Differential Scanning Calorimetry) technique, in which the combined system allows for a continual recording of both the mass variation and the heat flow exchanged between the sample and its surroundings. Time, mass and temperature are all measured and thus considered as base measurements in thermogravimetric analysis while many additional measures may be derived from these three variables. [124]

There are essentially three types of TGA: the **Isothermal** thermogravimetry, where the sample weight is recorded as a function of time at constant temperature; the **Quasistatic** thermogravimetry, in which the temperature is raised in sequential steps and the mass is recorded; or through **Dinamyc** thermogravimetry, where the sample is heated in an environment whose temperature changes in a linear constant matter. [124]

The typical thermogravimetric analysis consists of inserting the sample inside a scale, within a temperature-programmed furnace, where the heat increase is gradual and at constant rate in order to incur in a thermal reaction. This analysis may also occur for various atmospheres (e.g. ambient air, vacuum, inert gas, etc), and for various pressure conditions (e.g. high vacuum, controlled pressure, etc). On this weight scale, two samples are introduced, one is the sample for which results are put in for, whilst the other one is used as reference.

This technique was therefore used with the intent of knowing:

- the weight loss, resulting from the water removal previously adsorbed by the zeolite - determination of the dry weight of the catalyst;
- the hydrophobicity index (h), which is a measurement of the relative hydrophobicity, usually defined as the division between the weight lost by the zeolite at 150 °C and at 400 °C, as can be observed in equation 11.

$$h = \frac{Weightlossat150°C}{Weightlossat400°C} \tag{11}$$

All the referred analysis were carried out in the *Setsys Evolution TGA* equipment, by *Setaram Instruments*. They were carried out from 20 °C to 400 °C, under a heating rate of 10 °C/min. The procedure was performed twice, as a method of removing the background noise or possible errors. The air flow used was of 30ml/min. The mass of zeolite that was saturated in water was always between 20 and 25 mg.

3.2.4 N_2 Adsorption

Nitrogen adsorption is usually the standard way to characterize carbon-powdered compounds, since it supplies information on the textural properties of the catalyst, such as the specific area and the specific pore volume. [120]

According with IUPAC, there are three main types of pores (being L the diameter of a cylindrical pore): **micropores** (where L<2 nm), **mesopores** (where 2<L<50 nm) and **macropores** (where L>50 nm). [121]

Also according with IUPAC, there's also six types of adsorption equilibrium isotherms, and four types of hysteresis. The study of isotherms allow for a better understanding into the type of adsorption the catalyst performs, and enables to know the size of pores.

The total pore volume (V_{total}) is determined for atmospheric pressure. And, by applying the t-plot method of Lippens and Boer, it's possible to calculate the volume of micropores (V_{micro}) and the outer surface area (a_e^{ext}). Whilst the volume of mesopores (V_{meso}) will be determined afterwards through the difference of V_{total} and V_{micro}.

The studies were performed on an *Autosorb iQ* equipment from *Quantachrome*. Before adsorption, the samples were degassed in vacuum (90 °C for 1h, followed by 350 °C for 4h).

3.2.5 Transmission Electron Microscopy (TEM)

The microstructure of a sample in heterogeneous catalysis is deeply interconnected with its catalytic properties. Thus, TEM, which is a microanalytic technique where a beam of electrons is transmitted through a sample to form an image, is a powerful tool when it comes to characterising catalysts at an atomic level.

TEMs are capable of capturing significantly higher resolutions, thus enabling for the equipment to capture fine detail, such as columns of atoms. More recently, advances in technology have inclusively been able to achieve resolutions up to 0.5 Angstrom (50 pm) [130], thus allowing the imaging of lighter atoms.

This method, applied to the present catalysts, allows for a deeper understanding upon whether there was a preservation or destruction of the crystalline structure after the metal incorporation. It also allows for a determination of the average Ni°particle size, their respective variations with each different addition of promoters, as well as to infer their location on the framework of the support. [131]

TEM analysis was performed for several reduced samples using a *HRTEM 2010 JEOL LaB6* microscope (200kV).

3.3 Catalytic tests

3.3.1 Experimental Unit

The scheme of the setup used for the catalytic tests for the current report is shown in Figure 14 (adapted with permission from [116]).

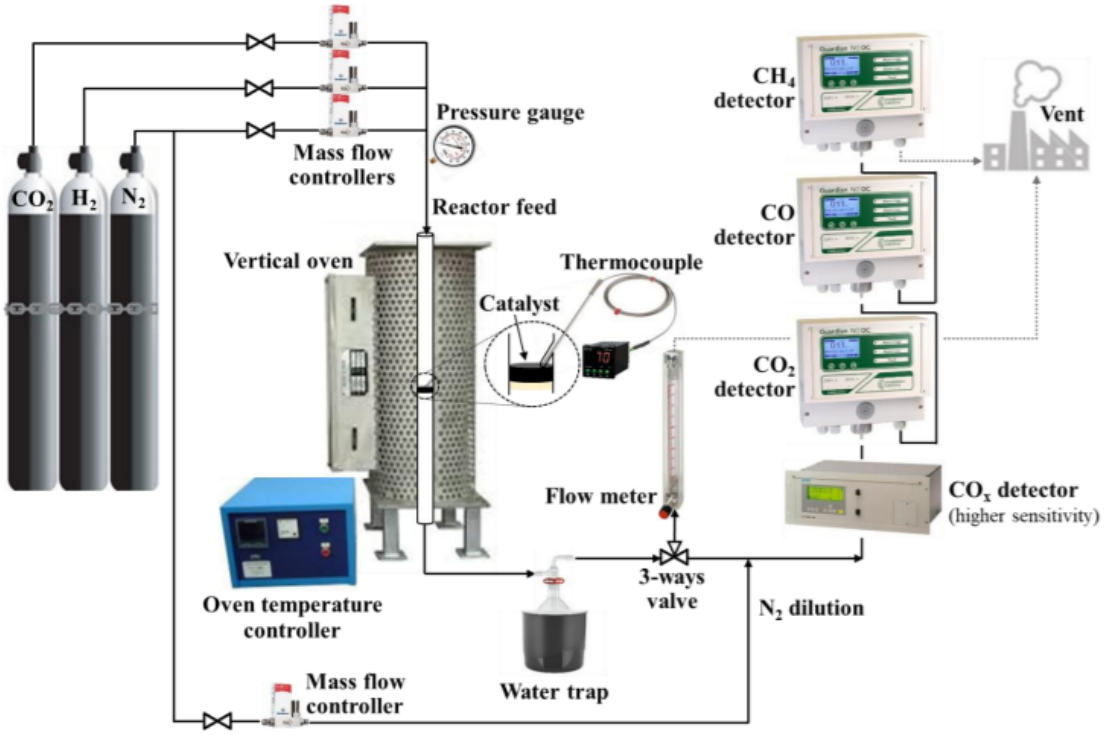

Figure 14: Scheme of the catalytic tests unit, for 1 bar, adapted with permission from [116].

The CO_2 methanation reaction tests were performed in a tubular fixed-bed quartz reactor heated by a vertical electrical furnace by *TermoLab*. Temperature control was carried out using a thermocouple installed in the middle of the catalyst bed, which is placed over a porous plate located in the middle of the reactor. The feed gas molar composition ratio was $CO_2/H_2/N_2$ = 9/36/10, with an inlet flow of 287 ml/min, which is the optimized gaseous inflow for the present operational setup, intending to avoid any external diffusion limitations. The reactor's outlet was analyzed using four gas IR detectors, one for CO_x (less than 1 vol.% of CO_2/CO, *Ultramat 23* from *Siemens*) and three other for larger ranges (less than 10 vol.% of $CO_2/CO/CH_4$, *Guardian NG* from *Edinburgh Sensors*. The use of the second CO detector with a smaller range was opted due to its (usually) low selectivity, which could reduce the accuracy of the values read in the detectors with larger range.

The outlet stream from the reactor passed through a water trap. Afterwards, a 3-ways valve allowed the measurement of total flow, being this required due to the reduction of the number of mol in this reaction. In order to guarantee that the compositions arising from the reactor are in the range of the detectors, a dilution consisting in 355 ml/min of N2 was incorporated to the reactor's outlet.

Catalytic tests were performed for a temperature range of 200 °C to 450 °C, keeping the sample at steady-state conditions for 30 minutes, for each temperature. Prior to the methanation reaction, a pretreatment was performed, which consisted of an *in situ* reduction of the sample at 470 °C and left at ambient temperature. The gas inflow used was 250 ml/min, composed of H_2/N_2 in a ratio of 4/1. The previous operational conditions can be better summarized in table 4.

Table 4: Operational conditions used for the pretreatment and methanation tests.

	Methanation Tests	Pre-treatment
Q_{total} **(ml/min)**	287	250
Q_{H_2} **(ml/min)**	188	200
Q_{N_2} **(ml/min)**	52	50
Q_{CO_2} **(ml/min)**	47	0
Q_{dil,N_2} **(ml/min)**	355	0
Pressure (atm)	1	1
Temperature range ($^{\circ}$**C)**	200 – 450	470
Heating rate ($^{\circ}$**C/min)**	5	2.5
Catalyst mass ($g_{drycatalyst}$**)**	0.200	0.200

After the system reached a stationary state, two measurements were performed for each temperature, and the average value was used, in order to obtain the most accurate values. In order for a possible reproduction of the current study, where the opted procedure should be as follows:

- Register the temperature of the thermocouple within the catalytic bed;
- Register the values obtained from the CO_2, CH_4 and CO detectors (which measure in % v/v);
- Register the value shown by the CO detector (measuring in ppm);
- Rotate the 3-way valve, in order to deviate the outflow from the detectors;
- Measure the output volumetric flow (Q_s);
- Rotate the 3-way valve again, sending the outflow for the detectors again;
- Await for the stabilization of the volumetric percentages of each compound to stabilize again, and redo the procedure;
- If two measurements for each temperature were already performed, then increase the temperature and wait for the system to stabilize (30 minutes) and repeat the procedure.

3.3.2 Calculation of CO_2 conversion, CH_4 selectivity and yield

Considering that the current system is in continuous flow, the carbon dioxide's conversion and methane's selectivity were calculated using equations 12 and 13, which use the inlet and outlet molar flows (F_{inlet} and F_{outlet}, respectively). This way, it is possible to represent the amount of CO_2 that reacted as ($F_{CO_2,inlet} - F_{CO_2,outlet}$).

$$\chi_{CO_2}[\%] = \frac{F_{CO_2,inlet} - F_{CO_2,outlet}}{F_{CO_2,inlet}} \times 100 \tag{12}$$

$$S_{CH_4}[\%] = \frac{F_{CH_4,outlet}}{F_{CO_2,inlet} - F_{CO_2,outlet}} \times 100 \tag{13}$$

As was previously stated, carbon monoxide was also measured at the reactor's outlet. This way, it is possible to also calculate the selectivity of CO_2 towards CO, which was determined using equation 14.

$$S_{CO}[\%] = \frac{F_{CO,outlet}}{F_{CO_2,inlet} - F_{CO_2,outlet}} \times 100 \tag{14}$$

The yield for CH_4 was afterwards calculated through equation 15, using both the CO_2 conversion and the CH_4 selectivity values.

$$Yield_{CH_4}[\%] = \frac{\chi_{CO_2} \times S_{CH_4}}{100} \tag{15}$$

4 Results and Discussion

In the current chapter, the results obtained shall be shown, as well as put into context and debated within a basis on literature.

4.1 Effect of the Metal Nature

4.1.1 XRD

X-Ray Diffraction aims to study the structural properties of catalysts, as well as determine the average particle size of both reduced metals (Ni °, Cu °, Fe °and Co °) and their respective oxides (i.e. NiO, CuO, Co_3O_4) from calcined, reduced and spent samples. All the diffraction peaks found for the current studied species can be found in Annex 1, section 7.1 of the present report.

As can be ascertained by the diffractograms (Fig. 15), the diffraction peaks referring to the faujasite's structure (FAU, red circles) are clearly identifiable in all the catalysts from this study. However, it is clear that, in the case of 15Co and 15Fe catalysts, FAU peaks intensity is lower than the found in 15Ni and 15Cu catalysts. This could indicate that the zeolite's crystallinity could be partially affected by the incorporation of these metals. In addition to this, the presence of Ni, Cu and Co oxides is clear in 15Ni, 15Cu and 15Co catalysts, respectively. On the contrary, no iron oxide peaks can be found in 15Fe, suggesting that these species will be highly dispersed over the support. Regarding reduced catalysts patterns, it is clear the presence of Ni°, Cu°and Co°on $15Ni_{Red}$, $15Cu_{Red}$ and $15Co_{Red}$ catalysts, respectively, while no peaks attributed to Fe°can be clearly found on $15Fe_{Red}$.

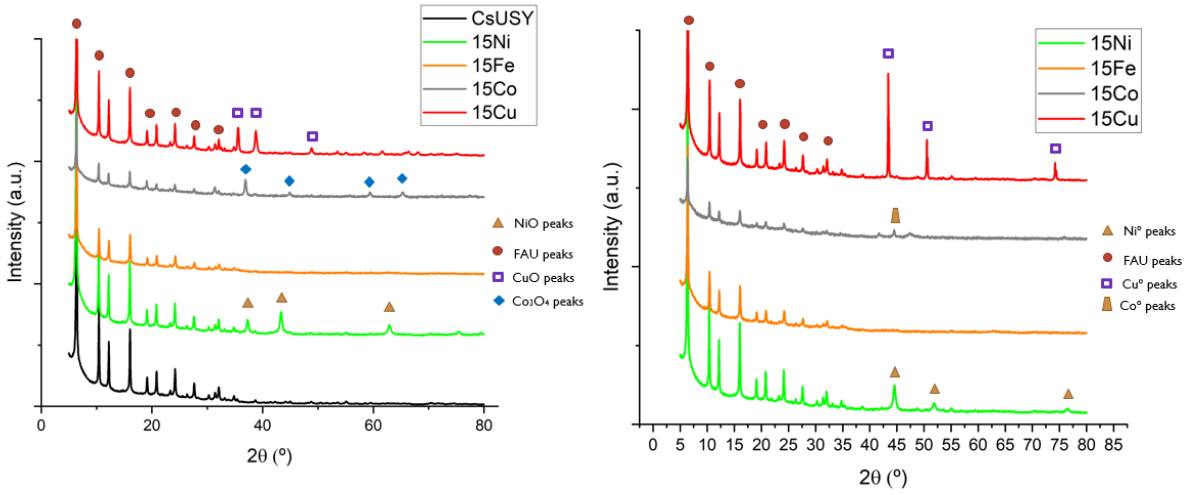

Figure 15: X-Ray Diffractograms for the calcined (on the left) and reduced (on the right) samples, referring to the first study.

By applying Scherrer's equation, it was possible to estimate the average crystallite sizes for the different oxides and metal species, being these values presented in Table 5. As observed, Ni and Cu oxides presented similar crystallite sizes, while larger Co oxide crystallites were formed in 15Co catalyst. In the case of 15Fe, the absence of clearly identifiable peaks did not allow the estimation of the crystallite sizes. Regarding the reduced catalysts properties, the smallest crystallites were found in 15Ni, being remarkable the growth of the crystallites in the case of 15Cu.

Furthermore, for 15Fe both reduced and spent samples, the inability to find any iron oxide particles may indicate that there wasn't any oxides' reduction, which is coherent with the findings for the TEM analysis, as shall be seen in section **??**ce those images couldn't ascertain for the presence of these particles.

Table 5: Grain size obtained for each catalyst, at each one of the phases it underwent, for the first study.

Catalyst	d_{Oxide} (nm)	d_{Metal} (nm)
15Ni	21	-
$15Ni_{Red}$	-	18
15Fe	n.a.	-
$15Fe_{Red}$	-	n.a.
15Cu	21	-
$15Cu_{Red}$	-	47
15Co	27	-
$15Co_{Red}$	-	29

4.1.2 H_2-TPR

The catalyst's reducibility was studied through the temperature reduction technique programmed with H_2 (H_2-TPR), being the profiles for the monometallic 15X catalysts obtained are represented in the figure 16.

Concerning the profile of the 15Ni catalyst, it can be inferred that the biggest fraction of nickel oxide (NiO) species was reduced at relatively low temperatures (below 470 °C, which is the temperature used for the reductions prior to the catalytic tests). This is an indicator of the presence of weak interactions between the nickel oxide and the zeolite, indicating that these species might be located on the external surface of the zeolite. [132] [133] [134] The highest peak occurred at approximately 368 °C, which agrees with the literature for the reduction of NiO, whilst situated in the outer layer of the surface of the support CsUSY. [135] In addition, the other peak observed at around 600 °C is related with stronger interactions, formed also between NiO and the zeolite, this time attributed to the reduction of the NiO particles located in the mesoporous cavities of the support. [134] [132]

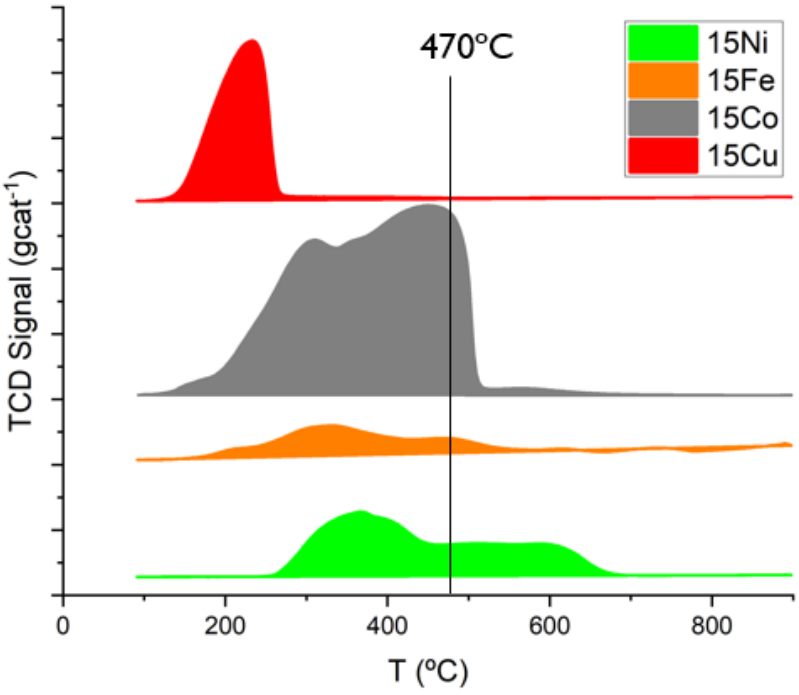

Figure 16: H_2-TPR profiles obtained for the 15X catalysts.

Regarding 15Cu and 15Co catalysts, it can be observed that their respective metal oxides are mostly reduced below 470 °C. Whilst for 15Fe, it appears to not be reduced entirely. When consulting the literature for previously developed Fe-zeolite catalysts [136] [137], this behavior seems to be common. The reduction peak found at 340 °C could be attributed to the reduction of Fe^{3+} into Fe^{2+} (from Fe_2O_3 into Fe_3O_4). [137] For the temperatures between 400 and 750 °C, the constant reduction peaks noticed can be attributed to the

reduction of Fe_3O_4 into Fe°, which may happen through the FeO mechanism ($Fe_3O_4 \rightarrow FeO \rightarrow Fe^{\circ}$).[138]

However, according with Chen Sachtler [139], when present as compensating cation, the reduction from Fe^{3+} to Fe^{2+} could occur at medium temperatures, while Fe^{2+} reduction to Fe°mainly occurs above 1000 °C, which should be expected to accompany the destruction of the zeolite. To be pointed out is that the high Fe loading (15 wt%) and the low Al content of the zeolite (hence, a very limited number of exchange positions) together with the preparation method (impregnation) do not promote the incorporation of iron as compensating cation.

4.1.3 TGA

Water is a product of this reaction, and according to literature, water also tends to adsorb at the same active sites as the carbon dioxide activation, having therefore a double inhibitory effect. Hence, it can be inferred that evaluating the catalysts hydrophobicity is an extremely important matter. Thus, a measurement of the calcined samples saturated on water was performed through TGA, for which were obtained the following hydrophobicity index (h index) displayed in table 6.

These hydrophobicity indexes of each sample after saturation with water, defined as the ratio between the mass losses at 150 °C and at 400 °C, inform on the interactions between the surface of the catalyst and water, whereas values near zero represent highly hydrophilic surfaces and values closer to the unit indicate weak interactions between water and the catalysts' surface. The latter values are usually preferred for this index, since they tend to have the least impediments, as for the reference of 15Ni/CsUSY its usual index is around 0.94 0.95. The incorporation of promoters usually reduces the hydrophobicity index, however when analyzing the results for the 15X catalysts series, it can be concluded that the nature of the transition metal does not strongly affect the hydrophobicity of the materials, as values above 0.90 were obtained in all cases. To be noted is that 15Ni presented the highest value, followed by 15Co, 15Cu and, finally, 15Fe.

Table 6: Hydrophobicity indexes calculated for the 15X catalysts.

Sample	h index
15Cu	0.93
15Co	0.94
15Fe	0.90
15Ni	0.95

Further studies on the mass loss (%) as a function of temperature can be found in Annex 3, section 7.3 of the present report.

4.1.4 N_2 Adsorption

Through the N_2 adsorption isotherms (Figure 17) it was possible to obtain the textural properties from the 15X samples after calcination, presented in Table 7.

By analyzing Figure 17, it is clear that all catalysts present the same type of isotherms (with a similar combination of both type I and II, which is characteristic of micro and mesoporous materials). When it comes to the textural properties (Table 7), it is possible to infer that the addition of any of the metals provoked a reduction on every parameter, when comparing with the CsUSY support, especially when it comes to the external surface area (S_{ext}). This indicates that a greater fraction of metals may be located on the external surface of the zeolite. The reduction of V_{micro}, more remarkable in the case of 15Co, may be related with a partial loss of zeolite's crystallinity or to pores blockage due to the location of metal species. Taking into account the results previously discussed in terms of XRD, the decrease in the intensity of the zeolite peaks for 15Co together with the reduction of the microporous volume could indicate that the incorporation of cobalt could be responsible for a partial damage of the zeolite structure. On the contrary, the decrease on the intensity of FAU diffraction peaks found for 15Fe could not be attributed to structural damage, as the microporous volume was similar to the obtained for the CsUSY support. Finally, the losses registered on the V_{meso} may be due to the presence of the oxides inside the mesoporous cavities of the zeolite. [140]

Where ^{1} represents the micropores volume and external surface area which were obtained from t-plot method; and ^{2} mesopores volume was obtained as V_total (at p/p0=0.95) - V_micro.

Table 7: Textural Properties in Calcined Catalysts.

Catalyst	V^1_{micro} (cm^3g^{-1})	V^2_{meso} (cm^3g^{-1})	S^1_{ext} (m^2g^{-1})
CsUSY	0.19	0.30	319
15Ni	0.12	0.23	259
15Co	0.08	0.19	182
15Cu	0.13	0.23	229
15Fe	0.18	0.17	164

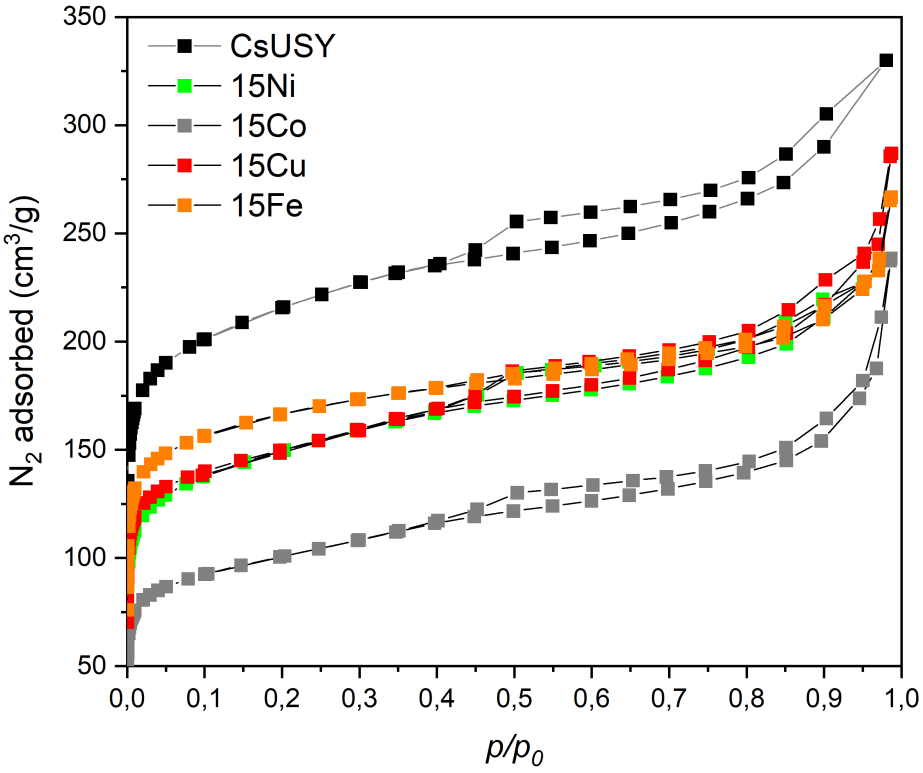

Figure 17: N_2 Adsorption Isotherms obtained for the support and catalysts of the first study.

4.1.5 TEM

The analysis of the reduced 15X catalysts by TEM (micrographs presented in Figure 18) indicated that no metallic Fe nor Cu seems to be clearly found in $15Fe_{Red}$ and $15Cu_{Red}$ catalysts, respectively. In the case of $15Fe_{Red}$, this information is coherent with XRD results, where the presence of diffraction peaks attributed to metallic iron or iron oxides was not clear. On the contrary, metallic particles were clearly observed in $15Ni_{Red}$ and $15Co_{Red}$ micrographs, being the sizes smaller and more homogeneously distributed in the case of $15Ni_{Red}$ catalyst.

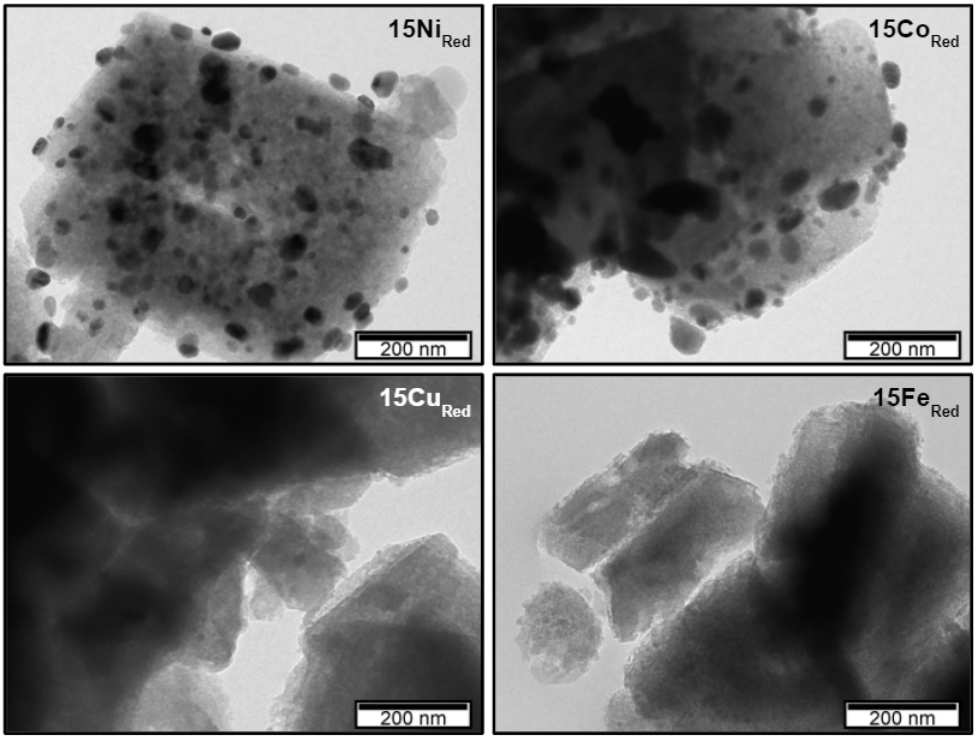

Figure 18: Images of each catalyst corresponding to the first study, obtained through Transmission Electron Microscopy, after their reduction.

4.1.6 Catalytic Results

The catalytic tests for the methanation of CO_2 were performed after a reduction at 470 °C, being the obtained CO_2 conversion, and CH_4 selectivity represented in Figure 19. As observed, CO_2 conversions followed the trend: 15Ni > 15Co > 15Cu > 15Fe, while CH_4 selectivity was higher for 15Fe than for 15Cu.

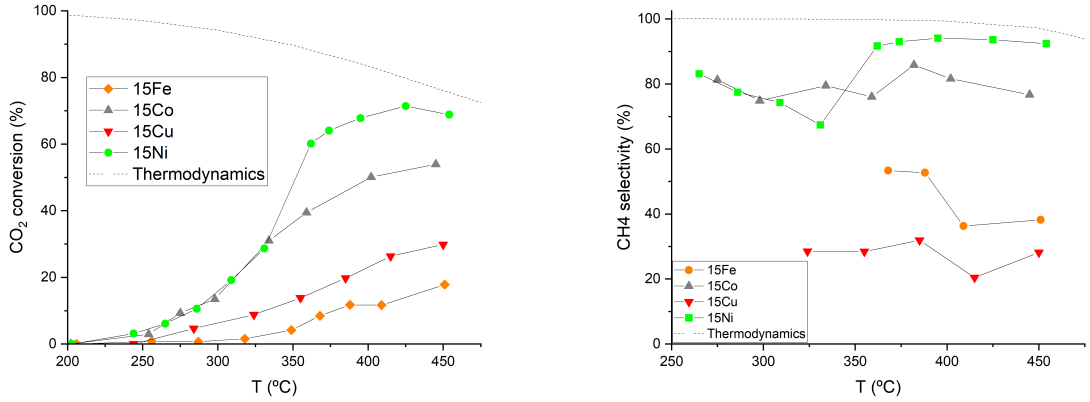

Figure 19: Methanation tests results for each one of the monometallic samples, after a reduction at 470 °C. In which each graph corresponds to a) CO_2 conversion; and b) CH_4 selectivity.

In order to compare the catalysts in a more appropriate way, methane yields were calculated and exhibited in Figure 20. As observed, 15Ni is the most outstanding catalyst, followed by 15Co and with 15Cu and 15Fe leading to similar performances. The higher performance of 15Ni catalyst could be related to this metal being known as more active for the reaction, together with the higher dispersion and smaller particle sizes achieved during the preparation, as already pointed out. For these reasons, in the following studies catalysts based on Ni and doped with low contents (<3 wt%) of a second transition metal were analyzed.

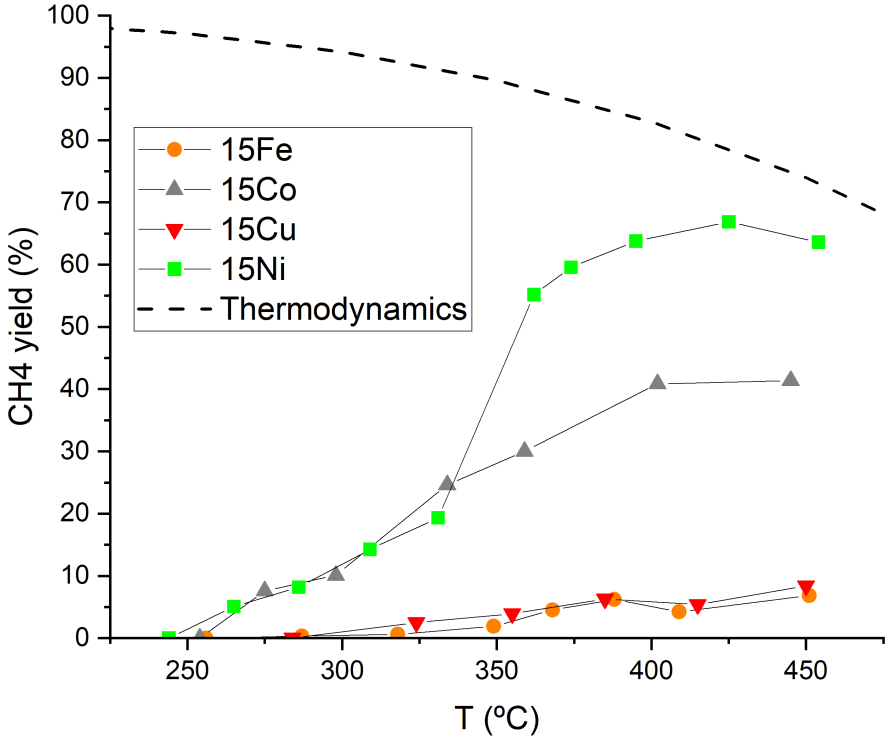

Figure 20: Methane yield obtained for 15X catalysts after reduction at 470 °C.

4.1.7 XRD of spent catalysts

After tests, catalysts were analyzed by XRD with the aim of identifying any influence of the test in the zeolite crystallinity and determining the average crystallite sizes. As observed in Figure 21, Ni °and Cu °diffraction peaks were found in the catalysts while no remarkable changes were observed in terms of FAU zeolite diffraction peaks. In terms of crystallite sizes, values were similar than those obtained for the reduced catalysts, with variations being lower than 2 nm in all cases. This suggests the absence of remarkable sintering processes during the catalytic tests.

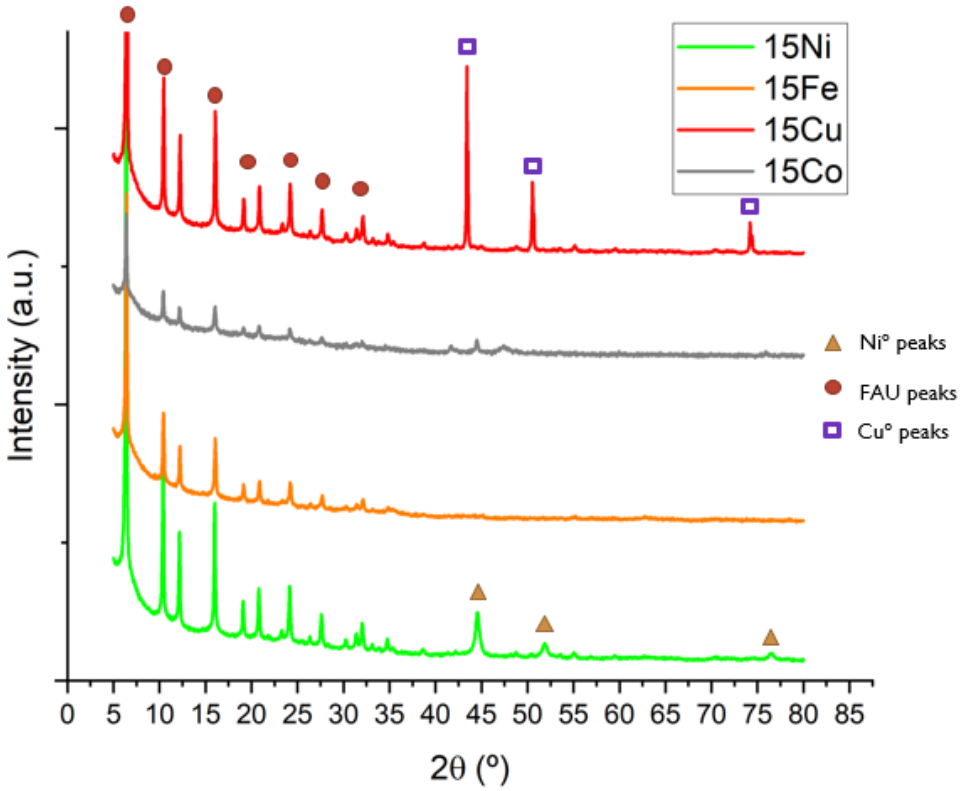

Figure 21: X-Ray Diffractograms for the spent samples belonging to the first study.

4.2 Effect of 15Ni doping with other transition metals

4.2.1 XRD

As can be ascertained by figure 22, FAU zeolite diffraction peaks can be found in all 15Ni1X catalysts. However, no peaks have been identified for Cu, Fe or Co oxides, which could be due to the low loading incorporated (1 wt%). In addition, NiO and Ni °peaks were found in all calcined and reduced catalysts, respectively. Thus, crystallite sizes were determined and presented in Table 8. As observed, Cu and Co addition did not induce a positive effect on NiO/Ni °crystallites sizes, while in the case of Fe the interaction of this metal with Ni seems to be responsible for a lower NiO reducibility, being both NiO and Ni°peaks found in this catalyst after reduction at 470 °C. This phenomenon, which did not allow the determination of the average particle size applying Scherrer's equation, could indicate a higher metallic dispersion of nickel in the bimetallic catalyst containing Fe.

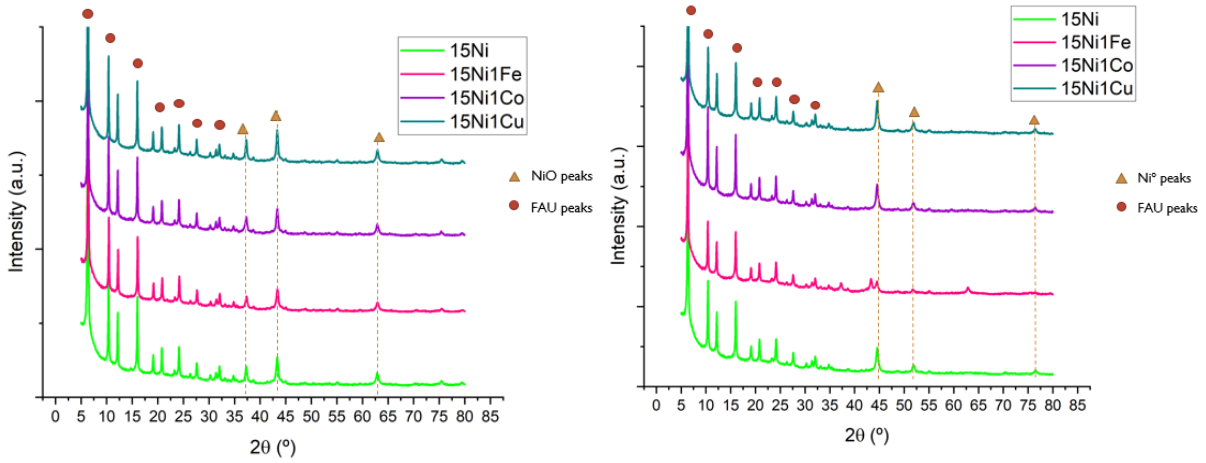

Figure 22: X-Ray Diffractograms for the calcined (on the left) and reduced (on the right) samples, for the second study.

Table 8: NiO and Ni°crystallite sizes obtained for the 15Ni1X catalysts after calcination and reduction.

Catalyst	dNiO (nm)	dNi^0 (nm)
15Ni	21	-
$15Ni_{Red}$	-	18
15Ni1Co	21	-
$15Ni1Co_{Red}$	-	19
15Ni1Cu	23	-
$15Ni1Cu_{Red}$	-	19
15Ni1Fe	21	-
$15Ni1Fe_{Red}$	-	n.a.

As can be ascertained by table 8, the incorporation of Cu and Co did not lead into improvements on grain size, whilst for the Fe incorporation, the interactions between this metal and Ni led to an inferior reducibility of NiO, thus making the reduction temperature (of 470 °C) insufficient to entirely reduce these oxides. Hence, it is expected that the addition of Fe has generated an improvement on the metallic dispersion, which may explain why Fe is the most interesting promoter.

4.2.2 H_2-TPR

In terms of H_2-TPR profiles, presented in Figure 23, it can be observed that the most remarkable reduction processes occur below the pre-reduction temperature (470 °C) for the 15Ni1X catalysts. In this way, by comparing the reduction extent below 470 °C, one can clearly observe that the weakest metal-support interactions, inducing reduction processes at lower temperatures, were established on 15Ni1Cu catalyst, followed by 15Ni1Co and, finally, 15Ni1Fe. This suggests that, while in 15Ni1Cu catalyst the oxides will be

fully reduced during the pre-treatment, unreduced species will be expectedly present in Co and, especially, Fe-containing samples. The stronger metal-support interactions found in 15Ni1Fe could be responsible for the clear coexistence of NiO and Ni°diffraction peaks in 15Ni1Fe diffractogram.

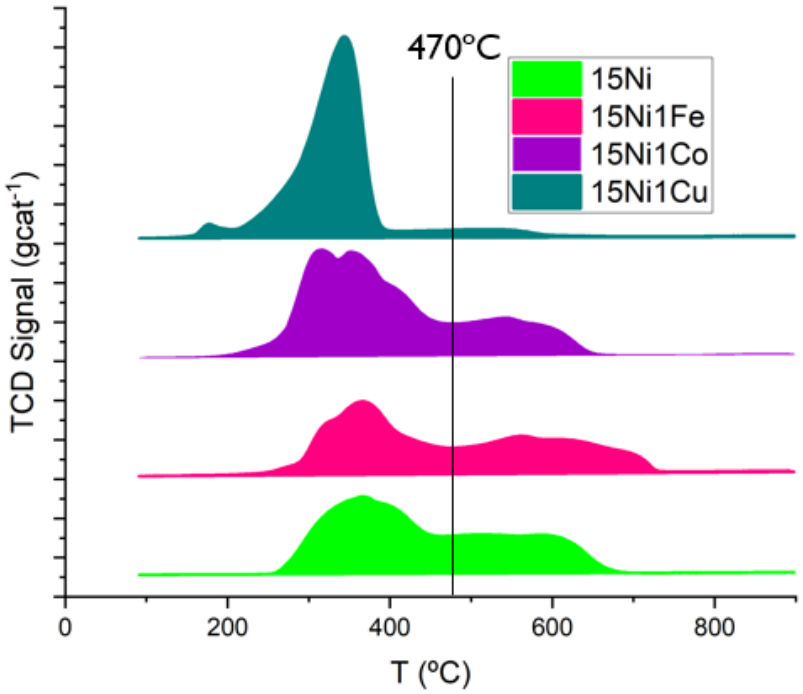

Figure 23: H_2-TPR profiles obtained for 15Ni1X catalysts.

4.2.3 TGA

In terms of hydrophobic character, again characterized by TGA through the calculation of h indexes (Table 9), it is clear that the incorporation of Cu, Co or Fe to the Ni-catalyst formulation did not lead to remarkable effects. Indeed, it is observed that h indexes are close to 1 (0.93-0.95) in all cases, indicating that all materials are highly hydrophobic.

Table 9: Hydrophobic indexes obtained for 15Ni1X catalysts.

Sample	h index
15Ni	0.95
15Ni1Cu	0.93
15Ni1Co	0.93
15Ni1Fe	0.94

4.2.4 TEM

In terms of TEM microscopy results (Figure 24), the incorporation of a second transition metal seems to induce a better distribution of the Ni°particles over the zeolite, especially when comparing the obtained micrographs with that presented for the monometallic Ni catalyst. In addition, when comparing among the bimetallic series, no remarkable changes in terms of Ni°particle sizes can be observed, in agreement with the crystallite sizes determined from XRD data applying Scherrer's equation. However, the presence of smaller particles can be suggested in 15Ni1Fe.

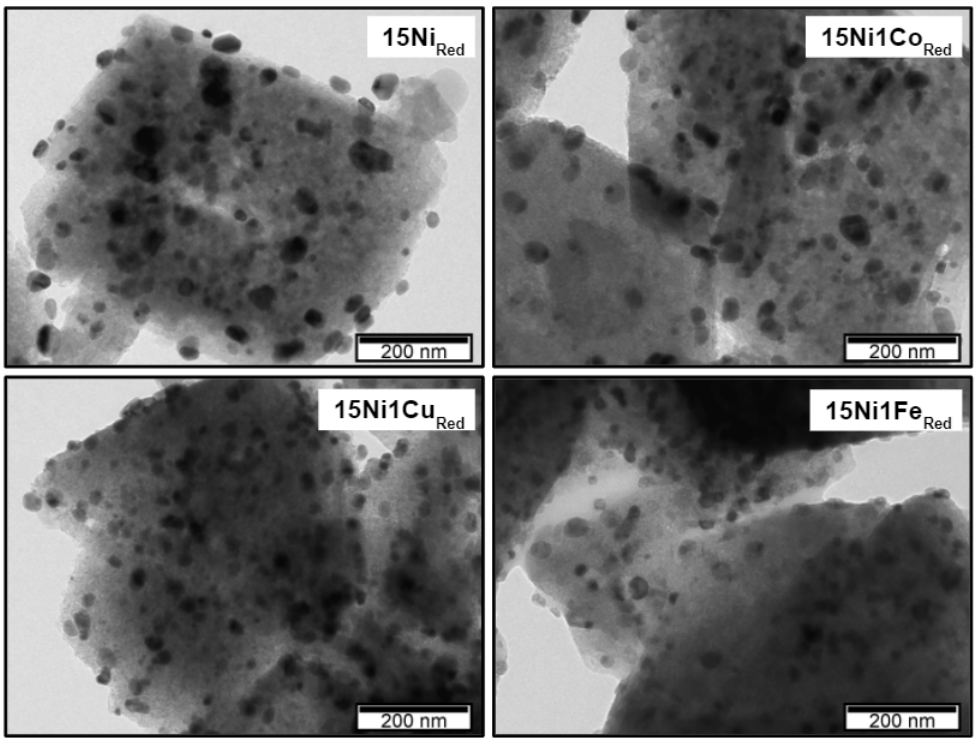

Figure 24: Images of each catalyst corresponding to the second study, obtained through Transmission Electron Microscopy, after their respective reduction.

4.2.5 Catalytic Results

In terms of catalytic performances, analyzed in terms of CO_2 conversions and CH_4 selectivity in Figure 25, it is clear that the incorporation of 1 wt% of Cu induced a significant reduction of the achieved activity. This effect could be due to the weakening of the metal-support interactions (H_2-TPR), which increases reducibility, and the lack of enhancements in terms Ni°particle size (XRD, TEM). Furthermore, Co incorporation, which did not induce changes in the metal-support interactions nor the average Ni°particle size, did not report significant changes in terms of performances, being the results similar to those exhibited by the monometallic 15Ni catalyst. Finally, 15Ni1Fe was the catalyst inducing the best performances, with a remarkable improvement of the CO_2 conversion and CH_4 selectivity in the 250 – 380 °C temperature range. This positive influence derived from Fe addition reveal the existence of potential beneficial synergies between both metals, resulting in stronger metal-support interactions and an enhancement in the dispersion of Ni°particles over the zeolite.

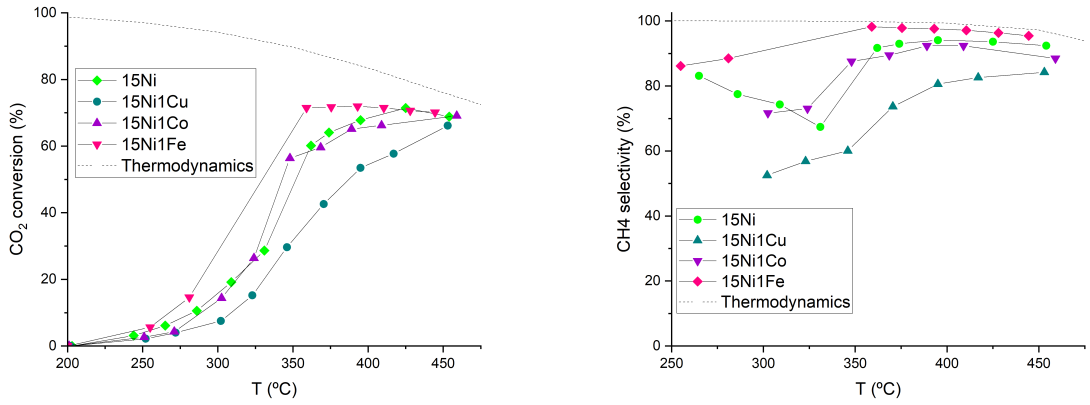

Figure 25: Methanation test results for each one of the bimetallic samples of the second study. In which each graph corresponds to a) CO_2 conversion; and b) CH_4 selectivity.

In addition, CH_4 yields were calculated and presented in Figure 26, to allow a proper comparison among the catalysts from this study. It is clear that results follow the order: 15Ni1Fe > 15 Ni ≈ 15Ni1Co > 15Ni1Cu. Since 15Ni1Fe proved to ascertain the best results, this catalyst was used as reference for the third study, and the content of Fe was then varied in order to determine which one would be optimal.

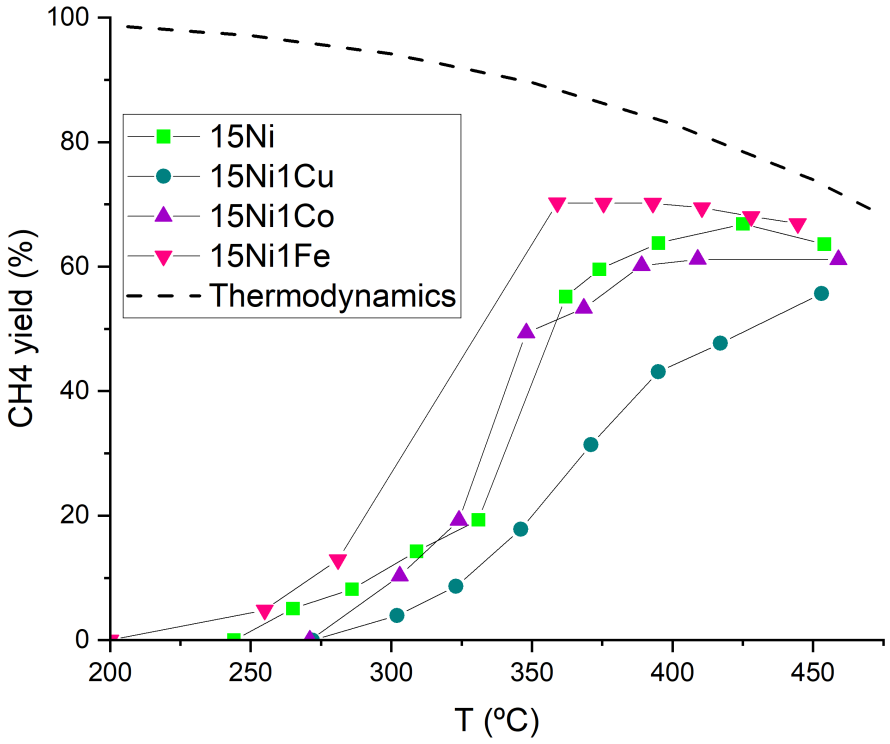

Figure 26: Methane yield obtained for each one of the bimetallic catalysts.

4.2.6 XRD of spent catalysts

As previously done for 15X catalysts, 15Ni1X spent samples were characterized by XRD, being the patters presented in Figure 27. As observed, FAU zeolite peaks can be found in all catalysts, indicating that the structure was preserved during the tests. In addition, the presence of Ni°peaks is clear in all cases, including the 15Ni1Fe samples, which exhibited both NiO and Ni°diffraction peaks after reduction (due to its lack of complete reduction). Thus, this indicates that unreduced NiO species in 15Ni1Fe were fully reduced during the test in presence of hydrogen. By applying Scherrer's equation it was possible to estimate the average Ni°crystallite sizes in spent samples, being the values similar (differences inferior to 2 nm) to those found in reduced catalysts. This is indicative of the lack of remarkable sintering processes occurring in the 15Ni and 15Ni1X series during the catalytic tests. Finally, it must be pointed out that in the case of 15Ni1Fe, for which Scherrer's equation was not applied in the reduced form, the average Ni°crystallite size in the spent catalyst was 16 nm, slightly lower than the obtained for 15Ni (18 nm), 15Ni1Co (20 nm) and 15Ni1Cu (21 nm), confirming the positive impact of Fe in the metallic dispersion.

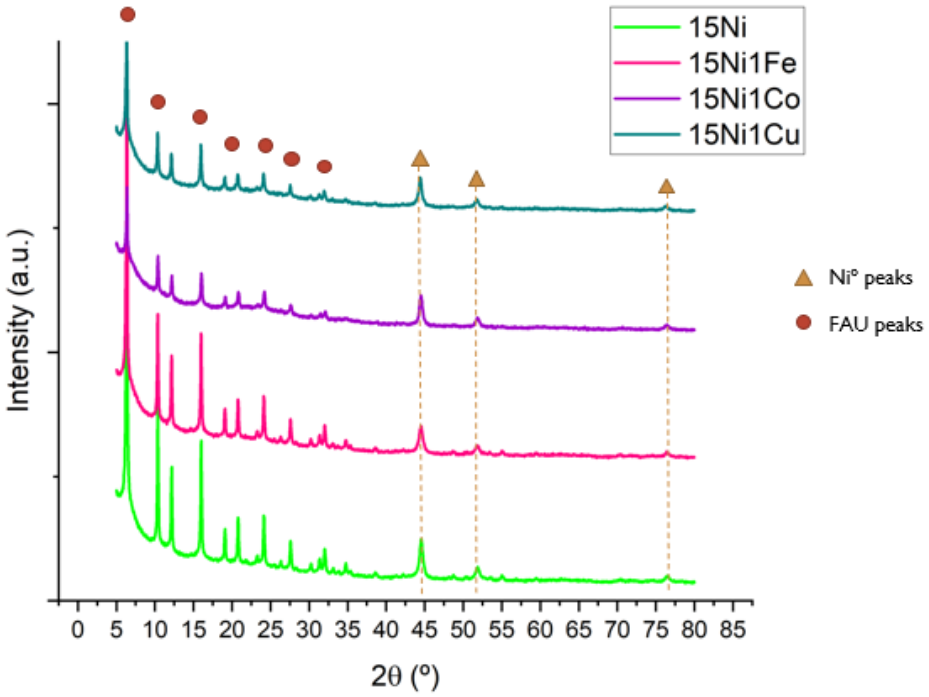

Figure 27: XRD patterns for spent 15Ni1X samples.

4.3 Effect of Fe Loading

4.3.1 XRD

As can be ascertained by the XRD patterns of 15NixFe catalysts exhibited in Figure 28, the variation of the Fe loading did not significantly affect the results. As so, FAU diffraction peaks are clearly observed in all samples, while NiO and Ni°diffraction peaks can be found in calcined and reduced catalysts patterns, respectively. In the case of 15Ni1Fe, as previously discussed in this work, both NiO and Ni°peaks can be found after reduction, while this behavior did not occur in the 15Ni2Fe and 15Ni3Fe samples. To be pointed out is that, despite the increase in the incorporated Fe loading, no peaks ascribed to iron oxides could be observed in the samples, which could be related to the low loadings and/or the high dispersion of these species over the support. By applying Scherrer's equation, Ni°crystallite sizes were again determined and presented in Table 10. As observed, the increase of Fe loading led to a progressive decrease in NiO and Ni°average crystallite sizes, indicating a positive impact of this metal on this parameter.

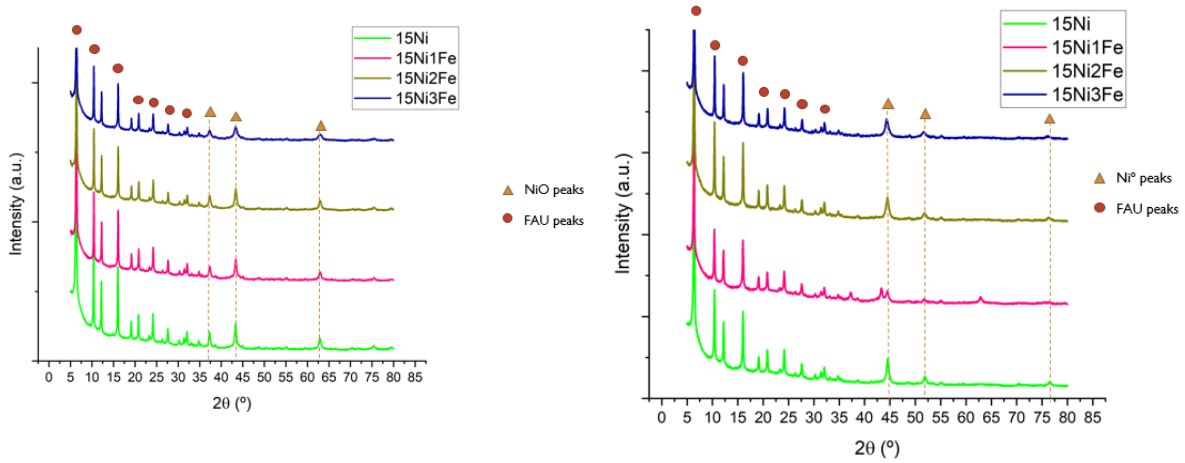

Figure 28: X-Ray Diffractograms for the calcined (on the left) and reduced (on the right) samples, for the third study.

Table 10: NiO and Ni°crystallite sizes obtained for the 15NixFe catalysts after calcination and reduction.

Catalyst	d_{NiO} **(nm)**	d_{Ni° **(nm)**
15Ni	21	-
$15Ni_{Red}$	-	18
15Ni1Fe	21	-
$15Ni1Fe_{Red}$	-	n.a.
15Ni2Fe	16	-
$15Ni2Fe_{Red}$	-	14
15Ni3Fe	12	-
$15Ni3Fe_{Red}$	-	13

4.3.2 H_2-TPR

In terms of reducibility, characterized by H_2-TPR, by observing the profiles presented in Figure 29 it is possible to infer that increasing the Fe loading leads to a displacement of the reduction peaks towards lower temperatures. Consequently, it is expected that the pre-reduction step at 470°C will lead to a greater presence of metallic species in the catalysts, justifying the absence of NiO diffraction peaks in the patterns of reduced 15Ni2Fe and 15Ni3Fe catalysts, contrary to what found for reduced 15Ni1Fe.

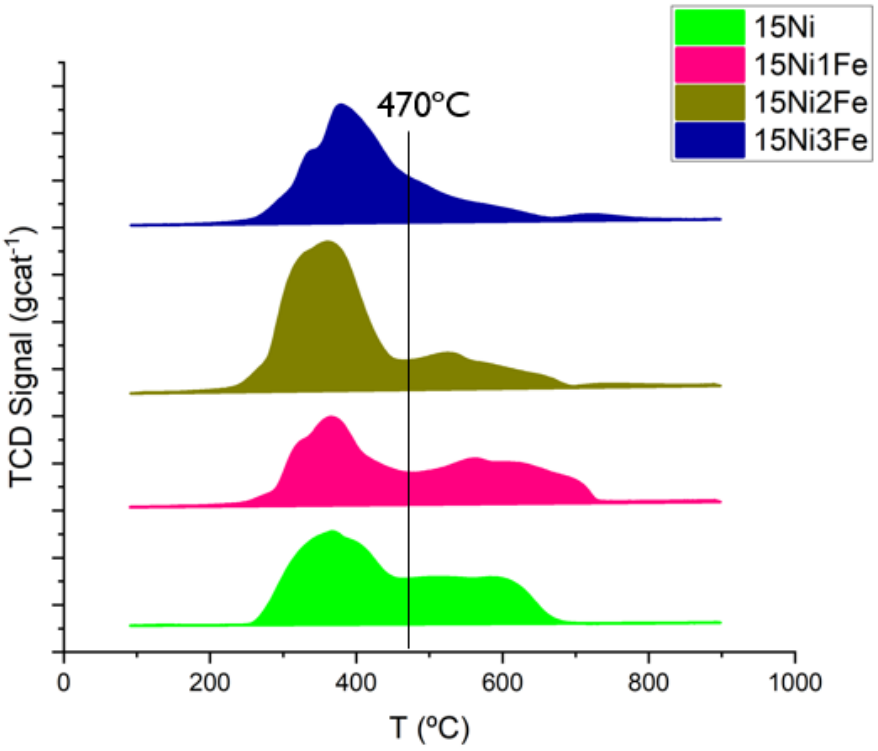

Figure 29: H_2-TPR profiles obtained for 15NixFe catalysts.

4.3.3 TGA

In terms of hydrophobic properties (TGA analysis, Table 11), the calculated h indexes reveal that all Fe-containing catalysts present weak interactions with water molecules (h indexes > 0.90 in all cases). However, the increase of Fe loading seems to lead to a more hydrophilic character, as the h index presented by 15Ni3Fe is the lowest from the series.

Table 11: Hydrophobic indexes obtained for 15NixFe catalysts.

Sample	h index
15Ni	0.95
15Ni1Fe	0.94
15Ni2Fe	0.95
15Ni3Fe	0.92

4.3.4 TEM

TEM micrographs were also collected for 15NixFe catalysts after reduction at 470 °C (Figure 30). As observed, the increase of the iron content appears to reduce the particle sizes of Ni°, in accordance with XRD results previously discussed. In addition, a more homogeneous distribution of Ni°particles is observed for higher Fe loadings, especially when comparing with the monometallic 15Ni.

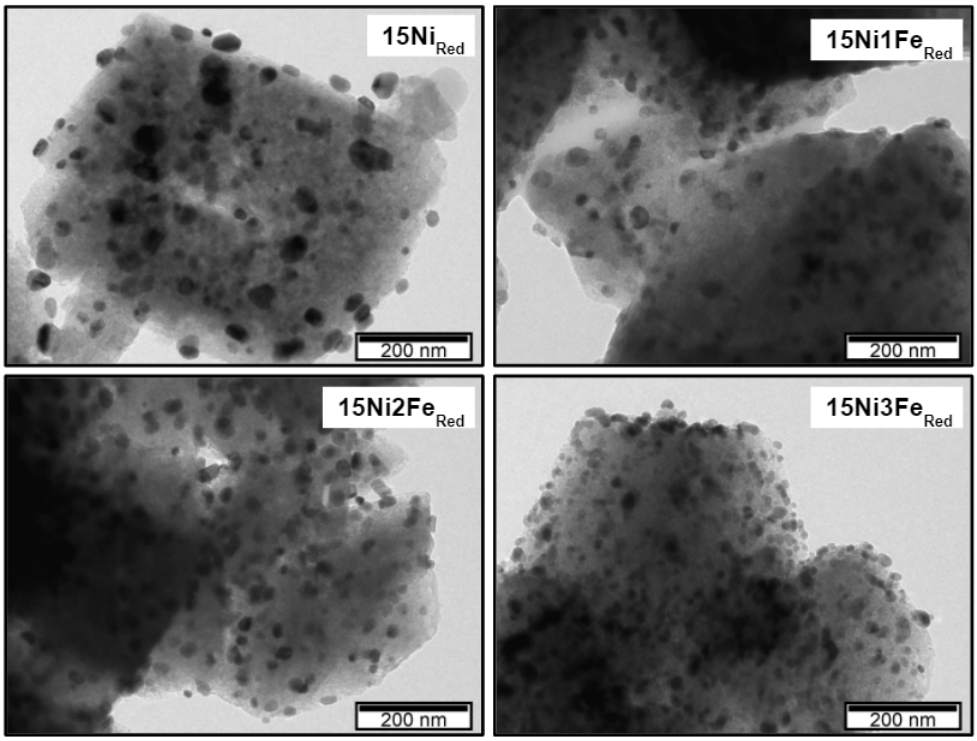

Figure 30: TEM micrographs obtained for 15NixFe catalysts after reduction at 470 °C.

4.3.5 Catalytic Results

Concerning the influence of Fe loading in the catalytic performances of 15NixFe samples, shown in Figure 31, it is clear that all Fe-containing catalysts exhibit higher methane selectivity than 15Ni. In terms of CO_2 conversion, increasing Fe loading leads to a reduction of the activity. In spite of the reduction in the Ni°particle sizes with the addition of increasing Fe loadings, the lack of catalytic enhancements in 2 and 3 wt% Fe samples could be due to the weakening of the metal-support interactions verified by H_2-TPR. To be pointed out is the activity tendency below 350 °C. Indeed, in this region 15Ni2Fe catalyst exhibited the best results. On the contrary, for temperatures above 350 °C, 15Ni1Fe sample portrays the most active catalyst. This could indicate that the metal-support interactions could present a predominant role at higher temperatures, while the metallic dispersion could be more relevant at lower temperatures. In the case of 15Ni3Fe, despite the lower Ni°particle size, the slightly lower hydrophobicity and weaker metal-support interactions could be in the origin of the displayed performances.

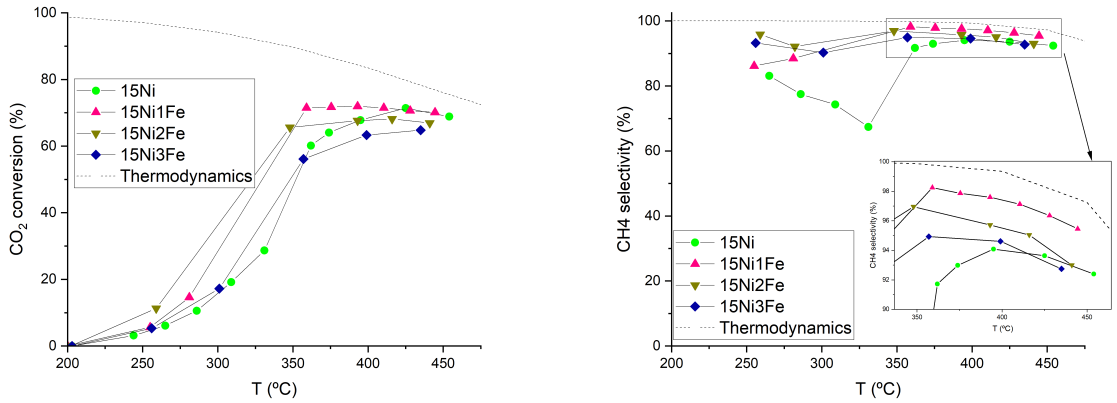

Figure 31: Methanation test results for the iron-based bimetallic samples of the third study. In which each graph corresponds to a) CO_2 conversion; and b) CH_4 selectivity.

In addition, the methane yields obtained for 15NixFe catalysts are shown in Figure 32. Despite the lower reducibility of the metal oxides below 470 °C (as was previously seen in section 4.2.2 of the present report), 15Ni1Fe obtained the best results, suggesting the establishment of promising synergies between iron and the nickel species in this sample. In addition, the lack of results for this sample in the range of temperature of 280 and 360 °C is due to the fact that since the reaction is exothermic, the high conversion rate in this region results in an overheating of the catalytic bed, precluding the temperature measurement in between that specific range.

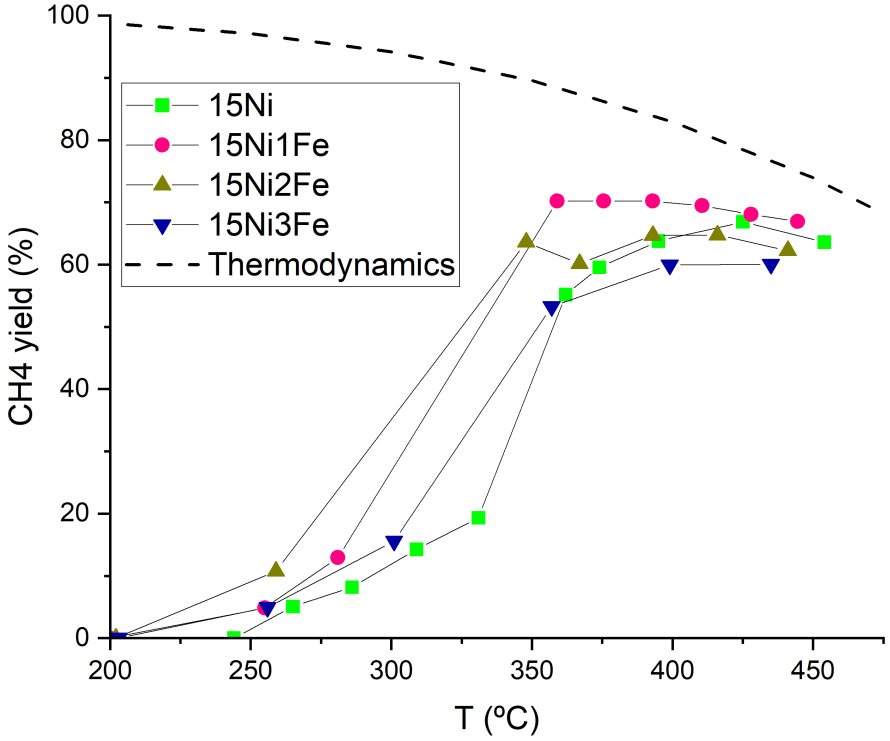

Figure 32: Methane yield obtained for each one of the iron-based bimetallic catalysts.

4.3.6 XRD of spent catalysts

As done in the previous chapters, spent samples were analyzed by XRD, being the collected patterns presented in Figure 33. As observed, both FAU zeolite and Ni°diffraction peaks can be found in the catalysts, and the determined Ni°crystallite sizes were similar (differences <1 nm) to those calculated for reduced catalysts.

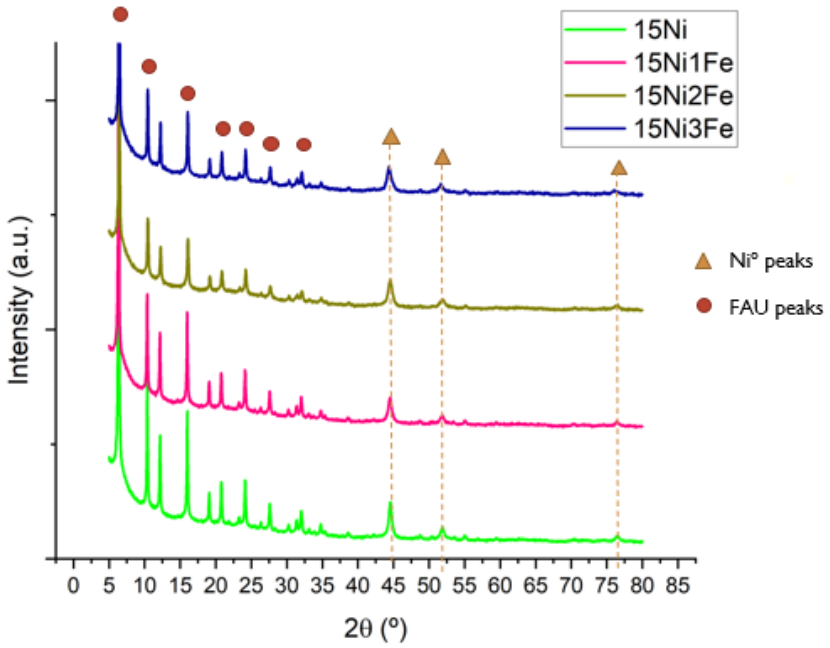

Figure 33: X-Ray Diffractograms for the spent samples belonging to the third study.

5 Conclusions and Future Perspectives

The utilization of carbon dioxide for the production of methane constitutes a promising alternative inserted in the concept of *Power-to-Gas*. Although, in most cases, the processes of feed purification and outlet upgrading are necessary, and thus costly, the value-added chemicals produced constitute an interest-rich alternative, both promising in economical and in ecological terms. However, on an economical study performed for the present process (in section 7.2), the conclusion was drawn that until the price of production for green hydrogen is lowered, the CO_2 methanation process can only be viable using hydrogen produced through fossil fuels, thus defeating its ecological principle.

The CO_2 methanation process has been thoroughly studied and zeolite-based catalysts have been showing promising results, mainly due to their highly adjustable properties and their high stability. In terms of active metals, mainly Ni-promoted zeolites have been reported. Thus, analyzing the effect of using alternative transition metals in the formulation of these catalysts can constitute an interesting research topic.

In this thesis, studies were carried out with the aim of identifying the potential utilization of Ni, Fe, Co and Cu as active metals for zeolite-based CO_2 methanation catalysts. In this way, and using a previously optimized USY zeolite as support, three series of catalysts were synthesized: (i) 15X catalysts (where X=Ni, Co, Cu or Fe), to compare among the four transition metals; (ii) 15Ni1X catalysts (where X=Co, Cu or Fe), to evaluate the effect of doping the Ni-based zeolite catalyst with low loadings of other transition metals; and (iii) 15NixFe (where x=1, 2 and 3 wt%), to analyze the effect of Fe loading.

Through the first study of the series, nickel proved to be the most active metal on itself, which was attributed to its well-known suitability towards carbon dioxide methanation and favored metallic dispersion. On the second study, 15Ni1Fe exhibited the highest performances, which was attributed to the establishment of proper synergies between the metals, improving the metal-support interactions and favoring the metallic dispersion. In the third study, it was concluded that both 15Ni1Fe and 15Ni2Fe had their own set of temperature range for which they were the most outstanding materials. However, the use of lower Fe loadings was found as more suitable, which was attributed to a slight reduction of the catalysts hydrophobicity and weakening of the metal-support interactions with higher Fe contents.

In a retrospective analysis of the current study, some improvements and future developments towards a better understanding of this system could be performed.

One of these corresponds to the **impregnation solvent** used. In a previous work developed by Bacariza *et al.* [141], where multiple impregnation solvents were tested for the preparation of nickel-supported zeolite catalysts, 2-propanol was found as responsible for an important enhancement of the metallic dispersion and, consequently, the catalytic performances. In the present work, distilled water was chosen as impregnation solvent for being the cheapest, and easiest to obtain, however the substitution of solvent to propanol could be potentially beneficial for the catalyst's activity.

Another possible alteration that could be tested would be the metals **impregnation order**, or even through the study of different **preparation methods**. This would be an important study due to the fact that iron has a really small quantity, and the separation of these impregnations could generate interesting phenomenon, since it could lead to the generation of different types of interactions or even alloy formations, which have proved better results already. [93]

Complementary **characterization methodologies** should be adopted besides the ones already considered. One of those would have to be Diffuse Reflectance Spectroscopy for the Ultraviolet and Visible region (DRS UV-Vis), in order to get more information regarding the type of metal species present in the catalysts. [59] Another methodology that could be performed is Chemical Analysis by Inductively Coupled Plasma (ICP Analysis), to confirm that the intended metals loadings were achieved. [143] Finally, characterizing the basicity of the catalysts by CO_2 temperature programmed desorption (CO_2-TPD) will be valuable to identify potential impacts of the metal's nature and loadings in this property. Also, Mössbauer Spectroscopy, where a solid sample is exposed to a beam of gamma rays, whilst a detector measures the intensity of the beam transmitted through the sample. The Mössbauer spectroscopy has an extremely fine energy resolution, thus allowing for the detection of small changes in the nuclear vicinities of the relevant atom. [144] The Mössbauer spectroscopy is usually used to characterize phase transformations in iron catalysts [145], and can give thorough information on which state of iron is found in the catalyst (whether it's Fe^0, Fe^{+2} or Fe^{+3}), as well as the type of coordination polyhedron is occupied by the iron atoms (e.g. triagonal, tetrahedral, octahedral). It can also be used to assist in the identification of iron oxide phases through the study of their magnetic properties. [146]

Yet another possible alteration would be to use an **inert within the catalytic bed**, in the reactor. This inert

could be such as silicon carbide (more commonly known as carborundum), although others have been used such as silica or alumina. However those would not behave as inert as they are commonly used as support for CO_2 methanation catalysts. This would be beneficial because it would avoid the overheating of the oven, thus affecting the temperature control and leading to important gaps in the reaction temperatures able to analyze.

In addition, and taking into account that this thesis was intended to be carried out at Sorbonne Université (Paris, France) with the aim of carrying out **plasma catalysis** experiments but this was not possible due to the COVID-19 pandemic, a further study where the most active catalysts could be tested under these non-conventional conditions is proposed. Plasma catalysis allows for an easier activation of CO_2 molecules, thus allowing for a more energetically efficient process. The combination of plasma and catalysts could create powerful synergies and thus present an even higher catalytic performances.

6 References

[1] IPCC, 2013: Climate Change 2013: The Physical Science Basis. Contribution of Working Group I to the Fifth Assessment Report of the Intergovernmental Panel on Climate Change [Stocker, T.F., D. Qin, G.-K. Plattner, M. Tignor, S.K. Allen, J. Boschung, A. Nauels, Y. Xia, V. Bex and P.M. Midgley (eds.)]. Cambridge University Press, Cambridge, United Kingdom and New York, NY, USA, 1535 pp.

[2] https://www.nationalgeographic.com/environment/global-warming/greenhouse-gases/ (consulted at 25/08/2021)

[3] Jurikova, H., Gutjahr, M., Wallmann, K. *et al.* Permian–Triassic mass extinction pulses driven by major marine carbon cycle perturbations. Nat. Geosci. 13, 745–750 (2020).

[4] Climate Change 2014: Synthesis Report. Contribution of Working Groups I, II and III to the Fifth Assessment Report of the Intergovernmental Panel on Climate Change. Core Writing Team, Pachauri, R.K., Meyer, L.A., Eds.; IPCC: Geneva, Switzerland, 2014.

[5] Earth's carbon dioxide levels on a daily basis. https://www.co2.earth/daily-co2 (consulted at 06/07/2021)

[6] Bill Gates How to Avoid a Climate Disaster Alfred A. Knopf, february 2021

[7] Pierre Friedlingstein *et al.* Global Carbon Budget 2020 Earth Syst. Sci. Data, 12, 3269–3340, 2020

[8] United Nations for Climate Change "The Paris Agreement" https://unfccc.int/process-and-meetings/the-paris-agreement/the-paris-agreement (consulted at 12/06/2021)

[9] Pierre Friedlingstein *et al.* Global Carbon Budget 2019 Earth Syst. Sci. Data, 11, 1783–1838, 2019

[10] https://ourworldindata.org/explorers/energy?tab=chartcountry=USA GBR CHN OWID_WRL IND BRA ZAFTotal+or+Breakdown=TotalEnergy+or+Electricity=Primary+energyMetric=Per+capita+consumption (consulted at 15/04/2021)

[11] C. Vogt, M. Monai, E. B. Sterk, J. Palle, A. E.M. Melcherts, B. Zijlstra, E. Groeneveld, P. H. Berben, J. M. Boereboom, E. J. M. Hensen, F. Meirer, I. A. W. Filot, B. M. Weckhuysen Understanding carbon dioxide activation and carbon–carbon coupling over nickel Nature Communications (2019) 10:5330

[12] Snoeckx, R.; Bogaerts, A. Plasma Technology - a Novel Solution for CO_2 Conversion? Chem. Soc. Rev. 2017, 46, 5805−5863.

[13] Vogt, C., Monai, M., Kramer, G. J. Weckhuysen, B. M. The renaissance of the Sabatier reaction and its applications on earth and in space. Nat. Catal. 2, 188–197 (2019).

[14] Pielke RA. An idealized assessment of the economics of air capture of carbon dioxide in mitigation policy. Environ Sci Policy 2009;12(3):216–25.

[15] Z. Abdin, K. Khalilpour, Single and Polystorage Technologies for Renewable-Based Hybrid Energy Systems, Polygeneration with Polystorage for Chemical and Energy Hubs, Academic Press, 2019, Pages 77-131.

[16] Q. Sun, H. Li, J. Yan, L. Liu, Z. Yu, X. Yu, Selection of appropriate biogas upgrading technology-a review of biogas cleaning, upgrading and utilisation, Renewable and Sustainable Energy Reviews, Vol. 51, 2015, P. 521-532

[17] M. A. A. Aziz, A. A. Jalil, S. Triwahyonoc and A. Ahmada, CO_2 methanation over heterogeneous catalysts: recent progress and future prospects Green Chem., 2015,17, 2647-2663.

[18] J. Kopyscinski, T.J. Schildhauer, S.M.A. Biollaz, Production of synthetic natural gas (SNG) from coal and dry biomass – A technology review from 1950 to 2009, Fuel 89 (2010) 1763–1783.

[19] Westermann A., Azambre B., Bacariza M.C., Graça I., Ribeiro M.F., Lopes J.M., Henriques C. (2015). Insight into CO_2methanation mechanism over NiUSY zeolites: Anoperando IR study. Appl Catal Environ B 174–175, 120–125

[20] Yentekakis, I.V.; Dong, F. Grand Challenges for Catalytic Remediation in Environmental and Energy Applications toward a Cleaner and Sustainable Future. Front. Environ. Chem. 2020, 1, 5.

[21] Press, R. J.; Santhanam, K. S. V.; Miri, M. J.; Bailey, A. V.; Takacs, Gerald A. (2008). Introduction to hydrogen Technology. John Wiley Sons. p. 249. ISBN 978-0-471-77985-8.

[22] https://4thgeneration.energy/life-cycles-emissions-of-hydrogen/ (consulted at 29/09/2021)

[23] Liu, K.; Song, C.; Subramani, V. (2009). Hydrogen and Syngas Production and Purification Technologies. ISBN: 9780470561256 American Institute of Chemical Engineers

[24] https://afdc.energy.gov/fuels/hydrogen_production.html (consulted at 29/09/2021)

[25] https://afdc.energy.gov/fuels/hydrogen_basics.html (consulted at 29/09/2021)

[26] https://www.bbc.com/news/world-europe-55931873 (consulted at 29/09/2021)

[27] Dr. U. Bünger, H. Landinger, E. Pschorr-Schoberer, P. Schmidt, W. Weindorf, J. Jöhrens, U. Lambrecht, K. Naumann, A. Lischke. "Power-to-Gas (PtG) in transport: Status quo and perspectives for development" Munich, Heidelberg, Leipzig, Berlin, 11 June 2014

[28] Martin Thema, Tobias Weidlich, Manuel Hörl, Annett Bellack, Friedemann Mörs, Florian Hackl, Matthias Kohlmayer, Jasmin Gleich, Carsten Stabenau, Thomas Trabold, Michael Neubert, Felix Ortloff, Raimund Brotsack, Doris Schmack, Harald Huber, Doris Hafenbradl, Jürgen Karl and Michael Sterner Biological CO_2-Methanation: An Approach to Standardization 1 May 2019 Energies 2019, 12, 1670

[29] S. Patel "Why Power-to-Gas May Flourish in a Renewables-Heavy World" (2019) https://www.powermag.com/why-power-to-gas-may-flourish-in-a-renewables-heavy-world/ (consulted at 06/06/2021)

[30] T. Schaaf, J. Grünig, M. R. Schuster, T. Rothenfluh, and A. Orth. Methanation of CO_2 - storage of renewable energy in a gas distribution system. Energy. Sustain. Soc., vol. 4, pp. 1–14, 2014.

[31] "STOREGO" https://www.storeandgo.info/ (consulted at 09/10/2021)

[32] L. Biacchi, Recovery of excess heat from methanation into WoodRoll® gasification and modelling of an integrated heat and mass balance 2015

[33] B. Khudenko, G. Gitman, and T. Wechsler Oxygen Based Claus Process for Recovery of Sulfur from H_2S Gases Journal of Environmental Engineering, Vol. 119 I. 6 - 1993

[34] S. Alexander, J. Winnick Removal of hydrogen sulfide from natural gas through an electrochemical membrane separator AIChE Journal, Vol. 40, I. 4 p. 613-620

[35] Amvrosios G. Georgiadis, Nikolaos D. Charisiou and Maria A. Goula Removal of Hydrogen Sulfide From Various Industrial Gases: A Review of The Most Promising Adsorbing Materials Catalysts 2020, 10, 521

[36] D. Chiche, C. Diverchy, A.-C. Lucquin, F. Porcheron, F. Defoort. Synthesis Gas Purification. Oil Gas Science and Technology - Revue d'IFP Energies nouvelles, Institut Français du Pétrole, 2013, 68 (4), pp.707-723.

[37] S. Sridhar, B. Smitha T. M. Aminabhavi (2007) Separation of Carbon Dioxide from Natural Gas Mixtures through Polymeric Membranes—A Review, Separation Purification Reviews, 36:2, 113-174.

[38] Nayef Ghasem. Chapter 21 - CO_2 removal from natural gas. Advances in Carbon Capture, Woodhead Publishing, 2020, Pages 479-501, ISBN 9780128196571.

[39] M. Vaccarelli, R. Carapellucci, L. Giordano, Energy and economic analysis of the CO_2 capture from flue gas of combined cycle power plants, Energy Procedia 45 (2014) 1165–1174

[40] R. Ahmed, G. Liu, B. Yousaf, Q. Abbas, H. Ullah, M.U. Ali, Recent advances in carbon-based renewable adsorbent for selective carbon dioxide capture and separation—a review, J. Clean. Prod. 242 (2020) 118409

[41] Vogt, C., Monai, M., Sterk, E.B. *et al.* Understanding carbon dioxide activation and carbon–carbon coupling over nickel. Nat Commun 10, 5330 (2019).

[42] Vogt, C. *et al.* Unravelling structure sensitivity in CO_2 hydrogenation over nickel. Nat. Catal. 1, 127–134 (2018).

[43] P.A. Ussa Aldana, F. Ocampo, K. Kobl, B. Louis, F. Thibault-Starzyk, M. Daturi, P. Bazin, S. Thomas, A.C. Roger, Catalytic CO_2 valorization into CH_4 on Ni-based ceria-zirconia. Reaction mechanism by operando IR spectroscopy, Catalysis Today, Volume 215, 2013, Pages 201-207, ISSN 0920-5861.

[44] Behrens, M. *et al.* The active site of methanol synthesis over Cu/ZnO/Al2O3. Science 336, 893–898 (2012).

[45] Liu, X. *et al.* Effective and highly selective CO generation from CO_2 using a polycrystalline -Mo2C catalyst. ACS Catal. 7, 4323–4335 (2017)

[46] Posada-Perez, S. *et al.* Highly activeAu/-MoC and Cu/-MoC catalysts for the conversion of CO_2: The metal/C ratio as a key factor defining activity, selectivity, and stability. J. Am. Chem. Soc. 138, 8269–8278 (2016).

[47] Wang, Y. *et al.* Exploring the ternary interactions in Cu-ZnO-ZrO2 catalysts for efficient CO_2 hydrogenation to methanol. Nat. Commun. 10, 1166 (2019).

[48] Ma, Z. Porosoff, M. D. Development of tandem catalysts for CO_2 hydrogenation to olefins. ACS Catal. 9, 2639–2656 (2019).

[49] Zhao, B., Liu, Y., Zhu, Z., Guo, H. Ma, X. Highly selective conversion of CO_2 into ethanol on Cu/ZnO/Al2O3 catalyst with the assistance of plasma. J. CO 2 Util. 24, 34–39 (2018).

[50] Lam, E. *et al.* Isolated Zr surface sites on silica promote hydrogenation of CO_2 to CH3OH in supported Cu catalysts. J. Am. Chem. Soc. 140, 10530–10535 (2018).

[51] Liu, X. *et al.* Selective transformation of carbon dioxide into lower olefins with a bifunctional catalyst composed of ZnGa2O4 and SAPO-34. Chem. Commun. 54, 140–143 (2018).

[52] Tsoukalou, A. *et al.* Structural evolution and dynamics of an In2O3 Catalyst for CO_2 hydrogenation to methanol: an operando XAS-XRD and in situ TEM study. J. Am. Chem. Soc. 141, 13497–13505 (2019).

[53] Dang, S. *et al.* Role of zirconium in direct CO_2 hydrogenation to lower olefins on oxide/zeolite bifunctional catalysts. J. Catal. 364, 382–393 (2018).

[54] F. Azzolina-Jury, F. Thibault-Starzyk, Mechanism of low pressure plasma-assisted CO_2 hydrogenation over Ni-USY by microsecond time-resolved FTIR spectroscopy, Top. Catal. (2017) 1–13.

[55] F. Azzolina-Jury, D. Bento, C. Henriques, F. Thibault-Starzyk Chemical engineering aspects of plasma-assisted CO_2 hydrogenation over nickel zeolites under partial vacuum Journal of CO_2 Utilization 22 (2017) 97–109

[56] Jiajian Gao, Yingli Wang, Yuan Ping, Dacheng Hu, Guangwen Xu, Fangna Gu and Fabing Su. A thermodynamic analysis of methanation reactions of carbon oxides for the production of synthetic natural gas. RSC Adv., 2012,2, 2358-2368

[57] Ye, RP., Ding, J., Gong, W. *et al.* CO_2 hydrogenation to high-value products via heterogeneous catalysis. Nat Commun 10, 5698 (2019).

[58] Jin, F. *et al.* High-yield reduction of carbon dioxide into formic acid by zero-valent metal/metal oxideredox cycles. Energ. Environ. Sci. 4, 881–884 (2011)

[59] Sun, Y. *et al.* In situ hydrogenation of CO_2 by Al/Fe and Zn/Cu alloy catalysts under mild conditions. Chem. Eng. Technol. 42, 1223–1231 (2019).

[60] Lyu, L., Zeng, X., Yun, J., Wei, F. Jin, F. No catalyst addition and highly efficient dissociation of H_2O for the reduction of CO_2 to formic acid with Mn. Environ. Sci. Technol. 48, 6003–6009 (2014)

[61] Zhong, H. *et al.* Selective conversion of carbon dioxide into methane with a 98% yield on an in situ formed Ni nanoparticle catalyst in water. Chem. Eng. J. 357, 421–427 (2019).

[62] Yang, Y. *et al.* Synergetic conversion of microalgae and CO_2 into value-added chemicals under hydrothermal conditions. Green Chem. 21, 1247–1252 (2019).

[63] P. J. Lunde and F. L. Kester, Carbon Dioxide Methanation on a Ruthenium Catalyst Ind. Eng. Chem. Process Des. Dev., 1974, 13, 27.

[64] T. Inui, T. Takeguchi, Effective conversion of carbon dioxide and hydrogen to hydrocarbons, Catalysis Today, Volume 10, Issue 1, 1991, Pages 95-106, ISSN 0920-5861.

[65] G. Centi, E. A. Quadrelli and S. Perathoner, Catalysis for CO_2 conversion: a key technology for rapid introduction of renewable energy in the value chain of chemical industries. Energy Environ. Sci., 2013, 6, 1711–1731.

[66] Ye, RP., Ding, J., Gong, W. *et al.* CO_2 hydrogenation to high-value products via heterogeneous catalysis. Nat Commun 10, 5698 (2019). https://doi.org/10.1038/s41467-019-13638-9

[67] Liu, X.; Lu, G.; Yan, Z.; Beltramini, J. Recent Advances in Catalysts for Methanol Synthesis via Hydrogenation of CO and CO_2. Ind. Eng. Chem. Res. 2003, 42, 6518−6530.

[68] Bansode, A.; Tidona, B.; von Rohr, P. R.; Urakawa, A. Impact of K and Ba Promoters on CO_2 Hydrogenation over Cu/Al2O3 Catalysts at High Pressure. Catal. Sci. Technol. 2013, 3, 767−778.

[69] S. G. Jadhav, P. D. Vaidya, B. M. Bhanage and J. B. Joshi, Catalytic carbon dioxide hydrogenation to methanol: A review of recent studies. Chem. Eng. Res. Des., 2014, 92, 2557–2567.

[70] Manfred Müller, Ute Hübsch, “Dimethyl Ether” in Ullmann’s Encyclopedia of Industrial Chemistry, Wiley-VCH, Weinheim, 2005

[71] Liu, Y.; Q. Fu; M.F. Stephanopoulos (1 September 2004). "Preferentialoxidation of CO in H_2 over CuO-CeO2 catalysts". Catalysis Today. 93–95: 241–246.

[72] Gokhale, A. A.; Dumesic, J. A.; Mavrikakis, M. (2008-01-01). "On the Mechanism of Low-Temperature Water Gas Shift Reaction on Copper". Journal of the American Chemical Society. 130 (4): 1402–1414.

[73] J. Ren, X. Qin, J.-Z. Yang, Z.-F. Qin, H.-L. Guo, J.-Y. Lin, Z. Li. Methanation of carbon dioxide over Ni–M/ZrO2 (M=Fe, Co, Cu) catalysts: Effect of addition of a second metal. Fuel Processing Technology, Volume 137, 2015, Pages 204-211, ISSN 0378-3820

[74] B.J. McBride, S. Gordon, M.A. Reno, NASA Lewis Research Center, Coefficients for calculating thermodynamic and transport properties of individual species (NASA-TM-4513), United States, (1993).

[75] Gao, J., Wang, Y., Ping, Y., Hu, D., Xu, G., Gu, F., Su, F. (2012). A thermodynamic analysis of methanation reactions of carbon oxides for the production of synthetic natural gas. RSC Advances, 2(6), 2358. doi:10.1039/c2ra00632d.

[76] J. Branco, A. Ferreira, F. Vieira, and J. Martinho. Cerium-Based Bimetallic Oxides as Catalysts for the Methanation of CO_2: Influence of the Preparation Method. Energy Fuels 2021, 35, 8, 6725–6737.

[77] Tsiotsias, A.I.; Charisiou, N.D.; Yentekakis, I.V.; Goula, M.A. Bimetallic Ni-Based Catalysts for CO_2 Methanation: A Review. Nanomaterials 2021, 11, 28.

[78] Lee, W.J.; Li, C.; Prajitno, H.; Yoo, J.; Patel, J.; Yang, Y.; Lim, S. Recent trend in thermal catalytic low temperature CO_2 methanation: A critical review. Catal. Today 2020

[79] H. Liu, X. Zou, X. Wang, X. Lu, W. Ding, Effect of CeO2 addition on Ni/Al2O3 catalysts for methanation of carbon dioxide with hydrogen, Journal of Natural Gas Chemistry, Volume 21, Issue 6, 2012, Pages 703-707.

[80] M. Cai, J. Wen, W. Chu, X. Cheng, Z. Li, Methanation of carbon dioxide on Ni/ZrO2-Al2O3 catalysts: Effects of ZrO2 promoter and preparation method of novel ZrO2-Al2O3 carrier, Journal of Natural Gas Chemistry, Volume 20, Issue 3, 2011, Pages 318-324, ISSN 1003-9953.

[81] S. Abelló, C. Berrueco, D. Montané, High-loaded nickel–alumina catalyst for direct CO_2 hydrogenation into synthetic natural gas (SNG), Fuel, Volume 113, 2013, Pages 598-609, ISSN 0016-2361.

[82] S. Kattel, B. Yan, J. G. Chen, P. Liu, CO_2 hydrogenation on Pt, Pt/SiO2 and Pt/TiO2: Importance of synergy between Pt and oxide support, Journal of Catalysis, Volume 343, 2016, Pages 115-126, ISSN 0021-9517.

[83] M.C. Bacariza, M. Biset-Peiró, I. Graça, J. Guilera, J. Morante, J.M. Lopes, T. Andreub, C. Henriques. DBD plasma-assisted CO_2 methanation using zeolite-based catalysts: Structure composition-reactivity approach and effect of Ce as promoter Journal of CO_2 Utilization, Volume 26, 2018, Pages 202-211, ISSN 2212-9820

[84] Everett, O.E.; Zonetti, P.C.; Alves, O.C.; de Avillez, R.R.; Appel, L.G. The role of oxygen vacancies in the CO_2 methanation employing Ni/ZrO2 doped with Ca. Int. J. Hydrogen Energy 2020, 45, 6352–6359.

[85] Q. Zheng, R. Farrauto, A. C. Nguyen Adsorption and Methanation of Flue Gas CO_2 with Dual Functional Catalytic Materials: A Parametric Study Ind. Eng. Chem. Res. 2016, 55, 24, 6768–6776

[86] R. Dębek, F. Azzolina-Jury, A. Travert, F. Maugé A review on plasma-calytic methanation of carbon dioxide – Looking for an efficient catalyst Renewable and Sustainable Energy Reviews 116 (2019) 109427

[87] J. Gao, Q. Liu, F. Gu, B. Liu, Z. Zhong, and F. Su, "Recent advances in methanation catalysts for the production of synthetic natural gas," RSC Adv., vol. 5, no. 29, pp. 22759–22776, 2015, doi: 10.1039/c4ra16114a

[88] J. L. Figueiredo and F. R. Ribeiro, Catálise Heterogénea, 3rd ed. Fundação Calouste Gulbenkian, 2015

[89] T. A. Le, M. S. Kim, S. H. Lee, T. W. Kim, and E. D. Park, "CO and CO_2 methanation over supported Ni catalysts," Catal. Today, vol. 293–294, pp. 89–96, 2017, doi: 10.1016/j.cattod.2016.12.036

[90] C. Mebrahtu, F. Krebs, S. Abate, S. Perathoner, G. Centi, and R. Palkovits, "CO_2 Methanation: Principles and Challenges," Stud. Surf. Sci. Catal., vol. 178, pp. 85–103, 2019, doi: 10.1016/B978-0-444-64127-4.00005-7

[91] J. Martins *et al.*, "CO_2 hydrogenation with shape-controlled Pd nanoparticles embedded in mesoporous silica: Elucidating stability and selectivity issues," Catal. Commun., vol. 58, pp. 11–15, 2015, doi: 10.1016/j.catcom.2014.08.027

[92] Liu, Q.; Bian, B.; Fan, J.; Yang, J. Cobalt doped Ni based ordered mesoporous catalysts for CO_2 methanation with enhanced catalytic performance. Int. J. Hydrogen Energy 2018, 43, 4893–4901.

[93] Mebrahtu, C.; Krebs, F.; Perathoner, S.; Abate, S.; Centi, G.; Palkovits, R. Hydrotalcite based Ni-Fe/(Mg,Al)OX catalysts for CO_2 methanation-tailoring Fe content for improved CO dissociation, basicity, and particle size. Catal. Sci. Technol. 2018, 8, 1016–1027.

[94] Mangla, A.; Deo, G.; Apte, P.A. NiFe local ordering in segregated Ni3Fe alloys: A simulation study using angular dependent potential. Comput. Mater. Sci. 2018, 153, 449–460

[95] Kang, S.H.; Ryu, J.H.; Kim, J.H.; Seo, S.J.; Yoo, Y.D.; Sai Prasad, P.S.; Lim, H.J.; Byun, C.D. Co-methanation of CO and CO_2 on the NiX-Fe1-X/Al2O3 catalysts; effect of Fe contents. Korean J. Chem. Eng. 2011, 28, 2282–2286.

[96] Sehested, J.; Larsen, K.E.; Kustov, A.L.; Frey, A.M.; Johannessen, T.; Bligaard, T.; Andersson, M.P.; Nørskov, J.K.; Christensen, C.H. Discovery of technical methanation catalysts based on computational screening. Top. Catal. 2007, 45, 9–13.

[97] Zhao, B.; Liu, P.; Li, S.; Shi, H.; Jia, X.; Wang, Q.; Yang, F.; Song, Z.; Guo, C.; Hu, J.; *et al.* Bimetallic Ni-Co nanoparticles on SiO2 as robust catalyst for CO methanation: Effect of homogeneity of Ni-Co alloy. Appl. Catal. B Environ. 2020, 278, 119307.

[98] Guo, M.; Lu, G. The regulating effects of cobalt addition on the catalytic properties of silica-supported Ni–Co bimetallic catalysts for CO_2 methanation. React. Kinet. Mech. Catal. 2014, 113, 101–113.

[99] M. Huš, D. Kopač, N. Štefančič, D. Jurković, V. Dasireddy, B. Likozara. Unravelling the mechanisms of CO_2 hydrogenation to methanol on Cu-based catalysts using first-principles multiscale modelling and experiments. Catalysis Science Technology, Issue 24, 2017, 7, 5900-5913

[100] K. Ray, R. Bhardwaj, B. Singh, G. Deo. Developing descriptors for CO_2 methanation and CO_2 reforming of CH_4 over Al2O3 supported Ni and low-cost Ni based alloy catalysts. Phys. Chem. Chem. Phys., 2018,20, 15939-15950

[101] P. Summa, B. Samojeden, M. Motak, D. Wierzbicki, I. Alxneit, K. Swierczek, P. Costa. Investigation of Cu promotion effect on hydrotalcite-based nickel catalyst for CO_2 methanation. Catalysis Today, May 2021, 0920-5861.

[102] Potential of an Alumina-Supported Ni3Fe Catalyst in the Methanation of CO_2: Impact of Alloy Formation on Activity and Stability B. Mutz, M. Belimov, W. Wang, P. Sprenger, M.-A. Serrer, D. Wang, P. Pfeifer, W. Kleist, and J.-D. Grunwaldt. ACS Catal. 2017, 7, 10, 6802–6814

[103] H. Lu, X. Yang, G. Gao, J. Wang, C. Han, X. Liang, C. Li, Y. Li, W. Zhang, X. Chen. Metal (Fe, Co, Ce or La) doped nickel catalyst supported on ZrO2 modified mesoporous clays for CO and CO_2 methanation. Fuel, Volume 183, 2016, 335-344, ISSN 0016-2361.

[104] Gonçalves, L.P.L.; Sousa, J.P.S.; Soares, O.S.G.P.; Bondarchuk, O.; Lebedev, O.I.; Kolen'ko, Y.V.; Pereira, M.F.R. The role of surface properties in CO_2 methanation over carbon-supported Ni catalysts and their promotion by Fe. Catal. Sci. Technol. 2020, 10, 7217–7225.

[105] Pastor-Pérez, L.; Le Saché, E.; Jones, C.; Gu, S.; Arellano-Garcia, H.; Reina, T.R. Synthetic natural gas production from CO_2 over Ni-x/CeO2-ZrO2 (x = Fe, Co) catalysts: Influence of promoters and space velocity. Catal. Today 2018, 317, 108–113

[106] Varun, Y.; Sreedhar, I.; Singh, S.A. Highly stable M/NiO–MgO (M = Co, Cu and Fe) catalysts towards CO_2 methanation. Int. J. Hydrogen Energy 2020, 45, 28716–28731

[107] Shafiee P *et al.* Solid-state synthesis method for the preparation of cobalt doped NieAl2O3 mesoporous catalysts for CO_2 methanation. International Journal of Hydrogen Energy, https://doi.org/10.1016/j.ijhydene.2020.10.221

[108] Jens Hagen, Industrial catalysis: a practical approach ,Wiley-VCH, 2006 ISBN 3-527-31144-0, page 197

[109] Boskovic G., Baerns M. (2004) Catalyst Deactivation. In: Baerns M. (eds) Basic Principles in Applied Catalysis. Springer Series in Chemical Physics, vol 75. Springer, Berlin, Heidelberg. https://doi.org/10.1007/978-3-662-05981-4_14

[110] Maca, Karel (2009). "Microstructure evolution during pressureless sintering of bulk oxide ceramics". Processing and Application of Ceramics. 3 (1–2): 13–17. doi:10.2298/pac0902013m

[111] https://www.catalystseurope.org/index.php/safety-and-regulation/catalyst-regeneration (consulted at 08/05/2021)

[112] Ewald, S., Kolbeck, M., Kratky, T., Wolf, M., Hinrichsen, O. (2018). On the deactivation of Ni-Al catalysts in CO_2 methanation. Applied Catalysis A: General. doi:10.1016/j.apcata.2018.10.033

[113] J. Branco, P. Brito, A. Ferreira, Methanation of CO_2 over nickel-lanthanide bimetallic oxides supported on silica, Chemical Engineering Journal, Volume 380, 2020, 122465, ISSN 1385-8947,

[114] X. Dong, B. Jin, S. Cao, F. Meng, T. Chen, Q. Ding, C. Tong, Facile use of coal combustion fly ash (CCFA) as Ni-Re bimetallic catalyst support for high-performance CO_2 methanation, Waste Management, Volume 107, 2020, Pages 244-251, ISSN 0956-053X.

[115] T. Zhang, Q. Liu. Mesostructured cellular foam silica supported bimetallic LaNi1-xCoxO3 catalyst for CO_2 methanation. International Journal of Hydrogen Energy, Volume 45, Issue 7, 2020, Pages 4417-4426, ISSN 0360-3199.

[116] Bacariza, C. (2018) CO_2 conversion to CH_4 using metallic catalysts supported on zeolites [Doctoral dissertation, Instituto Superior Técnico]

[117] A. M. Vos, P. Mignon, P. Geerlings, F. Thibault-Starzyk, R. A. Schoonheydt, Microporous Mesoporous Mater. 2006, 90, 370–376

[118] G. D. Pirngruber, P. Raybaud, Y. Belmabkhout, J. Čejka, A. Zukal, Phys. Chem. Chem. Phys. 2010, 12, 13534

[119] A. Temiloluwa. New Approach to the Preparation of Zeolite-based Catalysts for CO_2 Methanation. Instituto Superior Tecnico, Universidade de Lisboa, Portugal October, 2020

[120] Y. Tao, H. Kanoh, J. Groen, K. Kaneko, Characterization of alkaline post-treated ZSM-5 zeolites by low temperature nitrogen adsorption, Studies in Surface Science and Catalysis, Elsevier, Volume 160, 2007, P. 279-286, ISSN 0167-2991, ISBN 9780444520227

[121] B. Zdravkov, J. Cermák, M. Sefara, J. Janku. Pore classification in the characterization of porous materials: A perspective. Central European Journal of Chemistry. 5(2) 2007 385–395

[122] Coats, A. W.; Redfern, J. P. (1963). "Thermogravimetric Analysis: A Review". Analyst. 88 (1053): 906–924.

[123] M. Che and J. C. Védrine, Characterization of Solid Materials and Heterogeneous Catalysts: From Structure to Surface Reactivity, 1st ed. Wiley-VCH, 2012.

[124] Coats, A. W.; Redfern, J. P. (1963). "Thermogravimetric Analysis: A Review". Analyst. 88 (1053): 906–924. doi:10.1039/AN9638800906

[125] Blik, H.; Niemantsverdriet, J. (1984-05-15). Characterization of bimetallic FeRh/SiO2 catalysts by temperature programmed reduction, oxidation and Mössbauer spectroscopy. Applied Catalysis. 10 (2): 155–162.

[126] F. Sima, C. Ristoscu, L. Duta, O. Gallet, K. Anselme, I.N. Mihailescu, Laser thin films deposition and characterization for biomedical applications, Laser Surface Modification of Biomaterials, Woodhead Publishing, 2016, P. 77-125, ISBN 9780081008836

[127] R. Kohli, K. Mittal. Developments in Surface Contamination and Cleaning, Volume 12 - Methods for Assessment and Verification of Cleanliness of Surfaces and Characterization of Surface Contaminants Elsevier 2019 978-0-12-816081-7

[128] Resonant X-ray Scattering | Shen Laboratory. arpes.stanford.edu. (consulted at 23/09/2021)

[129] Patterson, A. (1939). The Scherrer Formula for X-Ray Particle Size Determination. Phys. Rev. 56 (10): 978–982.

[130] Erni, Rolf; Rossell, MD; Kisielowski, C; Dahmen, U (2009). Atomic-Resolution Imaging with a Sub-50-pm Electron Probe. Physical Review Letters. 102 (9): 096101

[131] M.C. Bacariza, I. Graça, S.S. Bebiano, J.M. Lopes, C. Henriques, Micro- and mesoporous supports for CO_2 methanation catalysts: a comparison between SBA-15, MCM-41 and USY zeolite, Chemical Engineering Science (2017), doi: http://dx.doi.org/10.1016/j.ces.2017.09.027

[132] Z. Zhang *et al.*, “Regulation the reaction intermediates in methanation reactions via modification of nickel catalysts with strong base,” Fuel, vol. 237, no. October 2018, pp. 566–579, Feb. 2019, doi: 10.1016/j.fuel.2018.10.052.

[133] J. A. Martins, A. C. Faria, M. A. Soria, C. V. Miguel, A. E. Rodrigues, and L. M. Madeira, “CO_2 Methanation over Hydrotalcite-Derived Nickel/Ruthenium and Supported Ruthenium Catalysts,” Catalysts, vol. 9, no. 12, p. 1008, Dec. 2019, doi: 10.3390/catal9121008.

[134] I. Graça *et al.*, “CO_2 hydrogenation into CH_4 on NiHNaUSY zeolites,” Appl. Catal. B Environ., vol. 147, pp. 101–110, 2014, doi: 10.1016/j.apcatb.2013.08.010

[135] M. C. Bacariza, I. Graça, A. Westermann, M. F. Ribeiro, J. M. Lopes, and C. Henriques, “CO_2 Hydrogenation over Ni-Based Zeolites: Effect of Catalysts Preparation and Pre-reduction Conditions on Methanation Performance,” Top. Catal., vol. 59, no. 2–4, pp. 314–325, 2016, doi: 10.1007/s11244-015-0435-4.

[136] Putluru, Siva Jensen, Anker Riisager, Anders Fehrmann, Rasmus. (2011). Alkali resistant Fe-zeolite catalysts for SCR of NO with NH3 in flue gases. Topics in Catalysis. 54. 10.1007/s11244-011-9750-6.

[137] Shirvani, S., Ghashghaee, M., Kegnæs, S. (2019). Dual Role of Ferric Chloride in Modification of USY Catalyst for Enhanced Olefin Production from Refinery Fuel Oil. Applied Catalysis A: General. doi:10.1016/j.apcata.2019.05.010

[138] Silva, E. Catalisadores à base de Cu, Co ou Fe trocados ou suportados em zeólita USY - avaliação na redução de NO com CO São Carlos, UFSCar, 2008, 105f.

[139] Chen, H., Sachtler, W. Activity and durability of Fe/ZSM-5 catalyst for lean burn NOx reduction in the presence of water vapor. Catalysis Today, 42, 78-83, 1998.

[140] M. C. Bacariza, M. Maleval, I. Graça, J. M. Lopes, and C. Henriques, “Power-to-methane over Ni/zeolites: Influence of the framework type,” Microporous Mesoporous Mater., vol. 274, no. July 2018, pp. 102–112, 2019, doi: 10.1016/j.micromeso.2018.07.037.

[141] M. Bacariza, S.Amjad, P. Teixeira, J. Lopes, C. Henriques. Boosting Ni Dispersion on Zeolite-Supported Catalysts for CO_2 Methanation: The Influence of the Impregnation Solvent. Energy Fuels, 34, 11, 14656-14666, 2020.

[142] L. Karam, M. C. Bacariza, J. M. Lopes, C. Henriques, P. Massiani, N. El Hassan, Assessing the potential of xNi-yMg-Al2O3 catalysts prepared by EISA-one-pot synthesis towards CO_2 methanation: An overall study, International Journal of Hydrogen Energy, Vol 45, I 53, 2020, P 28626-28639, ISSN 0360-3199.

[143] ICP Analysis. https://www.ohsu.edu/elemental-analysis-core/icp-ms-technique (consulted at 01/10/2021).

[144] Mössbauer Spectroscopy Group, Royal Society of Chemistry (RSC) website, Introduction to Mössbauer Spectroscopy. https://www.rsc.org/membership-and-community/connect-with-others/through-interests/interest-groups/mossbauer/ (consulted at 01/10/2021).

[145] Sarkar, A. (2007). "Fischer–Tropsch Synthesis: Characterization Rb Promoted Iron Catalyst". Catalysis Letters. 121 (1–2): 1–11.

[146] M. Darby Dyar Mössbauer Spectroscopy https://serc.carleton.edu/research_education/geochemsheets/techniques/mossbauer.html (consulted at 01/10/2021).

[147] M. M. J. Treacy, “Collection of simulated XRD powder patterns for zeolites,” Appl. Catal., vol. 21, no. 2, pp. 388–389, 1986, doi: 10.1016/S0166-9834(00)81382-2.

[148] M. C. Bacariza, I. Graça, S. S. Bebiano, J. M. Lopes, and C. Henriques, “Magnesium as Promoter of CO_2 Methanation on Ni-Based USY Zeolites,” Energy and Fuels, vol. 31, no. 9, pp. 9776–9789, 2017, doi: 10.1021/acs.energyfuels.7b01553.

[149] R. Delmelle *et al.*, “Development of improved nickel catalysts for sorption enhanced CO_2 methanation,” Int. J. Hydrogen Energy, vol. 41, no. 44, pp. 20185–20191, Nov. 2016, doi: 10.1016/j.ijhydene.2016.09.045

[150] Z. Zhang *et al.*, “Regulation the reaction intermediates in methanation reactions via modification of nickel catalysts with strong base,” Fuel, vol. 237, no. October 2018, pp. 566–579, Feb. 2019, doi: 10.1016/j.fuel.2018.10.052

[151] Pandey, D., Deo, G. (2014). Promotional effects in alumina and silica supported bimetallic Ni–Fe catalysts during CO_2 hydrogenation. Journal of Molecular Catalysis A: Chemical, 382, 23–30. doi:10.1016/j.molcata.2013.10.022

[152] Janlamool J, Praserthdam P, Jongsomjit B. Ti-Si composite oxide-supported cobalt catalysts for CO_2 hydrogenation. J Nat Gas Chem 2011;20(5):558e64

[153] Ray, K., Deo, G. (2017). A potential descriptor for the CO 2 hydrogenation to CH 4 over Al 2 O 3 supported Ni and Ni-based alloy catalysts. Applied Catalysis B: Environmental, 218, 525–537. doi:10.1016/j.apcatb.2017.07.009

[154] https://www.edf.org/true-cost-carbon-pollution (consulted at 13/07/2021)

[155] https://www.scientificamerican.com/article/cost-of-carbon-pollution-pegged-at-51-a-ton/ (consulted at 13/07/2021)

[156] https://cleantechnica.com/2012/04/10/zero-carbon-cement-production-with-solar-thermal/ (consulted at 13/07/2021)

[157] https://www.globalpetrolprices.com/methane_prices/ (consulted at 13/07/2021)

[158] https://www.spglobal.com/marketintelligence/en/news-insights/latest-news-headlines/experts-explain-why-green-hydrogen-costs-have-fallen-and-will-keep-falling-63037203 (consulted at 13/07/2021)

[159] J. Albo, M. Alvarez-Guerra, P. Castaño and A. Irabien, Green Towards the electrochemical conversion of carbon dioxide into methanol Chem., 2015, 17, 2304–2324.

[160] I. Ganesh, Conversion of carbon dioxide into methanol – a potential liquid fuel: Fundamental challenges and opportunities (a review) Renewable Sustainable Energy Rev., 2014, 31, 221–257.

[161] E. V. Kondratenko, G. Mul, J. Baltrusaitis, G. O. Larrazabal, G. O. Larrazábal and J. Pérez-Ramírez, Status and perspectives of CO_2 conversion into fuels and chemicals by catalytic, photocatalytic and electrocatalytic processes. Energy Environ. Sci., 2013, 6, 3112–3135.

[162] G. A. Olah, A. Goeppert and G. K. S. Prakash, J. Chemical Recycling of Carbon Dioxide to Methanol and Dimethyl Ether: From Greenhouse Gas to Renewable, Environmentally Carbon Neutral Fuels and Synthetic Hydrocarbons Org. Chem., 2009, 74, 487–498.

[163] J. Qiao, Y. Liu, F. Hong and J. Zhang, A review of catalysts for the electroreduction of carbon dioxide to produce low-carbon fuels Chem. Soc. Rev., 2014, 43, 631–675.

[164] S. Das and W. M. A. Wan Daud, A review on advances in photocatalysts towards CO_2 conversion. RSC Adv., 2014, 4, 20856–20893.

[165] G. P. Smestad and A. Steinfeld, Review: Photochemical and Thermochemical Production of Solar Fuels from H_2O and CO_2 Using Metal Oxide Catalysts. Ind. Eng. Chem. Res., 2012, 51, 11828–11840.

[166] J. R. Scheffe and A. Steinfeld, Oxygen exchange materials for solar thermochemical splitting of H_2O and CO_2: a review Mater. Today, 2014, 17, 341–348.

[167] Y. Izumi, Recent advances in photocatalytic conversion of carbon dioxide into fuels with water and/or hydrogen using solar energy and beyond Coord. Chem. Rev., 2013, 257, 171–186.

[168] S. C. Roy, O. K. Varghese, M. Paulose and C. A. Grimes, Toward Solar Fuels: Photocatalytic Conversion of Carbon Dioxide to Hydrocarbons. ACS Nano, 2010, 4, 1259–1278.

[169] Götz, M.; Lefebvre, J.; Mörs, F.; McDaniel Koch, A.; Graf, F.; Bajohr, S.; Reimert, R.; Kolb, T. Renewable Power-to-Gas: A technological and economic review. Renew. Energy 2016, 85, 1371–1390

[170] Ye, RP., Ding, J., Gong, W. *et al.* CO_2 hydrogenation to high-value products via heterogeneous catalysis. Nat Commun 10, 5698 (2019). https://doi.org/10.1038/s41467-019-13638-9

[171] Rönsch, S.; Schneider, J.; Matthischke, S.; Schlüter, M.; Götz, M.; Lefebvre, J.; Prabhakaran, P.; Bajohr, S. (2016-02-15). "Review on methanation – From fundamentals to current projects". Fuel. 166: 276–296

[172] Bailera, M.; Lisbona, P.; Romeo, L.M.; Espatolero, S. Power to Gas projects review: Lab, pilot and demo plants for storing renewable energy and CO_2. Renew. Sustain. Energy Rev. 2017, 69, 292–312

[173] Martin, M.R.; Fornero, J.J.; Stark, R.; Mets, L.; Angenent, L.T. A Single-Culture Bioprocess of Methanothermobacter thermautotrophicus to upgrade Digester Biogas by CO_2-to-CH_4 Conversion with H_2. Archaea 2013, 2013, 157529

[174] L. Brennan and P. Owende, Biofuels from microalgae—A review of technologies for production, processing, and extractions of biofuels and co-products. Renewable Sustainable Energy Rev., 2010, 14, 557–577.

[175] Total cost of carbon capture and storage implemented at a regional scale: northeastern and midwestern United States. W. J. Schmelz, G. Hochman and K. G. Miller. 14 August 2020 The Royal Society.

[176] https://www.statista.com/statistics/1171389/co2-emissions-european-union/ (consultado a 01/04/2021)

[177] Albert Hans Baur Greenhouse Gas Emissions in European Cities: A straightforward approach for estimating urban emissions by focusing on relevant socioeconomic and spatial drivers Technischen Universität Berlin, 2015

[178] https://cembureau.eu/about-our-industry/key-facts-figures/ (consultado a 01/04/2021)

[179] Analysis of the industrial sectors in the European Union EU-MERCI HORIZON 2020 Project Nr. 693845

[180] Greenhouse gas and gold mines Nearly 1 ton of CO_2 emitted per ounce of gold produced in 2019. https://www.spglobal.com/marketintelligence/en/news-insights/blog/greenhouse-gas-and-gold-mines-nearly-1-ton-of-co2-emitted-per-ounce-of-gold-produced-in-2019 (consultado a 05/04/2021)

[181] Carbon Dioxide Separation Technologies. R. Czarnota, E. Knapik, P. Wojnarowski, D. Janiga, J. Stopa. Arch. Min. Sci. 64 (2019), 3, 487-498. DOI 10.24425/ams.2019.129364

[182] Wang M., Lawal A., Stephenson P., Sidders J., Ramshaw C., 2011. Post-combustion CO_2 capture with chemical absorption: a state-of-the-art review. Chemical Engineering Research and Design 89 (9), 1609-1624.

[183] J. Gao, Y. Wang, Y. Ping, D. Hu, G. Xu, and F. Su. A thermodynamic analysis of methanation reactions of carbon oxides for the production of synthetic natural gas. RSC Adv., vol. 2, pp. 2358–2368, 2012.

[184] S. Amjad Renewable energy storage in the natural gas network: Enhancing CO_2 conversion into synthetic natural gas over zeolite catalysts by tuning Ni particle size July 2019

[185] Zyryanova, M.M., Snytnikov, P.V., Amosov, Y.I. *et al.* Selective methanation of CO in the presence of CO_2 in hydrogen-containing mixtures on nickel catalysts. Kinet Catal 51, 907–913 (2010).

[186] Khorsand, K. (2007). "Modeling and simulation of methanation catalytic reactor in ammonia unit". Petroleum Coal. 49: 46–53.

[187] The Sabatier System: Producing Water on the Space Station https://www.nasa.gov/mission_pages/station/research/news/sabatier.html

[188] D.P. VanderWiel, J.L. Zilka-Marco, Y. Wang, A.Y. Tonkovich, R.S. Wegeng. Carbon Dioxide Conversions in Microreactors. American Institute of Chemical Engineers, 2000.

[189] Kopyscinski, J.; Schildhauer, T. J.; Biollaz, S. M. A. (2010-08-01). "Production of synthetic natural gas (SNG) from coal and dry biomass – A technology review from 1950 to 2009". Fuel.Volume 89, Issue 8, 2010, P. 1763-1783, ISSN 0016-2361.

[190] https://www.basf.com/global/en/media/news-releases/2019/06/p-19-249.html (consulted at 24/04/2021)

[191] Kothandaraman, J., Goeppert, A., Czaun, M., Olah, G. A. Prakash, G. K. Conversion of CO_2 from air into methanol using a polyamine and a homogeneous ruthenium catalyst. J. Am. Chem. Soc. 138, 778–781 (2016).

[192] L. Wang, Y. Yi, H. Guo, and X. Tu. Atmospheric Pressure and Room Temperature Synthesis of Methanol through Plasma-Catalytic Hydrogenation of CO_2. ACS Catal. 2018, 8, 1, 90–100 Publication Date:November 14, 2017

[193] Z. Luo, S. Tian, and Z. Wang. Enhanced Activity of Cu/ZnO/C Catalysts Prepared by Cold Plasma for CO_2 Hydrogenation to Methanol. Ind. Eng. Chem. Res. 2020, 59, 13, 5657–5663 Publication Date:March 2, 2020

[194] J.-J. Zou, Y-p Zhang, C.-J. Liu, Y. Li, B. Eliasson Starch-enhanced synthesis of oxygenates from methane and carbon dioxide using dielectric-barrier discharges Plasma Chem Plasma Process, 23 (2003), pp. 69-82

[195] B. Eliasson, U. Kogelschatz, B.Z. Xue, L.M. Zhou Hydrogenation of carbon dioxide to methanol with a discharge activated catalyst Ind Eng Chem Res, 37 (1998), pp. 3350-3357

[196] Yu-Long Men, Yi Liu, Qianqian Wang, Zheng-Hong Luo, Shuai Shao, Yi-Bao Li, Yun-Xiang Pan, Highly dispersed Pt-based catalysts for selective CO_2 hydrogenation to methanol at atmospheric pressure, Chemical Engineering Science, Volume 200, 2019, Pages 167-175, ISSN 0009-2509.

[197] Joshi, N, Loganathan, S. Methanol synthesis from CO_2 using Ni and Cu supported Fe catalytic system: Understanding the role of nonthermal plasma surface discharge. Plasma Process Polym. 2021.

[198] R. Burch, R. J. Chappell, Appl. Catal. 1988, 45, 131.

[199] M. Behrens Heterogeneous Catalysis of CO_2 Conversion to Methanol on Copper Surfaces Angewandte Chemie International Edition Volume 53, Issue 45 November 3, 2014 Pages 12022-12024

[200] J. Graciani, K. Mudiyanselage, F. Xu, A. E. Baber, J. Evans, S. D. Senanayake, D. J. Stacchiola, P. Liu, J. Hrbek, J. Fernández Sanz, J. A. Rodriguez, Science 2014, 345, 546.

[201] T. Fujitani, I. Nakamura, T. Uchijima, J. Nakamura, Surf. Sci. 1997, 383, 285.

[202] W. Baumjohann, R. Treumann. Basic Space Plasma Physics. World Scientific, 1996

[203] A. Bogaerts, X. Tu, J. C. Whitehead, G. Centi, L. Lefferts, O. Guaitella, F. Azzolina-Jury, H. Kim, A. B. Murphy, W. F Schneider, T. Nozaki, J. C. Hicks, A. Rousseau, F. Thevenet, A. Khacef and M. Carreon. The 2020 plasma catalysis roadmap. J. Phys. D: Appl. Phys. 53 (2020) 443001

[204] P. Mehta, P. Barboun, D. B. Go, J. C. Hicks, W. F. Schneider Catalysis Enabled by Plasma Activation of Strong Chemical Bonds: A Review ACS Energy Lett., 2019, 4 1115–33

[205] P. Tang, Q. Zhu, Z. Wua and D. Ma Methane activation: the past and future Energy Environ. Sci., 2014,7, 2580-2591

[206] K. H. R. Rouwenhorst, Y. Engelmann, K. van't Veer, R. S. Postma, A. Bogaerts and L. Lefferts. Plasma-driven catalysis: green ammonia synthesis with intermittent electricity Green Chem., 2020, 22, 6258-6287.

[207] R. Morent, J. Dewulf, N. Steenhaut, C. Leys, and H. V. Langenhove Hybrid Plasma-Catalyst System for the Removal of Trichloroethylene in Air J. Adv. Oxid. Technol. Vol. 9, No.1, 2006

[208] M. Nizio, A. Albarazi, S. Cavadias, J. Amouroux, M. E. Galvez, P. Costa, Hybrid plasma-catalytic methanation of CO_2 at low temperature over ceria zirconia supported Ni catalysts, International Journal of Hydrogen Energy, Volume 41, Issue 27, 2016, Pages 11584-11592, ISSN 0360-3199.

[209] Kim H H, Teramoto Y, Negishi N and Ogata A 2015 A multidisciplinary approach to understand the interactions of nonthermal plasma and catalyst: a review. Catal. Today 256 13–22

[210] Mehta P, Barboun P, Herrera F A, Kim J, Rumbach P, Go D B, Hicks J C and Schneider W F 2018. Overcoming ammonia synthesis scaling relations with plasma-enabled catalysis Nat. Catal. 1 269–75

[211] Fridman, A. Plasma Chemistry; Cambridge University Press: New York, 2008

[212] Rettner, C. T.; Stein, H. Effect of Vibrational Energy on the Dissociative Chemisorption of N2 on Fe(111). J. Chem. Phys. 1987, 87, 770−771

[213] Holmblad, P. M.; Wambach, J.; Chorkendorff, I. Molecular Beam Study of Dissociative Sticking of Methane on Ni(100). J. Chem. Phys. 1995, 102, 8255−8263.

[214] Luntz, A. C. A Simple Model for Associative Desorption and Dissociative Chemisorption. J. Chem. Phys. 2000, 113, 6901−6905

7 Annexes

7.1 Annex 1: Peak angles in the XRD diffractogram ($^{\circ}$)

Upon the following table 12 can be observed the peak values obtained for the different components used, and that could be visible in the X-Ray Diffraction graphs.

Table 12: Peak angles corresponding to each compound on the X-ray diffractograms.

Compound	**Peak angles in the XRD diffractogram ($^{\circ}$)**	**Reference**
FAU	6.0; 10.0; 16.0; 20.0; 24.0; 27.0; 31.0	[147]
NiO	37.0; 43.0; 63.0; 75.2	[148]
Ni $^{\circ}$	44.5; 51.9; 76.3	[149], [150]
Fe $^{\circ}$	45; 65	[76]
Fe_3O_4	30.5; 35.5; 36.5; 43.5; 54; 63	[76]
Fe_2O_3	34; 36; 42; 49; 54.5; 57; 63	[76], [151]
Ni-Fe alloy	44; 51; 75	[151]
Co_3O_4	31.22; 36.80; 44.83; 59.43; 64.55	[152]
$NiCo_2O_4$	19.19; 31.54; 37.07; 44.92; 59.61; 65.43	[107]
Cu $^{\circ}$	43.3; 50.4; 74.06	[153]
CuO	32.4; 35.5; 38.1; 48.4; 58.2; 62.0; 61.7; 72.1; 74.8	[153]
$NiCuO_x$	43.9; 63.0	[153]

7.2 Annex 2: Tecnico-Economical study into the system

In order to better understand the current feasibility of this process, it is necessary to develop an economical study. For that, the costs of the different components were procured, and can be found in table 13.

Table 13: Prices for each one of the components involved in the process. Water was despised as its value is far lower than the others.

Component	Price (€/ton)	Ref.
CO_2	42.37	[154], [155]
CH_4	2589.34	[157]
H_2	4046.61 (green hydrogen)	[158]
	1525.42 (fossil fuel hydrogen)	[158]
CO	508.47	[156]

Whereas, carbon dioxide can be considered as a profit, even if counting as a reactant, since companies will pay to remove it, hence it could be a good business opportunity to capitalise on that waste other companies produce. In addition, carbon monoxide can also be considered a profitable secondary-product, since it could be commercialised for its syngas addition purposes.

Afterwards, a mass balance was performed, considering 100 tons of CO_2, whilst using the values of CO_2 conversion and CH_4 selectivity for the best catalyst developed in the current study. Those results can be therefore found in the table 14.

Table 14: Mass balance performed for both the Sabatier reaction and the reverse water gas shift reaction, according to their respective selectivity.

Mass Balance		
(ton)	Prior Reaction	After Reaction
CO_2	100	28.08
H_2	18.32	5.38
CH_4	0	25.58
H_2O	0	58.17
CO	0	1.10

The gross margin was calculated using both prices of hydrogen, in order to understand the viability of acquiring green hydrogen and yet remain a profitable process. For the calculation of the gross margin, the equation 16 was used, and its values can be found in table 15.

$$GM = \frac{Profit}{Sales} \times 100(\%) = \frac{Sales - Costs}{Sales} \times 100(\%) \tag{16}$$

Table 15: Profit and Gross Margin obtained both for green and fossil fuel hydrogen.

	Profit (1000€)	**GM (%)**
for green hydrogen	-3.11	-4.4
for fossil fuel hydrogen	43.09	60.6

Hence, solely considering the gross margin of the process, one can infer that without reducing the green hydrogen prices, it would be impossible to accomplish a viable process. However, for when considering hydrogen originated from fossil fuels, this process can become quite a viable option, in spite of contradictory in terms of ecological responsibility.

7.3 Annex 3: Mass Loss (%) vs Temperature

Through the TGA, it can be obtained the Figure 34, a graph depicting the mass loss (%) as a function of temperature for the monometallic catalysts.

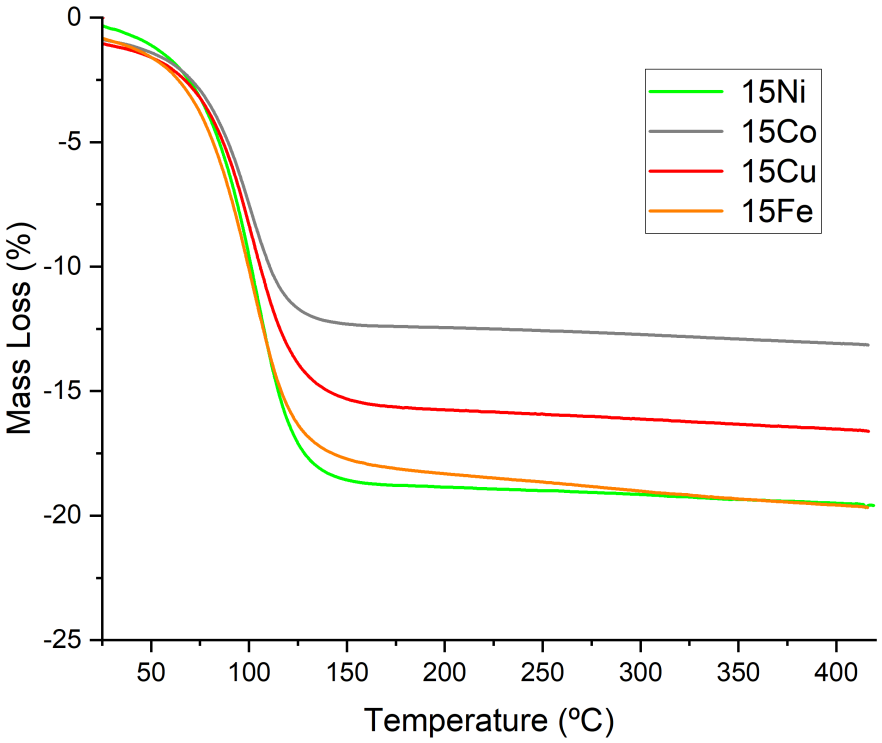

Figure 34: Mass Loss (%) as a function of temperature for 15X catalysts.

In addition, through the observation of figure 35, a graph depicting the mass loss (%) as a function of temperature for the 15Ni1X catalysts.

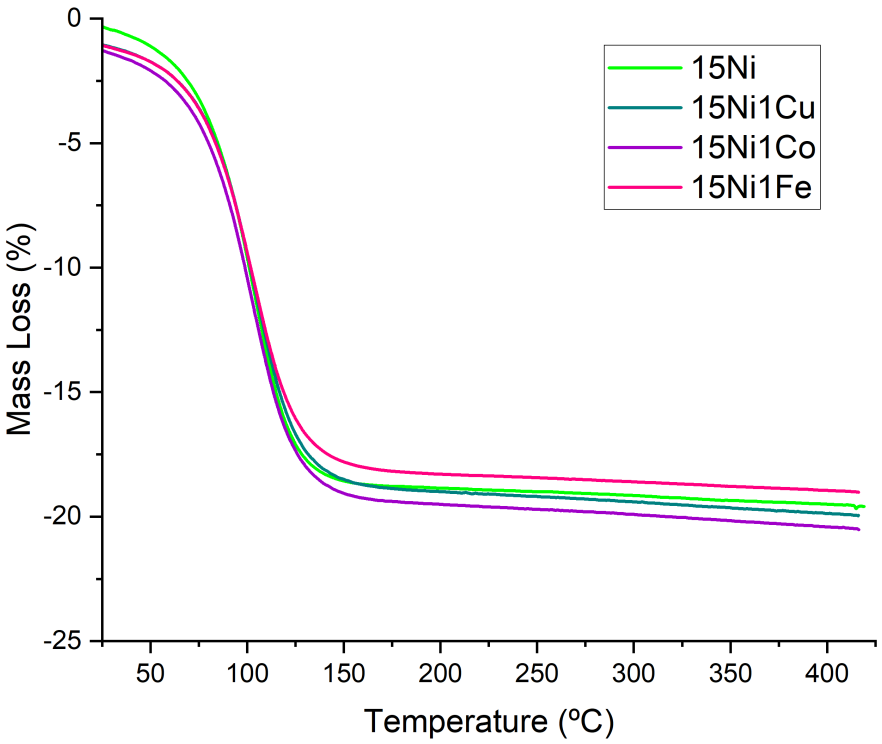

Figure 35: Mass Loss (%) as a function of temperature for the bimetallic catalysts pertaining the second study.

In addition, the observation of figure 36, a graph depicting the mass loss (%) as a function of temperature for the 15NiXFe catalysts.

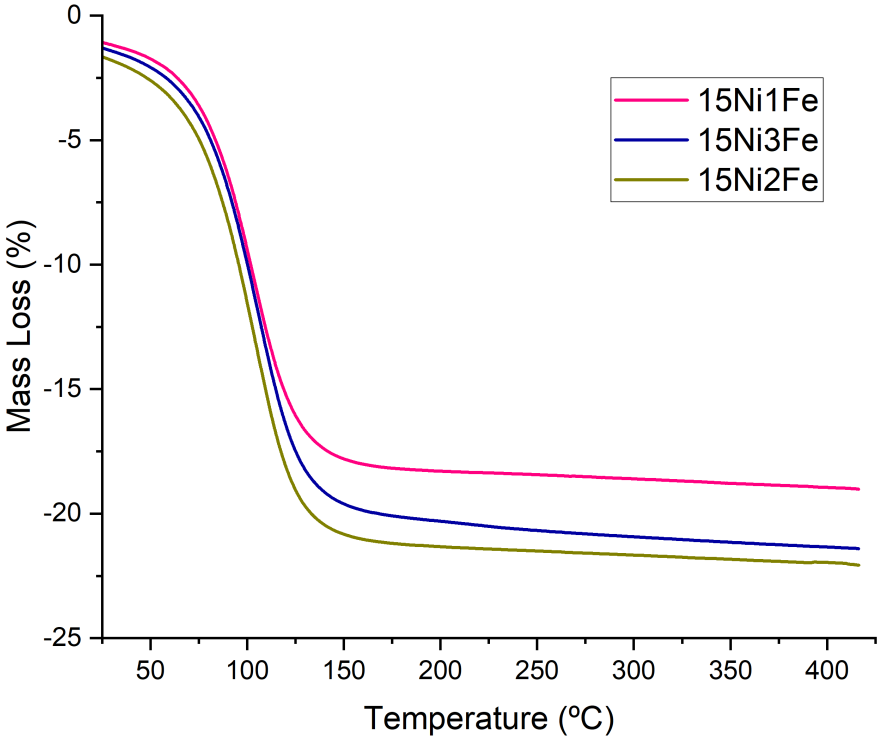

Figure 36: Mass Loss (%) as a function of temperature for the iron-based bimetallic catalysts.

7.4 Annex 4: Other Technologies for the conversion of CO_2

Besides thermal catalysis and plasma-assisted catalysis, there are also other alternative methods for conversion of CO_2 into high valued-chemicals and fuels.

7.4.1 Electrochemical Conversion

From all the alternative technologies, this is the closest one to plasma-assisted catalysis. This closeness derives from the fact that these two technologies rely on (preferably renewable) eletrical energy to operate, whereas the other novel technologies only utilize renewable energy, i.e. solar, both for its focused radiation heat and its emitted photons. [159] [160] [161] [162]

The electrochemical valorisation of CO_2 is a novel technology in which electrical energy is supplied to establish a potential between two electrodes, and CO_2 is transformed into a value-added chemicals under mild conditions. [159] [160]

Multiple variables can influence the products that are obtained from this technology, such as the catalyst, the electrode materials, the reaction medium, the electrolyte solution the buffer strength, pH, CO_2 concentration and pressure as well as the reaction temperature. [163] The major reduction products that can be obtained are carbon monoxide, formic acid (or formate, when in basic solution), formaldehyde, methanol, oxalic acid (or oxalate, in basic solutions), methane, ethylene and ethanol. [159] [162] [163]

For this wide variety of products to be made, besides the direct electrochemical reduction of CO_2 to methanol, it is also possible to produce syngas at the cathode in a H_2/CO ratio close to 2, while at the anode, a pure oxygen stream is generated, as can be seen by figure 37. [162] And, through methanol and/or syngas, it is possible to obtain a multitude of other products.

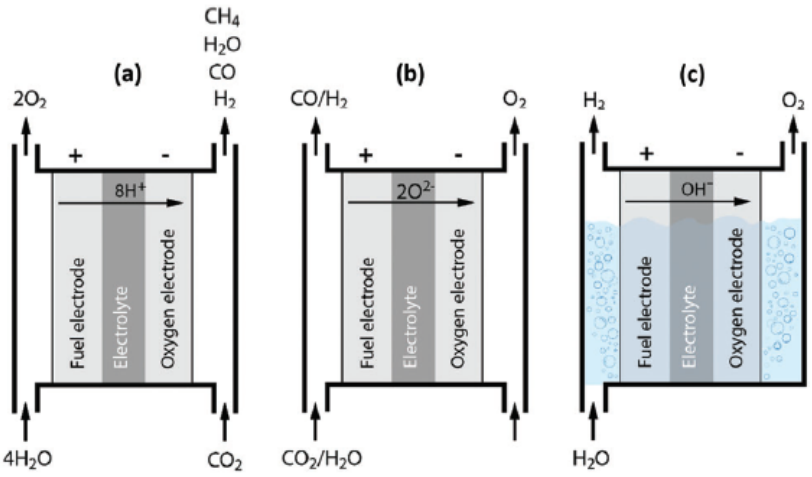

Figure 37: Diagram representing the principles of a solid proton conducting electrolysis cell (a) solid oxide electrolysis cell (b) an alkine electrolysis cell (c) for the conversion of CO_2 and/or H_2

There are a number of reasons why the electrochemical reduction process is a good option: for instance, the process is controllable by several reaction parameters, including the electrode potential and temperature. [159] [163] [162] Another advantage is that it can use a wide variety of renewable electricity sources, not just solar. [163] Also, a wide variety of valuable products can be made. Additionally, electrochemical reaction systems are compact, modular, on-demand and thus relatively easy to utilize both for small and industrial-scale applications. [163]

Although it still requires significant technical and catalytic advances for its large scale use, electrochemical conversion is becoming a mature technology for H_2 splitting. When it comes to CO_2 reduction, several important challenges still remain. [159] [160] [161]

7.4.2 Solar Thermochemical Conversion

There are multiple ways to reduce CO_2 using renewable solar energy, whereas the use of direct solar light irradiation is probably the most effective method because there is no additional extra energy required and no negative influence on the environment. [164] Both direct and indirect solar irradiation could provide energy for several conversion applications. Two forms of direct solar energy conversion can be distinguished: (i) thermal conversion, where heating can be produced after sunlight is absorbed; and (ii) quantum conversion, where the work output can be taken directly from the light absorbed. [165]

Through a two-step thermochemical cycle which uses metal oxides in order to promote redox reactions, it is possible to bypass the separation problem and allows for operation at relatively moderate temperatures. More specifically, as shown in figure 38, solar processes enable a thermochemical cycle for CO_2/H_2O-splitting. [165] [166]

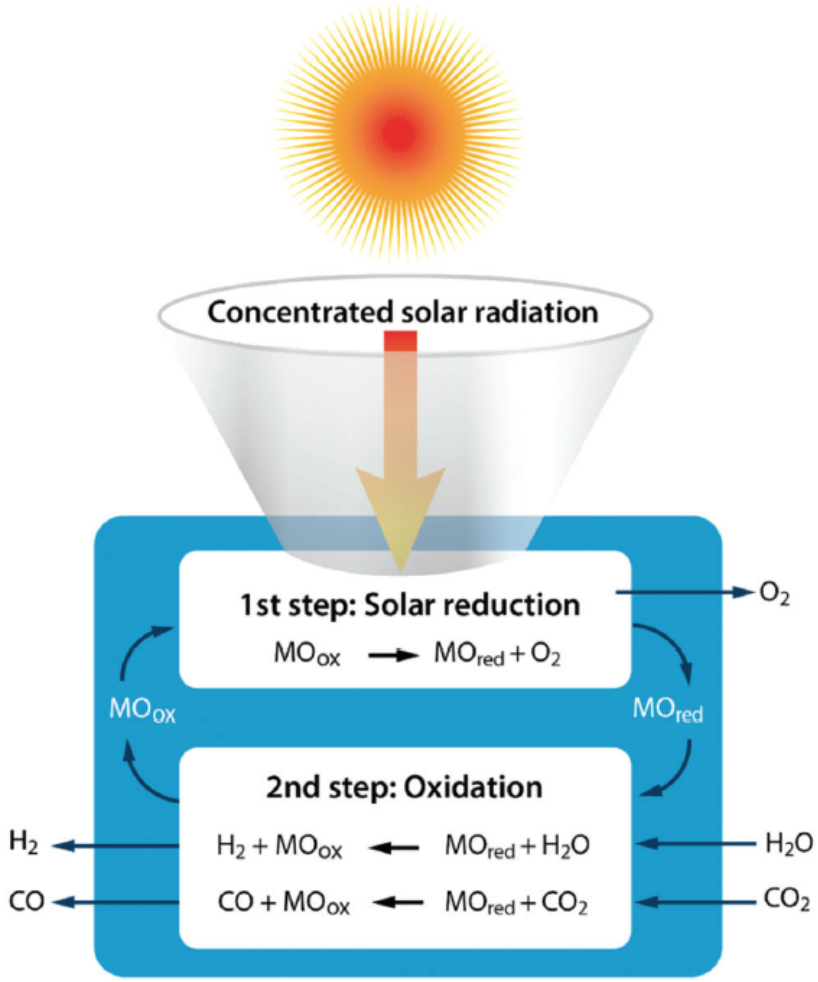

Figure 38: Schematic of the two-step solar thermochemical conversion cycle for CO_2 and H_2 splitting based on metal oxide redox reactions.

The first step is the solar thermal reduction of the metal oxide MO_{ox} (where M is usually Ce, Zn or Fe [167]) to the metal or the metal oxide (MO_{red}). The second step consists on the oxidation of the reduced metal oxide with CO_2/H_2O, to form CO/H_2, whilst allowing for the metal oxide catalyst to be reused. [165] [166]

The thermochemical conversion rates are higher than, for example, the photocatalytic rates, but although conceptually simple, the material necessary for sunlight capturing and high-temperature reactors can incur in high initial investment costs. [167]

7.4.3 Photochemical Conversion

Photochemical conversion differs from solar thermochemistry in the way the solar energy is used, since the former uses the energy of a photon in the chemical reaction, [167] whilst the latter uses that photon to power the thermal necessities to overcome the activation barriers and to affect the chemical equilibrium. [165]

Photoreduction of CO_2 to formaldehyde and methanol in purified water was achieved, using semiconductors such as TiO_2, ZnO, CdS, GaP, SiC and WO_3. [167] Based in a correlation between the conduction band energy potential and the yield of methanol, it is possible to infer a mechanism, suggesting that the photoreduction of CO_2 proceeds through the photoexcited electrons in the conduction band, moving towards CO_2. This principle mechanism of selective photocatalysis under light irradiation can be observed in figure **??**. [167]

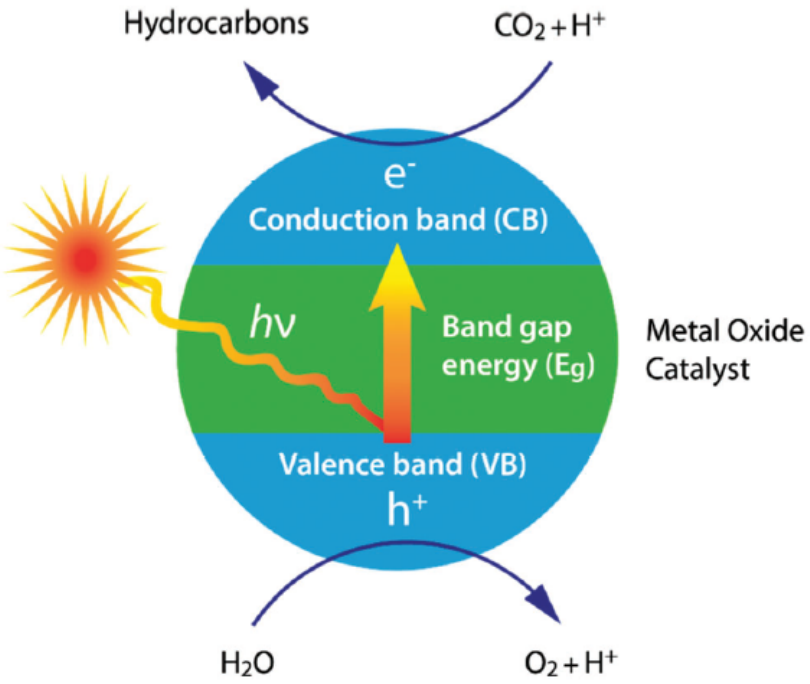

Figure 39: Schematic of the photochemical reduction of CO_2 by water on a metal oxide catalyst.

The efficiency of the photocatalytic materials is influenced by several factors, such as catalyst dosage, reactant ration, reaction temperature, time, pressure, pH, and both light intensity and wavelength. [164] A wide variety of reduction products can be obtained, including carbon monoxide, formic acid, formaldehyde, methanol, methane, ethylene, ethane and ethanol. [168]

Currently, most research work is performed using artificial UV light sources [164] [168], because the large band gap of metal oxides result in a poor response to visible light; hence, a band gap between 2 and 2.4 eV is optimal, which limits the maximum attainable efficiency to 17%. [168] Yet, solar energy conversion efficiencies obtained to date, are far lower (at present, around 2% [165]). Thus, it can be perceived that, at the moment, the existing techniques are inefficient and insufficient, and further efforts are yet required. [161] [162] [164] [168]

7.4.4 Biochemical Conversion

Biochemical conversion distinguishes itself from Thermal (or thermocatalytic, or catalytic) methanation [169], because instead of using metal catalysts (e.g. Fe/Al_2O_3 [170] [28]), high temperatures (usually between 200 and 550 °C), and pressure up until 100 bars [28] [171], they use microalgae to catalyze the reaction. As a result, reactors work normally at temperatures between 37 and 65 °C, and pressures from one up to 15 bars, in order to reach the optimal growth conditions for these organisms. [172] This process can also be known as biological methanation, when methanogenic microorganisms are used in order to catalyze the reaction and produce specifically methane. [172] [173]

Microalgae are photosynthetic microorganisms with simple growing requirements (light, sugars, CO_2, N, P, and K) that can produce lipids, proteins and carbohydrates in large amounts over short periods of time. These products can be processed into both biofuels and valuable co-products. [174]

Microalgae can typically be used to capture CO_2 from three different sources: atmospheric CO_2, CO_2 emissions from power plants and industrial processes, and CO_2 from soluble carbonates. [174] A descriptive diagram of this bioconversion of CO_2 can be observed on figure 40.

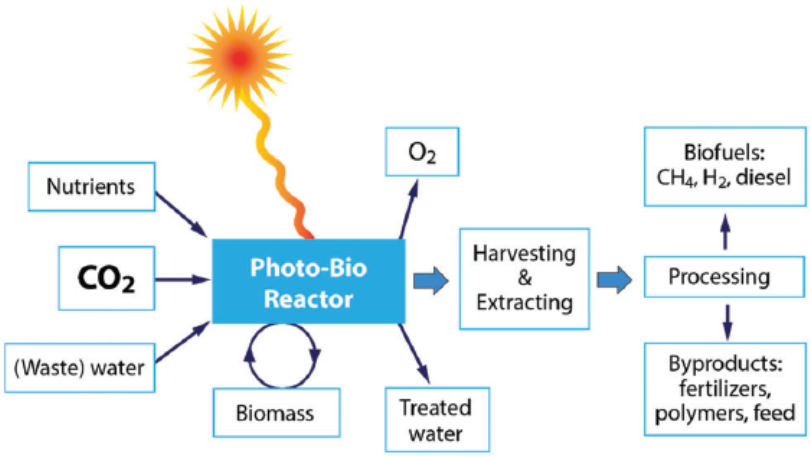

Figure 40: Schematic of the photo-bioreactor application for CO_2 conversion. [12]

However, there's currently yet a significant drawback which consists on the big share of the cost of cultivation. Therefore, they aren't currently suitable to be cultivated solely for bioenergy applications, and should instead be integrated with the production of other value-added products. [12] Within the process itself, the major limitation of the biological process corresponds to the slow hydrogen gas-liquid mass transfer, which leads to low space-time yields and requires therefore larger reactor dimensions than for chemical methanation. [28]

7.5 Annex 5: CO_2 Procurement

The fact that CO_2 is the most abundant GHG in the atmosphere doesn't mean it's capture and usage directly from the atmosphere would be easy nor cheap. [175] That's why it'd be wise to look for CO_2 production hubs, in which this carbon dioxide is so abundant it might sometimes not only be free, but also this project could be paid to get rid of other companies' CO_2. Companies as such could be involved with the cement and the oil industry.

When referring to the general CO_2 emissions, Germany has been the european leader emitter for the past decades, followed by the UK and Italy. These three nations combined produce around 34% of all CO_2 emissions in Europe. [176]

Although, this isn't a straightforward method of calculating where the problem really is, since it's really the urban activities that drive the majority of global energy use, and account for more than 75% of the world's energy-related CO_2 emissions. [177] So a succinct investigation into which cities and industries specifically produce more was conducted.

Even though the focus of scientific investigation is going mainly into the transport necessities (oil industry) and to clean electricity, those aren't the main producers of GHG. The main carbon emitter necessity is our necessity to build things, such as cement, steel and plastics, which represents about 31% of the total GHG emitted. [6] Cement, specifically, has an emission rate of one ton of CO_2 per each ton of cement produced. [6] As so, the focus shifted on the behalf of the latter.

When comparing values from the cement industry worldwide, it is easy to infer that the main producer is China, with around 54.5% of the world cement production, followed by India with 8.2% and by Europe with 6.4%. [178] In the EU, the main cement producers are Germany (17%), Italy (14%), Spain (11%) and France (10%). [179] This is specially accentuated for cities such as Bordeaux, which possesses a vast hub of cement producing companies, such as Cemex Bétons, Unibéton, F2I, Garandeau Bétons Cavignac, Lafarge Ciments and Ciments Calcia, and even mining industries such as Sablières de Guyenne and MinéralCo (by Cemex Granulats), which also have a high emission rate of CO_2 (e.g. of around 0.8 tons of CO_2 emitted for each ounce of gold extracted [180]). Bordeaux could potentially be the ideal place to install the current project. The abundance of CO_2 emitting industries in the surroundings of the city assures a continuous supply of carbon, whilst its closeness to the sea could become advantageous if the possibility of obtaining H_2 through direct water electrolysis was to be carried on.

7.5.1 Cleaning the Cement

Once the procurement of the CO_2 issue is resolved, another issue arises. This gaseous output from the cement industries isn't just pure CO_2, and is expected to contain several impurities such as SO_2, O_2 and N_2. Gases which can constitute a problem, specially when it comes to plasma catalysis, since the presence of O_2 and N_2 would automatically result in the formation of NOx products, incredibly toxic and great contributors to the formation of smog and acid rain, as well as affecting the ozone present in the troposphere.

However, when considering using a direct line from some other industries' waste, that can be a beneficial initiative. According with Czarnota *et al.* [181], the capture of CO_2 from a stream of gases is the best option, since the capture of CO_2 from the atmosphere can lead up to 60 70 % of the entire costs of the operation.

CO_2 has plenty of possibilities when considering its separation from other compounds, as can be observed in figure 41. [182]

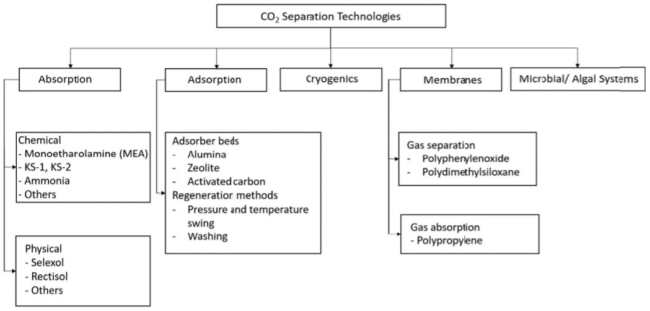

Figure 41: Separation techniques available for the removal of CO_2 on the post-combustion stage. [182]

So as can be ascertained, through figure 41, there are multiple methods for the separation of CO_2 from other compounds, such as chemical or physical absorption, adsorption, membrane technology, or even through cryogenic CO_2 capture.

7.6 Annex 6: Aspen simulation of thermodynamic conditions for methanation and methanolation

Use Aspen in order to obtain the variation of the selectivity of CH_4 and the conversion of CO_2 as a function of temperature, pressure and dilution of N2. Obtain and expose graphs. Comment those. Compare with other work performed on this?

For this project, a simulation on the ASPEN Plus V11 program to the current reactional system was performed, in order to better understand the thermodynamic equilibrium of the current reaction, and to develop a novel study of interactions between the compounds, associated with the variation of temperature, pressure and N_2 dilution.

The results were interpreted through the variables obtained for CO_2 conversion and CH_4 and CH_3OH selectivities. A variation on the ratio H_2/CO_2 was also performed, in order to study its effect on the CH_3OH and CH_4 selectivity.

Several sensibility analysis were performed, using the reactor model **RGibbs**, which based on thermodynamic equilibrium (especially on Gibbs free energy) calculates the extent of each product formed on the reactor's outlet. And, knowing the reaction's stoichiometry, this method allows for a calculation of conversion of CO_2 and selectivity towards CH_4.

As is known, whenever the Gibbs free energy is negative, it means the products of the considered reaction are spontaneously formed. When its positive, then the compounds have the tendency to react in favour of the reactants. If this Gibbs free energy happens to be equal to zero, then that means thes system is in equilibrium.

7.6.1 Temperature

As can be ascertained by figure 42, temperature has a clear effect on the selectivity of these products. Specially for CH_4, there is a total dependence on temperature, since for higher temperatures, this reaction ceases to occur, whilst for relatively low temperatures (up until around 350 °C), there is practically 100% selectivity for this product. This happens due to a higher selectivity for the dissociation of CO_2 into CO and O_2 reaction, resulting in a depletion of CH_4 for higher temperatures. For CH_3OH, the dependence can although be despised, since its selectivity is so low for the current set of temperature, that its existence can practically be despised as an end-product of the current system.

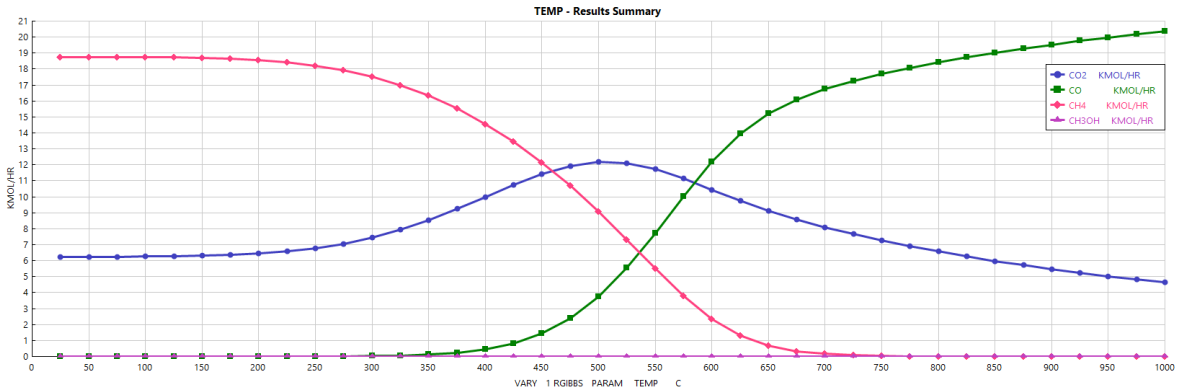

Figure 42: Graph representing the quantity of each respective product obtained for the ASPEN simulation, as a function of temperature, for a H_2/CO_2 ratio of 3, pressure of 1 bar, no catalyst.

Now for the conversion of CO_2, figure 43, for low temperatures, there's 75% of CO_2 conversion, which is the maximum possible conversion that can be obtained, if the reaction considered is the CO_2 methanation, although for this ratio of H_2/CO_2 of 3, it should tend to the formation of methanol instead. Now, for higher temperatures, what starts happening is a tendency towards the dissociation of the CO_2 molecule into CO and O_2, which results in an undesired low selectivity for CH_4, as was observed in figure 42.

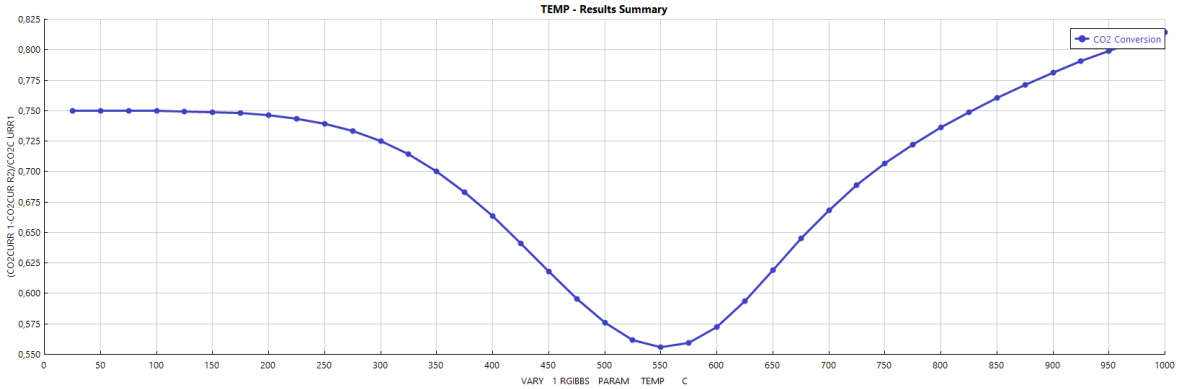

Figure 43: Graph representing the conversion of CO_2 as a function of temperature, for a H_2/CO_2 ratio of 3, pressure of 1 bar, without a catalyst.

This change in the system's behavior for the preferred reaction observed in figure 42 was already previously documented by Gao *et al.* [183], which reported that the theoretical operating temperature window for the CO_2 conversion into methane shifts at around 500 °C, due to the overall exothermic nature of the reactions. For higher temperatures than 500 °C, the RWGS reaction is preferred, hence the higher formation of CO than that of methane. Thus being this previously stated range of temperatures the ideal for the methanation process.

Higher temperatures could, although, increase the reaction rate, however this could also compromise the catalyst's stability, and could also be responsible for carbon deposition. [184]

7.6.2 Pressure

By altering the pressure, between 0.1 bars up until 50 bars, it was possible to evaluate how this variable altered the selectivities of CH_4 and CH_3OH, figure 45, and the conversion of CO_2, figure 45.

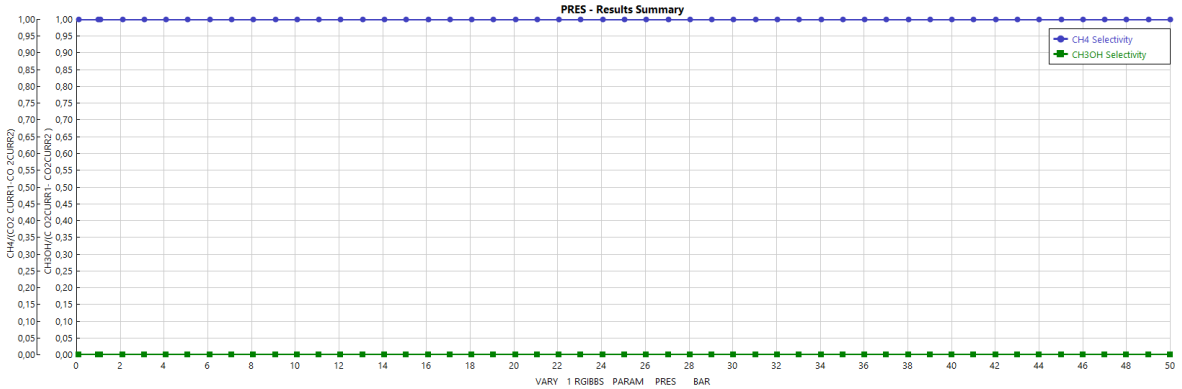

Figure 44: Graph representing the selectivities of CH_3OH and CH_4 as a function of pressure, for a H_2/CO_2 ratio of 3, constant temperature of 25 °C, without a catalyst.

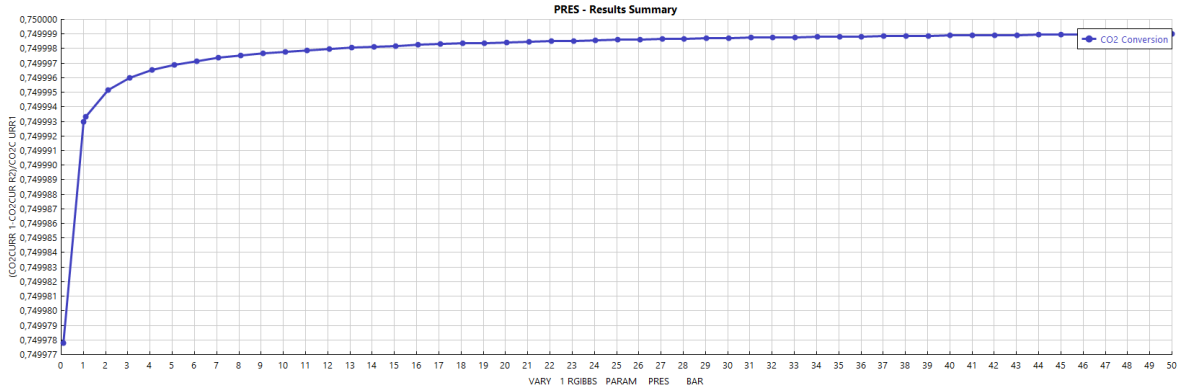

Figure 45: Graph representing the conversion of CO_2 as a function of pressure, for a H_2/CO_2 ratio of 3, constant temperature of 25 °C, without a catalyst.

As can be ascertained from figures 45 and 44, both the selectivities of CH_4 and CH_3OH and for the conversion of CO_2 don't seem to be much affected by the variation of pressure.

This situation in which the CH_3OH selectivity is so low should somewhat be expected. Even for a ratio of H_2/CO_2 equal to three, which is optimal for the conversion to methanol, CH_4 appears to be a preferable product. This happens because, as stated previously in section 2.2, CH_4 has a lower enthalpy than any other alcohol or molecule that could be formed, hence it is expected to have methane as the main product, unless a specific catalyst were to be introduced, in order to facilitate other pathways and therefore generate other products.

7.6.3 N_2 Dilution

As could be expected, N_2 doesn't have a significant effect either on the CO_2 conversion, nor on the selectivities of both CH_4 and CH_3OH; and for relatively low temperatures, it is important also to affirm that N_2 doesn't react with any loose oxygen, creating undesirable compounds such as NO_2, NO or N_2O.

Although, not directly a concern, but with the possibility of the usage of air as solvent, or even an inability to purge the same of the system, could result in a preference of the hydrogen, which is usually the most costly reactant, to react with the free O_2 in the air, resulting in a conversion of those two compounds into water.

Since the system is expected to explore higher temperatures, a study upon the variation of how N_2 reacts as a function of temperature was performed, figure 46.

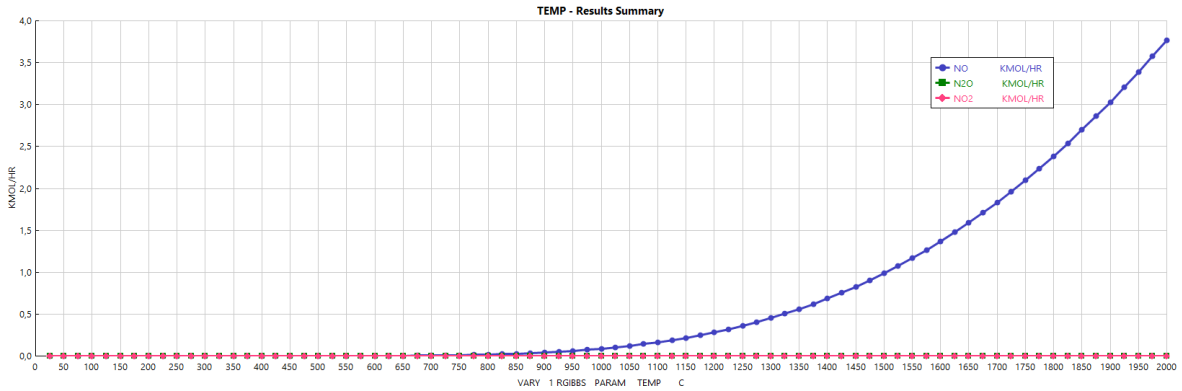

Figure 46: Graph representing the thermodynamic conversion of 200 kmol/h of N_2 into NO, NO_2 and N_2O as a function of temperature.

As can be perceived through figure 46, the N_2 conversion isn't very significant (less than 2%), and only starts reacting for relatively high temperatures (around 1000 K), which aren't expected to be reached on thermal CO_2 methanation reactions. And the only product formed appeared to be NO. For these reasons, for thermal catalysis, the effect of N_2 dilution can therefore be despised.

7.6.4 H_2/CO_2 ratio

All the simulations and results presented previously were performed for a ratio of H_2/CO_2 of three, now for a comparison of how this ratio can effect the dispersion of products obtained, a study for a H_2/CO_2 ration of four was performed, represented in figure 47.

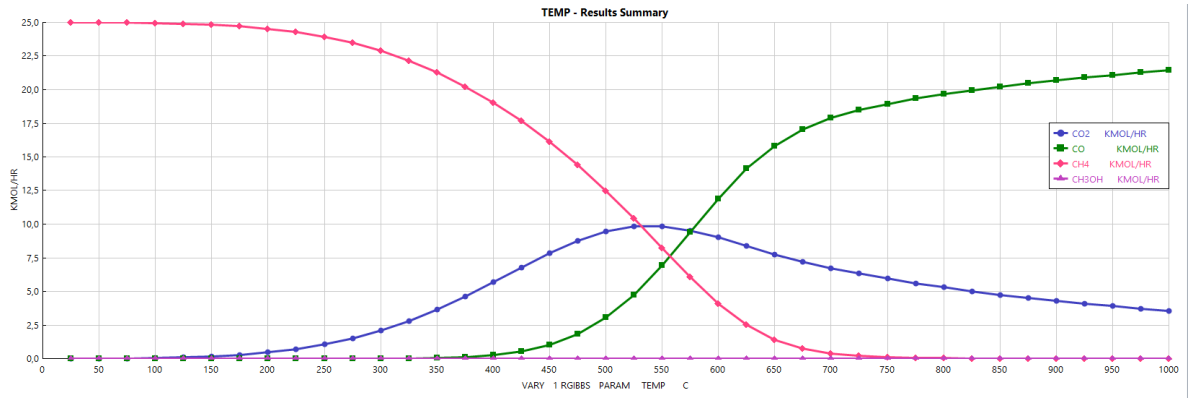

Figure 47: Graph representing the products obtained for the conversion of CO_2 with H_2 for a ratio of four between the two, as a function of temperature.

As can be perceived, the variation of products obtained, between figures 47 and 42, isn't very significant, since the same reactions are observed for around the same temperatures. Both figures display a clear preference for the conversion into methane in detriment of methanol, which, as explained before, is due to the lower enthalpy value for methane. However, for higher temperatures, the dissociation of CO_2 into carbon monoxide and oxygen is preferable, when in the absence of a catalyst.

7.7 Annex 7: Uses for Methanation

Carbon dioxide methanation, in the fuel cell and ammonia synthesis industry, can be used for the removal of trace CO and CO_2 from H_2-rich stream to prevent catalyst poisoning. [17] [185] [186]

The National Aeronautics Space Administration (NASA) has also demonstrated interest in the Sabatier's reaction for their manned missions, in which their special interest resides in the water production, associated with the methanation of CO_2. [187] Besides this goal, they also intend to produce oxygen through water electrolysis, whilst the carbon dioxide that's formed though respiration should be recirculated, along with the hydrogen formed from the electrolysis, providing a full-circle regeneration cycle. [63] These systems are also planned to be used in the future manned missions to Mars, in which they'll convert the Martian carbon dioxide atmosphere into methane and water for fuel and astronaut life support systems. [188].

Methanation is also an important step for the production of synthetic natural gas (SNG) from coal and dry biomass. [189] The first synthetic gas plant was founded in 1984, in Beulah, North Dakota (USA) and is known as the Great Plains Synfuel Plant. [171]

BASF, altogether in a partnership with *Linde* and *Lutianhua*, are planning the construction of a new pilot plant for the development of a direct production of DME from CO_2. [190]

CO_2-to-methanol (CTM) (CH3OH and MeOH) has already been industrialized in Reykjavik, Iceland using heterogeneous catalysis and geothermal energy. [191] [62]

7.8 Annex 8: Catalysts used for Methanol Conversion

Similarly to methane, methanol is also a promising product which can be obtained through CO_2 conversion. And despite having a well-developed process for CO hydrogenation into methanol, the use of CO_2 as a feedstock has been under-explored, in part due to its challenges, such as its need for high pressure (between 30 and 300 atm) and relatively high temperatures (around 250 and 400 °C). [192]

Hence, the necessity of plasma catalysis arises, as a simple low-energy requiring method of activating the CO_2 molecule. Wang *et al.* [192] tested whether using a DBD plasma reactor at room temperature and pressure would increase the conversion of CO_2 and the methanol yield. Both catalysts used, $Cu/\gamma - Al_2O_3$ and $Pt/\gamma - Al_2O_3$, obtained relatively high selectivities towards methanol, specially copper, which obtained a conversion of CO_2 of 21.2% and a selectivity towards methanol of 53.7%. This study has also shown that without plasma, at room temperature and pressure, no production of methanol occurred.

In another study, performed by Luo *et al.* [193], cold plasma was used to fabricate and produce the activated catalysts of Cu/ZnO/C for CO_2 hydrogenation to methanol. And the following was stated "The Cu/ZnO/C catalyst prepared by cold plasma showed an obvious increase in CO_2 conversion, methanol selectivity, and productivity in the catalytic evaluation of catalysts". [193] Which proves that just this type of enhancement of the catalyst using plasma can be advantageous for the process, in addition to plasma catalysis.

Zou *et al.* [194] performed a study on the synthesis of different oxygenates, using a feedstock of CH_4 and CO_2, and using starch and a DBD. The starch was found to prevent the production of C_xH_y, and significantly improve the selectivity towards oxygenates (CH_2O, CH_3OH, C_2H_6O). The total selectivity towards oxygenates was about 10 to 40%, and the conversion of CH_4 and CO_2 was up to 20%.

In table 16, a succinct summary of previously used catalysts for CO_2 conversion into methanol can be observed. The main conditions used were described and the results obtained for both CO_2 conversion (%) and CH_4 selectivity (%) were used for comparison.

Table 16: Descriptive table of previously used catalysts for the conversion of CO_2 into methanol and their respective results.

Catalyst	Method	T (°C)	P (bar)	Other Conditions	CO_2 conversion (%)	CH3OH selectivity (%)	Methanol yield (%)	Ref.
Cu/gamma-Al2O3	DBD	30	1	H_2/CO_2=3	21.2	53.7	11.3	[192]
Pt/gamma-Al2O3	DBD	30	1	H_2/CO_2=3	n.a.	∼52	∼9.0	[192]
Cu/ZnO/Al_2O_3	DBD	60∼250	8	H_2/CO_2=3 Q=1 NL/min power=400W	14	10	1.0	[195]
Pt/film/In2O3	DBD	30	1	-	37	62.6	n.a.	[196]
film	DBD	30	1	-	3.2	6.2	n.a.	[196]
Pt/film	DBD	30	1	-	8.8	14.1	n.a.	[196]
In2O3	DBD	30	1	-	13.1	24.6	n.a.	[196]
film/In2O3	DBD	30	1	-	15.3	26.1	n.a.	[196]
Pt/In2O3-C	DBD	30	1	-	24.9	36.5	n.a.	[196]
Cu/ZnO/Al2O3	DBD	30	1	-	25.6	35.1	n.a.	[196]
CuO/Fe2O3/QW	DBD	200	1	H_2/CO_2=3 Q=0.1 NL/min power=2W	16.7	32.7	n.a.	[197]
NiO/Fe2O3/QW	DBD	200	1	H_2/CO_2=3 Q=0.1 NL/min power=2W	1.7	33.3	n.a.	[197]
CuO/ZnO/Al2O3	DBD	220	1	H_2/CO_2=3 Q=0.5 NL/min power=500W	11.0	1.9	n.a.	[198]

The investigation towards finding the best catalyst for the CO_2 conversion to methanol using plasma reactors hasn't been advancing as swiftly as the methane has. Hence, there aren't currently many certainties into which catalysts should be expected to have a good performance in such reactors. Therefore, due to a lack of previous focused research on plasma catalysis, the catalysts that have been studied in this field have been mainly imported from thermal catalysis.

As was previously stated, the CH_3OH selectivity for CO_2 conversion is mainly obtained through a Cu catalyst. [73] [199] Some other metals that have been associated with copper in order to augment the activity of the catalyst are Zn [201], Ce [200] and their respective oxides.

The mechanism by which this reaction occurs is not yet fully understood, however, Graciani *et al.* [200] proposed a mechanism consisting of reverse water–gas shift and CO hydrogenation (CO_2 + H_2 →CH_3OH)

for the copper/ceria catalyst. Whilst for the copper/zinc-oxide catalyst, the mechanism favored appears to be the direct hydrogenation of CO_2 via a formate intermediate. [199]

7.9 Annex 9: Plasma

Plasma is usually referred to as the "fourth state of matter", due to the fact that with the increase of temperature, matter transforms itself in the following sequence: solid, liquid, gas (neutral), ionized gas (or plasma). The concept of plasma is still highly unknown, yet it is estimated that 99% of the visible matter in the universe is in plasma state, considering the observations made to stars and interstellar matter. [202]

This allows for a distinction between two different types of plasma: natural occuring, e.g. the auroras (Borealis and Australis), and the Saint Elmo's fire; and the man-made plasmas, which applications include tokomaks, stellarators, plasma pinches, and many others.

A second, and more relevant, distinction can be made based on whether the plasma is in thermal equilibrium or not. Due to the impossibility of measuring the real temperature of a plasma, this variable is usually determined by the average energies of the different species. When the temperature in a localized area is the same of all the species within, the plasma is said to be in Local Thermodynamic Equilibrium (LTE), which are usually distinguished as thermal plasmas. When there are multiple different temperatures within the plasma, then it's far from thermodynamic equilibrium, and is known as non-local thermodynamic equilibrium (non-LTE), and these discharges are usually known as Non-Thermal Plasmas (NTP).

7.9.1 Plasma Catalysis

However, plasma, on itself, isn't capable of producing significant amounts of CH_4 since, as described before, NTPs can contain a diverse mix of highly reactive species, so it can become difficult to operate in such a way as to produce single products with high yield and/or high selectivity. Hence, there's the reason why it needs to use both plasma and catalysts together, promising to combine the advantages of the two, to effect transformations that are currently difficult to achieve with only thermal catalysis. [203] [204] [86]

Plasma Catalysis has been gaining some interest in the academic field for various gas conversion applications, such as CO_2 conversion into more valuable chemicals and fuels, CH_4 conversion into carbon monoxide and hydrogen [205], higher hydrocarbons or oxygenates, and even NH_3 synthesis. [206] Some other applications are already more established, such as air pollution control, e.g. VOC remediation, PM and NOx removal. [203] [207]

The study performed by Nizio *et al.* [208] has proven that, within certain conditions, plasma catalysis can outperform thermal catalysis. These results have shown that the catalytic performances of Ni/ZrCe were enhanced by the application of non-thermal plasma. An increase of CO_2 conversion from 0 to 97% and a CH_4 selectivity higher than 90% was obtained at around 260 °C, whilst in the absence of this catalytic plasma system, only a conversion of 5% was obtained, and the final product was mainly CO.

Although, despite the growing interest in plasma catalysis for various environmental and energy applications, the fundamental mechanisms of plasma catalysis are not yet fully understood, since its interactions are not entirely and thoroughly documented. It's a rather complex system, as the catalyst affects the plasma behaviour, and vice versa. This is why currently optimization of plasma catalysis is somewhat of a trial-and-error process, since a lack of fundamental understanding of the ruling physical processes and interactions makes progress rather challenging. The catalysts used and studied for plasma catalysis are often the ones adopted by thermal catalysis, yet this doesn't necessarily comprise an optimal relationship between catalyst and plasma, due to their different reactionary interactions. In spite of that, many are the cases in which plasma-catalyst synergy has been reported, in which the combined effect of plasma and catalyst is superior to that of those when separated.

As far as can be ascertained, currently there isn't any fully extensive research into the screening for a large number of catalysts, so it is within this scope that research on plasma catalysis of the CO_2 methanation should be headed.

One of the difficulties of Plasma Catalysis is that the information from one study is hardly transferable into the whole field. This happens due to the diverse possibilities of catalyst (since the catalyst may be films, powders, foams, pellets, or incorporated in other materials) and to the different local electric field variations that may modify the catalytic reactions. [203] Hence, the reproducibility of previously made essays are not nearly as accurately guaranteed as they are for thermal catalysis, which complicates the wide spread usability of such a technology.

However, for plasma catalysis it is still possible to decrease aggressive conditions or improve the synergies between catalyst and plasma and thus performance, either via shifting operation temperatures to lower values, whilst increasing CH_4 yield and selectivity or via decreasing influence of side reactions, e.g. reverse water-

gas shift reaction (RWGS). [86] For this purpose, the investigation towards finding a better CO_2 methanation catalyst is not yet finished.

7.9.2 Catalysts for Plasma-Assisted Methanation

As described before, a series of catalysts have been studied for this particular reaction, both for thermal and plasma catalysis. In the present section, an enumeration of previously studied catalysts under DBD reactors is presented on table 17.

Table 17: Comparison with some of the catalysts reported in the literature for CO_2 methanation under DBD plasma assisted conditions.

Catalyst Used	CH_4 Selectivity (%)	CO_2 Conversion (%)	T (°C)	P (atm)	Other Conditions	Ref.
Zeolite- H-USY Ni (14 %wt)	7	60	20 to 470	0.0028	H_2/CO_2 =4 GHSV=48 000 h^-1	41
Ni/SiO2	100	90	180 to 320	1	H_2/CO_2 =2 GHSV=7200 h^-1	43
Ni-Ce-Zr/HT	100	80	110 to 430	1	H_2/CO_2=4 GHSV=20 000h^-1	31
CeNi/Cs-USY	95	70	200 to 450	1	H_2/CO_2=4 GHSV=32 000h^-1	36
Ni/BEA	n.a.	95	180 to 360	1	GHSV=15 000h^-1	40
Ni/Al2O3	97	85	260	1	H_2/CO_2=4	45
Mn/$\gamma - Al2O3$	7.5	10.2	135	1	H_2/CO_2=1	39
Cu-Mn/$\gamma - Al2O3$	7.0	9.0	135	1	H_2/CO_2=1	39
Cu/$\gamma - Al2O3$	8.6	8.0	135	1	H_2/CO_2=1	39

As can be observed from table 17, Ni appears to be the best metal catalyst, both for thermal, as previously stated, but also for DBD plasma-assisted catalysis. When it comes to the support, there are more options, specially associated with the Ni catalysts. The best supports tested so far appear to be SiO_2 and Al_2O_3.

In spite of the selection of the catalyst, there's also the selection of when to introduce it, in which three cases can be distinguished. Case 1 involves the operation of the catalyst in the downstream of the plasma, also termed as PPC. Whilst cases 2 and 3 deal with IPC, although with different types of activation of reactants, being the first mild preactivation via excitation-vibration, while the latter corresponds to activation via dissociation of molecules. [203]

PPC is only relevant for relatively stable species, i.e. unconverted reactants, product molecules formed in the upstream plasma and possible relatively stable activated species, e.g. OH radicals. [209] IPC implies the interaction of relatively unstable species with the catalyst surface, causing complex mutual influence of plasma and catalyst. [210]

According with Bacariza *et al.* [83], higher Si/Al ratios led to better performances, not only in thermal catalysis, but specially in non-thermal DBD plasma conditions, which were attributed to the lower affinity of this sample with water. Furthermore, it was also concluded that the addition of Cerium (Ce) would be beneficial, since it acts as a promoter favouring the dielectric properties of the materials and by giving additional sites for the CO_2 activation to occur. Leading therefore to better results than those obtained for Ni/ $\gamma - Al_2O_3$ or Ni/zeolite, specially in plasma conditions. The best catalyst observed in this work was the NiCe/zeolite, which obtained a 75% yield of CH_4 and consumed 25 W.

7.9.3 Physicochemical Interactions of Plasma and Catalyst

A wide variety of complex physical and chemical interactions take place between catalyst and plasma. In thermal catalysis, only ground-state molecules are present in the gas phase. In a plasma, vibrationally and electronically excited molecules, radicals, atoms, ions and electrons are all present, leading to a much larger range of possible chemical reactions. The physical interactions between plasma and catalyst involve charge transfer, electric field modifications and heat transfer, which can affect both the plasma and the catalyst, and therefore shall affect the chemical reactions.

Although there has been plenty of experimental and theoretical studies on the penetration of plasmas into

pores in the catalyst and substrate, a general and complete understanding of these interactions is still lacking. Yet, it is currently known that the influence of plasma on the catalytic surface includes charging, heating and possible alterations of the morphology and structure of the catalyst. [203]

Plasma energy transfers are normally initiated by collisions between energized electrons and the gas molecules. The activation energy thresholds of the four most significant electron impact activation channels typically follow the order (i) Vibrational excitation, (ii) Electronic excitation, (iii) Bond dissociation, (iv) Ionization. The values for the threshold energies of these such electron interactions in CH_4 and CO_2 molecules can be found in table **??**.

Table 18: Bond Dissociation Energies (E_diss), Vibrational Energies (E_vib), First Electronically Excited State (E_elect), Ionization Energies (E_ion), and Electron Impact Dissociation Energy Thresholds ($E_diss, impact$) for the CH_4 and CO_2 molecules, all the variables in eV.

Molecule	E_{diss}	E_{vib}	E_{elect}	E_{ion}	$E_{diss,impact}$
CH_4	4.5	0.37	8.8	13.0	9.0
CO_2	5.5	0.29	7.0	13.8	11.5

Electron impact dissociation typically corresponds to the excitation of the molecule into a repulsive electronic state, which is above the bond dissociation energy limit.

In CO_2 plasmas, as reproduced through figure 48 [12], there are different discharge types which can be performed on the reactant molecule. Electrons receive their share of energy from the electric field generated in NTP, and, through collisions, this energy is then distributed to different channels of excitation, such as dispersed energy in vibrational and electronic excitation, and even ionization, all competing with the intended purpose of dissociation of this molecule.

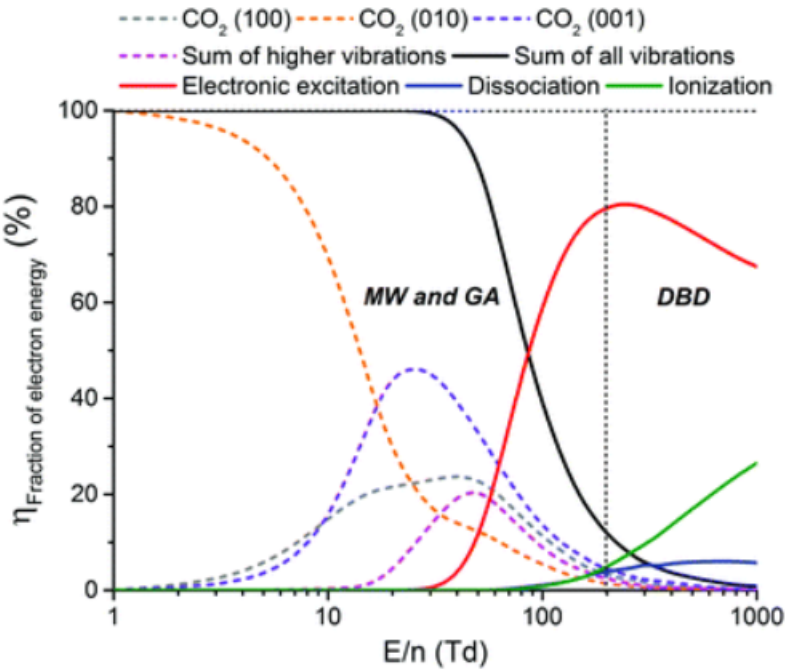

Figure 48: Fraction of electron energy transferred to different channels of excitation, as well as to the ionization and dissociation of CO_2. [12]

According with figure 48, for low electric fields, a significant fraction of the electron energy goes into rotational and vibrational excitations. While at higher-energy electronic excitations, both ionization and dissociation become significant at a value of electric fields of 200 Td or higher. At this reduced electric fields value is where the DBD regime starts. [12] [204]

Due to their low excitation energy threshold, vibrational kinetics have particular relevance in non-equilibrium plasma reactions. [211] Even tho dissociation only receives a small fraction (around 5%) of the electron en-

ergy, the energy going into vibrational excitation is also very important in order to obtain an efficient dissociation of CO_2. [12]

Direct electron-impact dissociation could also be a possible pathway to obtain dissociation of CO_2. However, this pathway would need enough energy (more than 7 eV) to excite CO_2 into a repulsive electronic state. [12] Thus, this energy supply is higher than that of the necessary for C=O bond breaking (5.5eV), and vibrational excitation offers therefore a more efficient dissociation path. It has also been thoroughly proven that vibrationally excited molecules have higher dissociation rates, both for homogeneous reactions [211] and for surface chemisorption. [212] [213] [214]